



FACULTAD DE CIENCIAS

**DEPARTAMENTO DE QUÍMICA INORGÁNICA, CRISTALOGRAFÍA Y
MINERALOGÍA**

TESIS DOCTORAL

**“Preparation and hydration of model
ecocement phases. Characterization by
diffraction and cognate methods”**

Ana María Cuesta García

Málaga, 2015



Publicaciones y
Divulgación Científica

AUTOR: Ana María Cuesta García

 <http://orcid.org/0000-0002-8634-2241>

EDITA: Publicaciones y Divulgación Científica. Universidad de Málaga



Esta obra está bajo una licencia de Creative Commons Reconocimiento-NoComercial-SinObraDerivada 4.0 Internacional:

<http://creativecommons.org/licenses/by-nc-nd/4.0/legalcode>

Cualquier parte de esta obra se puede reproducir sin autorización pero con el reconocimiento y atribución de los autores.

No se puede hacer uso comercial de la obra y no se puede alterar, transformar o hacer obras derivadas.

Esta Tesis Doctoral está depositada en el Repositorio Institucional de la Universidad de Málaga (RIUMA): riuma.uma.es

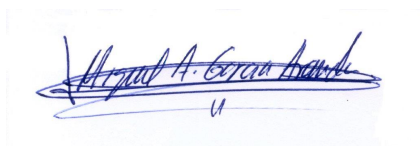
Preparation and hydration of model ecocement phases. Characterization by diffraction and cognate methods

MEMORIA presentada por la Licenciada en Química D^a Ana María Cuesta García para aspirar al grado de Doctora en Ciencias, Sección de Químicas, con la mención de “**Doctorado Internacional**”



Fdo.: Ana María Cuesta García

Los Directores,



Fdo.:

Dr. Miguel Ángel García Aranda
Catedrático de la Universidad



Fdo.:

Dra. M^a Ángeles Gómez de la Torre
Profesora Titular de Universidad



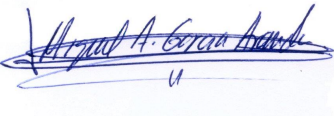
Fdo.:

Dr. Enrique Ramírez Losilla
Profesor Titular de Universidad


D. MIGUEL ÁNGEL GARCÍA ARANDA, Catedrático de la Universidad de Málaga, D^a M^a ÁNGELES GÓMEZ DE LA TORRE, Profesora Titular de la Universidad de Málaga, y D. ENRIQUE RAMÍREZ LOSILLA, Profesor Titular de Universidad, todos pertenecientes al Departamento de Química Inorgánica, Cristalografía y Mineralogía de la Facultad de Ciencias de la Universidad de Málaga, certifican:

Que la presente memoria realizada por D^a Ana María Cuesta García, titulada: **“Preparation and hydration of model ecocement phases. Characterization by diffraction and cognate methods”**, ha sido realizada bajo nuestra dirección en el Departamento de Química Inorgánica, Cristalografía y Mineralogía de la Facultad de Ciencias de la Universidad de Málaga. Este trabajo reúne, a nuestro juicio, contenido científico suficiente y las condiciones necesarias para ser presentado y defendido ante el tribunal correspondiente para optar al Grado de Doctora.

Málaga a 28 de Julio de 2015

Fdo.: 

Dr. Miguel Ángel García Aranda
Catedrático de Universidad

Fdo.: 

Dra. M^a Ángeles Gómez de la Torre
Profesora Titular de Universidad

Fdo.: 

Dr. Enrique Ramírez Losilla
Profesor Titular de Universidad

D. PEDRO JESÚS MAIRELES TORRES, Catedrático de la Universidad y Director del Departamento de Química Inorgánica, Cristalografía y Mineralogía de la Facultad de Ciencias de la Universidad de Málaga.

Informa:

Que la presente memoria realizada por D^a Ana María Cuesta García, titulada: “Preparation and hydration of model ecocement phases. Characterization by diffraction and cognate methods”, ha sido realizada bajo la dirección del Catedrático D. Miguel Ángel García Aranda, la Profesora Titular D^a M^a Ángeles Gómez De la Torre y el profesor Titular D. Enrique Ramírez Losilla en el Departamento de Química Inorgánica, Cristalografía y Mineralogía de la Facultad de Ciencias de la Universidad de Málaga. Este trabajo constituye la Memoria de Tesis Doctoral de la interesada, cuya presentación autorizo en Málaga a 28 de Julio de 2015.



Fdo.: D. Pedro Jesús Maireles Torres.

Acknowledgements

Firstly, I would like to thanks to Inorganic Chemistry, Crystallography and Mineralogy Department of University of Málaga which gave me the opportunity of prepared this PhD Thesis under the direction of Prof. Dr. Miguel Angel García Aranda, Dr. María de los Ángeles Gómez de la Torre and Dr. Enrique Ramirez Losilla.

I would like to express my sincere gratitude to my supervisors Prof. Dr. Miguel Angel García Aranda, Dr. María de los Ángeles Gómez de la Torre and Dr. Enrique Ramirez Losilla for the continuous support during my PhD Thesis, for their patience, motivation, and immense knowledge sharing. Their guidance have helped me in all the time of research and writing up of this thesis.

Besides my supervisor, I would like to thank the rest of the members of the Inorganic Chemistry Crystallography and Mineralogy Department for their help and for accompanying me along these four years.

I would like also thank to Prof. Dr. Reinhard Neder for giving me the opportunity of doing a PhD stage under his supervision.

I would like to acknowledge the financial contribution supported by “Ministerio de Educación, Cultura y Deporte” thought AP2010-0019 FPU-research grant.

Last but not the least; I would like to thank my family, especially my mother and my boyfriend for supporting me with my Thesis and with my life in general.

Agradecimientos

Este espacio de la Tesis está dedicado especialmente a agradecer a todas las personas que me han ayudado y que han hecho posible la finalización de esta Tesis doctoral. Esta Tesis doctoral se ha podido completar gracias a la ayuda de muchas personas que directa o indirectamente han aportado sus conocimientos e ideas para ayudarme a alcanzar mi objetivo final. Para empezar, me gustaría agradecer a la Universidad de Málaga y al Departamento de Química Inorgánica, Cristalografía y Mineralogía por darme la oportunidad de poder desarrollar todo este trabajo bajo la dirección del Prof. Dr. Miguel Ángel García Aranda, la Dra. María de los Ángeles Gómez De la Torre y el Dr. Enrique Ramírez Losilla.

Mis primeras palabras estás dedicadas a mis tres directores de Tesis sin los cuales no habría sido posible realizar esta Tesis doctoral. Me gustaría agradecer al Dr. Miguel Ángel García Aranda por confiar en mí, darme la oportunidad de comenzar este proyecto y por enseñarme que no hay límites para crecer profesionalmente, porque él es un claro ejemplo a seguir. A la Dra. María de los Ángeles Gómez De la Torre por enseñarme tantas cosas día a día y por todo el tiempo que me ha dedicado durante estos cuatro años. Finalmente, agradecer al Dr. Enrique Ramírez Losilla por solucionarme todos los problemas en el laboratorio y porque cada día he podido aprender algo distinto gracias a sus consejos.

Me gustaría agradecer también al resto de profesores del departamento, que por falta de espacio no puedo nombrarlos a todos, empezando por Pedro, director del departamento. Destacar a Maribel, que aunque no ha sido directora de mi Tesis hemos llevado a cabo muchos proyectos en común y he podido aprender muchas cosas de ella. A Aurelio, porque aunque trabaje en otro tema me ha ayudado mucho y me enseñado también muchas cosas relacionadas con la difracción. Por supuesto,

quiero agradecer a Laura por recibirme siempre con una sonrisa cuando iba a llevarle muestras y por su ayuda incondicional que me ha dado cuando la he necesitado.

Por supuesto, quiero agradecer a todos mis "compis" de despacho por todos los momentos compartidos y por las risas que hemos tenido en ese despacho, en el laboratorio, en la sala "vip" y por supuesto en nuestras "quedadas outside". A mis niñas de cementos, Gemita, por enseñarme tantas cosas sobre todo en los primeros años y ayudarme a resolver mis dudas comparando sus cementos con mis "no cementos", Marta, por buscarme "CIFs" de forma ilimitada y por los buenos ratos que hemos pasado tanto dentro como fuera del despacho y por supuesto a Diana, la experta en normativa, que aunque llegó la última a nuestro minigrupo también me ha aportado mucho. También agradecer a los del grupo de "pilas", a Lucia, por ser una muy buena compañera y una excelente cocinera y a Jose Porras (que se fue y luego volvió) por enseñarme "a apuntarse en los hornos" poniendo una línea continua para toda la semana y por su ayuda en el laboratorio, especialmente, durante mi primera etapa. A las niñas "de fosfonatos", Rosario con la cual he podido compartir muchas comidas sobre todo en el "scai" y ha sido mi compañera "brilliant" y "super" en las clases de inglés y Montse, por compartir también muy buenos ratos en el despacho y en el laboratorio. A Jose M. Compañía por su gran conocimiento sobre todas las cosas y por contarnos tantas historias interesantes. Además, a la gente de catálisis, destacando los que han sido compañeros de despacho: Toñi, Cristina, Juanmi, María José... y por supuesto a Mercedes ("la mami") por querernos engordar día a día. Finalmente al resto de compañeros que han pasado por allí, Susana, M^a Jose, Antonio, Sara...

Al Professor Reinhard Neder, de la universidad Friedrich-Alexander de Erlangen (Alemania), por aceptarme para que formara parte de su grupo durante mi estancia.

Agradecer también a mi familia y amigos, por haberme apoyado y ayudado en todos los momentos, tanto buenos como malos y por hacerme ver que esta ha sido una etapa muy importante en mi vida. A mi abuela, porque siempre se ha sentido muy orgullosa de su nieta.

En especial, me gustaría agradecer a mi madre porque todo lo que tengo y lo que soy se lo debo a ella, ya que siempre se ha sacrificado por mí en todos los aspectos y ha antepuesto mi felicidad a la suya. Gracias, mama, por darme siempre tantos valiosos consejos y por comprender todos mis problemas.

A Víctor, por su paciencia, comprensión y apoyo en todos los momentos y estados de ánimo por los que he pasado a lo largo de esta etapa. Por animarme a afrontar todos los problemas y por ser uno de los pilares más importantes en mi vida. Gracias por hacerme sonreír cada día.

Finalmente, me gustaría agradecer la ayuda económica recibida de la beca FPU (AP2010-0019) del “Ministerio de Educación, Cultura y Deporte” sin la cual no habría sido posible la realización de esta Tesis doctoral.

A mi madre.

Table of contents

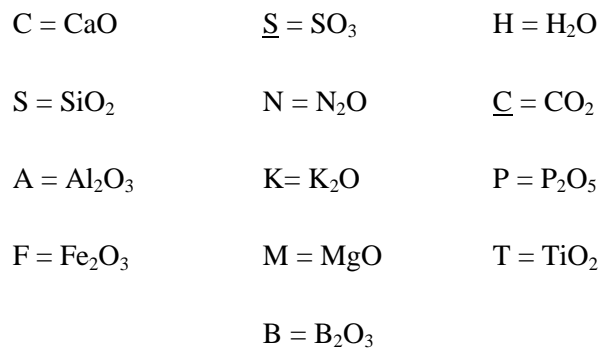
Nomenclature	1
Chemical reactions	5
Abstract	9
Resumen.....	21
1. Introduction to cements.....	35
1.1. Ye'elimites-containing cements	35
1.2. Pure phases of interest in calcium sulfoaluminate cements.....	41
1.2.1. Dicalcium silicate (Ca_2SiO_4 , C_2S)	41
1.2.1.1. Dicalcium silicate chemical compositions and structures	42
1.2.1.2. Hydration mechanisms of dicalcium silicate.....	48
1.2.2. Ye'elimites ($\text{Ca}_4[\text{Al}_6\text{O}_{12}]\text{SO}_4$, $\text{C}_4\text{A}_3\text{S}$).....	50
1.2.2.1. Ye'elimites chemical compositions and structures.....	51
1.2.2.2. Ye'elimites hydration mechanisms	54
1.2.3. Tetracalcium aluminoferrite ($\text{Ca}_4\text{Al}_2\text{Fe}_2\text{O}_{10}$, C_4AF)	56
1.2.3.1. C_4AF chemical compositions and structures	56
1.2.3.2. C_4AF hydration mechanisms	58
1.2.4. Ettringite or AFt ($\text{Ca}_6\text{Al}_2(\text{OH})_{12}(\text{SO}_4)_3 \cdot 26\text{H}_2\text{O}$ $\text{C}_6\text{AS}_3\text{H}_{32}$)	60
1.2.5. AFm-type phases	62
1.2.6. Other hydrated phases: hydrogarnet phases and amorphous aluminium hydroxide $\text{Al}(\text{OH})_3 \cdot n\text{H}_2\text{O}$	65

1.3. Methodologies.....	69
1.3.1. Laboratory X-Ray Powder Diffraction (LXRPD) and Rietveld Method.....	69
1.3.2. Synchrotron X-Ray Powder Diffraction (SXRPD) (BL04 – MSPD, ALBA)	73
1.3.3. Isothermal conduction calorimetry	74
1.3.4. Thermal measurements	76
1.3.5. Scanning electron microscopy (SEM)	76
2. Objectives.....	81
3. Articles section	(not numerated)
a#1: Mechanism of stabilization of dicalcium silicate solid solution with aluminium	
a#2: Reactive belite stabilization mechanisms by boron-bearing dopants	
a#3: Structure, atomistic simulations, and phase transition of stoichiometric ye'elimite	
a#4: Pseudocubic crystal structure and phase transition in doped ye'elimite	
a#5: Hydration mechanisms of two polymorphs of synthetic ye'elimite	
a#6: Ye'elimite: structures and hydration mechanisms	
a#7: Hydration of C ₄ AF in the presence of other phases: a synchrotron X-ray powder diffraction study	
4. General results and discussion	85
4.1. Dicalcium silicate.....	85
4.1.1. Synthesis and sample characterization of dicalcium silicate.....	85
4.1.2. Dicalcium silicate structural study.....	91
4.2. Ye'elimite.....	93

4.2.1. Ye'elinite synthesis.....	93
4.2.2. Ye'elinite structural study.....	95
4.2.3. Thermodiffractometric study and phase transition	99
4.2.4. HT-polymorphs of ye'elinite: structural study.....	102
4.3. Synthesis of C ₄ AF	103
4.4. Application of the structural studies to the analysis of CSA and BCSA cements	105
4.5. Hydration studies.....	107
4.5.1. Hydration of ye'elinite.....	109
4.5.2. Reactivity of ye'elinite with gypsum.....	115
4.5.3. Reactivity of ye'elinite with C ₄ AF	118
4.5.4. Reactivity of ye'elinite with dicalcium silicate.....	124
4.5.5. Hydration of C ₄ AF	129
4.5.6. Reactivity of C ₄ AF with gypsum.....	133
4.5.7. Influence of ye'elinite in C ₄ AF hydration	135
4.6. On-going research	136
5. Conclusions	145
5. Conclusiones	151
6. References	157
Annex I: Collaborations.....	183
Annex II: Copyright permissions	187

Nomenclature

In order to simplify the writing and presentation of chemical formulations, cement nomenclature will be used hereafter:



The compounds are written as follows:

Formula	Oxides	Cement nomenclature	Name
$2\text{Al}(\text{OH})_3 \cdot n\text{H}_2\text{O}$	$\text{Al}_2\text{O}_3 \cdot (3+n)\text{H}_2\text{O}$	$\text{AH}_3 \cdot n\text{H}$	Amorphous aluminium hydroxide
CaSO_4	$\text{CaO} \cdot \text{SO}_3$	CS	Anhydrite
$\text{CaSO}_4 \cdot 0.5\text{H}_2\text{O}$	$\text{CaO} \cdot \text{SO}_3 \cdot 0.5\text{H}_2\text{O}$	$\text{CSH}_{0.5}$	Bassanite
CaCO_3	$\text{CaO} \cdot \text{CO}_2$	CC	Calcite or vaterite
CaAl_2O_4	$\text{CaO} \cdot \text{Al}_2\text{O}_3$	CA	Calcium aluminate
$\text{Ca}_2\text{Al}(\text{OH})_6[\text{Al}(\text{OH})_4 \cdot 3\text{H}_2\text{O}]$	$2\text{CaO} \cdot \text{Al}_2\text{O}_3 \cdot 8\text{H}_2\text{O}$	C_2AH_8	Dicalcium aluminate hydrate
Ca_2SiO_4	$2\text{CaO} \cdot \text{SiO}_2$	C_2S	Dicalcium silicate/ Belite
$\text{Ca}_6\text{Al}_2(\text{OH})_{12}(\text{SO}_4)_3 \cdot 26\text{H}_2\text{O}$	$6\text{CaO} \cdot \text{Al}_2\text{O}_3 \cdot 3\text{SO}_3 \cdot 32\text{H}_2\text{O}$	$\text{C}_6\text{AS}_3\text{H}_{32}$	Ettringite (AFt)
$\text{Ca}_3\text{Al}_2(\text{SiO}_4)_3$	$3\text{CaO} \cdot \text{Al}_2\text{O}_3 \cdot 3\text{SiO}_2$	C_3AS_3	Garnet
$\text{Ca}_2\text{Al}_2\text{SiO}_7$	$2\text{CaO} \cdot \text{Al}_2\text{O}_3 \cdot \text{SiO}_2$	C_2AS	Gehlenite
$2\text{Al}(\text{OH})_3$	$\text{Al}_2\text{O}_3 \cdot 3\text{H}_2\text{O}$	AH_3	Gibbsite
$\text{CaSO}_4 \cdot 2\text{H}_2\text{O}$	$\text{CaO} \cdot \text{SO}_3 \cdot 2\text{H}_2\text{O}$	CSH_2	Gypsum

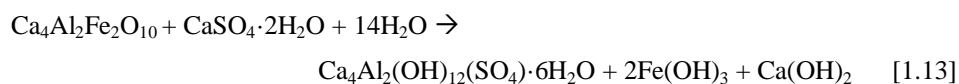
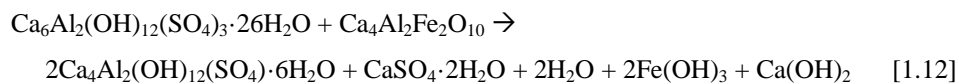
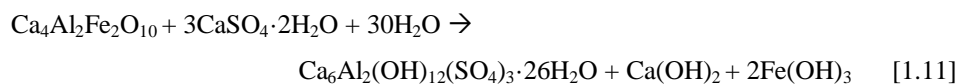
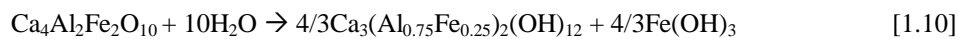
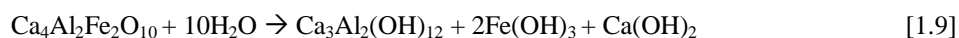
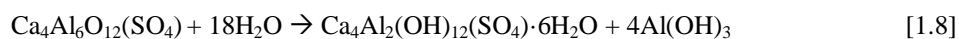
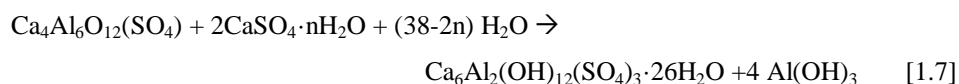
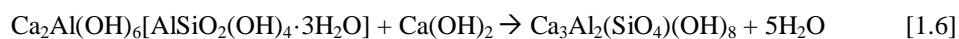
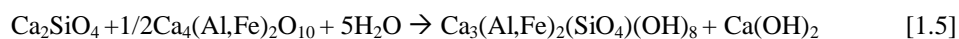
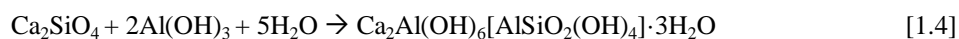
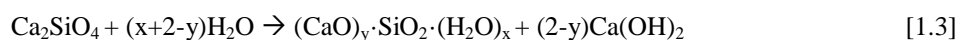
Formula	Oxides	Cement nomenclature	Name
$\text{Ca}_3\text{Al}_2(\text{OH})_{12}$	$3\text{CaO}\cdot\text{Al}_2\text{O}_3\cdot 6\text{H}_2\text{O}$	C₃AH₆	Hydrogarnet or katoite
$2\text{Fe}(\text{OH})_3$	$\text{Fe}_2\text{O}_3\cdot 3\text{H}_2\text{O}$	FH₃	Iron hydroxide
$\text{Ca}_3(\text{Al}_{0.5}\text{Fe}_{0.5})_2(\text{SiO}_4)(\text{OH})_8$	$3\text{CaO}\cdot 0.5\text{Al}_2\text{O}_3\cdot 0.5\text{Fe}_2\text{O}_3\cdot \text{SiO}_2\cdot 4\text{H}_2\text{O}$	C₃A_{0.5}F_{0.5}SH₄	Iron (siliceous) hydrogarnet or iron-katoite
$\text{Ca}_{12}\text{Al}_{14}\text{O}_{33}$	$12\text{CaO}\cdot 7\text{Al}_2\text{O}_3$	C₁₂A₇	Mayenite
$\text{Ca}_4\text{Al}_2(\text{OH})_{12}(\text{SO}_4)\cdot 6\text{H}_2\text{O}$	$4\text{CaO}\cdot \text{Al}_2\text{O}_3\cdot \text{SO}_3\cdot 12\text{H}_2\text{O}$	C₄ASH₁₂	Monosulfate (AFm)
$\text{Ca}(\text{OH})_2$	$\text{CaO}\cdot \text{H}_2\text{O}$	CH	Portlandite
$\text{Ca}_3\text{Al}_2(\text{SiO}_4)(\text{OH})_8$	$3\text{CaO}\cdot \text{Al}_2\text{O}_3\cdot \text{SiO}_2\cdot 4\text{H}_2\text{O}$	C₃ASH₄	Silicious hydrogarnet
$\text{Ca}_2\text{Al}(\text{OH})_6[\text{AlSiO}_2(\text{OH})_4\cdot 3\text{H}_2\text{O}]$	$2\text{CaO}\cdot \text{Al}_2\text{O}_3\cdot \text{SiO}_2\cdot 8\text{H}_2\text{O}$	C₂ASH₈	Stratlingite
$\text{Ca}_5(\text{SiO}_4)_2(\text{SO}_4)$	$5\text{CaO}\cdot 2\text{SiO}_2\cdot \text{SO}_3$	C₅S₂S	Ternesite
$\text{Ca}_4\text{Al}_2\text{Fe}_2\text{O}_{10}$	$4\text{CaO}\cdot \text{Al}_2\text{O}_3\cdot \text{Fe}_2\text{O}_3$	C₄AF	Tetracalcium aluminoferrite
$\text{Ca}_3\text{Al}_2\text{O}_6$	$3\text{CaO}\cdot \text{Al}_2\text{O}_3$	C₃A	Tricalcium aluminate
Ca_3SiO_5	$3\text{CaO}\cdot \text{SiO}_2$	C₃S	Tricalcium silicate/ Alite
$\text{Ca}_4\text{Al}_6\text{O}_{12}(\text{SO}_4)$	$4\text{CaO}\cdot 3\text{Al}_2\text{O}_3\cdot \text{SO}_3$	C₄A₃S	Ye'elinite

Abbreviated names or initials to refer to some terms are listed below in alphabetical order:

- a#x: article number x
- ACn: Amorphous and Crystalline non-quantified
- ADP: Atomic Displacement Parameter
- AFm: $\text{Al}_2\text{O}_3\text{-Fe}_2\text{O}_3\text{-mono}$

- AFt: $\text{Al}_2\text{O}_3\text{-Fe}_2\text{O}_3\text{-tri}$
- ATR-FTIR: Attenuated Total Reflectance-Fourier Transform Infrared Spectroscopy
- BCSA: Belite Calcium Sulfo-Aluminate
- BCSAF: Iron-rich Belite Calcium Sulfo-Aluminate
- BSE: BackScattered Electrons
- B.M. EoS: Birch-Murnaghan Equation of State
- CAC: Calcium Aluminate Cement
- CSA: Calcium Sulfo-Aluminate
- DAC: Diamond Anvil Cell
- DSC: Differential Scanning Calorimetry
- DTA: Differential Thermal Analysis
- FW: Free Water
- FWHM: Full Width at Half Maximum
- HT-LXRPD: High-Temperature Laboratory X-Ray Powder Diffraction
- LXRPD: Laboratory X-Ray Powder Diffraction
- NPD: Neutron Powder Diffraction
- OPC: Ordinary Portland Cement
- PXCT: Ptychographic X-ray Computed Tomography
- RQPA: Rietveld Quantitative Phase Analysis
- RT: Room Temperature
- SEM: Scanning Electron Microscopy
- SXRPD: Synchrotron X-Ray Powder Diffraction
- TGA: ThermoGravimetric Analysis
- w/s: water to solid ratio
- XRPD: X-Ray Powder Diffraction

Chemical reactions



Abstract

Abstract

The manufacture of CSA cements is more environmentally friendly than that of OPC as it releases less CO₂ than the latter. This reduction, which depends on CSA composition, is due to three factors: i) CSA cements are less calcite demanding materials than OPC, with the consequent diminution of carbon dioxide emissions from decarbonation in the kilns; ii) OPC clinkering temperature is ~1450°C, while for CSA can be as low as ~1250°C depending on the composition and consequently less fuel is needed, and iii) these CSA cements are easier to grind, implying an energetic saving and so, indirect emission depletion. For example, the production of one ton of OPC clinker composed of 65 wt% of C₃S, 15 wt% of C₂S, 10 wt% of C₃A and 10 wt% of C₄AF released 0.97 tons of carbon dioxide. However one ton of CSA clinker composed by 65 wt% of C₄A₃S, 20 wt% of C₂S, 9 wt% of C_S and 6 wt% C₄AF releases 0.61 tons of CO₂. Consequently, a reduction in carbon dioxide emissions by 37% taking into account the three contributions can be attained.

CSA cements are prepared by mixing the clinker with different amounts of a calcium sulfate set regulator. The main performances of CSA cements are fast setting time (followed by a rapid hardening), good-chemical resistance properties and, depending on the amount of the added sulfate source they are shrinkage controllers.

CSA cements present a wide range of phase assemblages, but all of them contain over 50 wt% of ye'elinite jointly with belite, tetracalcium aluminoferrite and other minor components such as CA, C₄AF, CS, C_SH₂ and so on.

This phase, ye'elinite, is also included (~25 wt%) in BCSA. The most common formulation of these cements consists on β-C₂S, C₄A₃S and C₄AF. These cements always contain as main phase dicalcium silicate. The stabilization of α'_H-C₂S polymorph, which is more hydraulically active than the others

polymorphs of dicalcium silicate, plays an important role in the preparation of active BCSA cements in the laboratory and industrial trials.

Ca_2SiO_4 or dicalcium silicate (belite in cement nomenclature) presents five stoichiometric forms γ , β , α'_L , α'_H and α . The low temperature polymorph is $\gamma\text{-C}_2\text{S}$, however, this phase is avoided in cement manufacture because it is hydraulically non-active. The β -form is usually found in OPC and in almost all CSA cements. In addition, α -phases are supposed to be more reactive and they are mainly found in some active BCSA cements. The stabilization of α' -polymorph by introduction of foreign oxides has been studied over the years. Recently, it has been reported that the addition of a combination of B_2O_3 and Na_2O successes to stabilize $\alpha'_H\text{-C}_2\text{S}$ (Wesselsky and Jensen 2009). Dicalcium silicate hydration may yield C-S-H and portlandite or stratlingite in case an aluminum source is present and portlandite is absent. However, the hydration kinetic of dicalcium silicate is slow when compared to other phases.

Ye'elimite, $\text{Ca}_4[\text{Al}_6\text{O}_{12}]\text{SO}_4$, present a sodalite type-structure with general composition, $\text{M}_4[\text{T}_6\text{O}_{12}]\text{X}$. Nevertheless, stoichiometric ye'elimite crystal structure at room temperature was poorly understood since it has been reported to be orthorhombic, tetragonal or cubic. Furthermore, it was know that the presence of different amounts of Na^+ and Fe^{3+} can stabilize the cubic form. On the other hand, ye'elimite is very reactive and most of its hydration heat is released during the first eight hours. During early age hydration, ettringite (AFt) phase is the main crystalline hydration product formed from the dissolution of ye'elimite in the presence of calcium sulfate(s). However, monosulfate (AFm) phase is mainly formed in the absence of a source of soluble sulfate. A similar hydration mechanism can be found in the early age hydration of CSA and BCSA cements because their hydration procedure is mainly dominated by the ye'elimite phase. For this reason, commercial cements with large amounts of ye'elimite have special applications such as high strength developments at early-ages.

Tetracalcium aluminoferrite, is the major iron-containing phase in OPC and is also present in BCSA. However, the reactivity of tetracalcium aluminoferrite during hydration in these cements is slower than that for ye'elimite and it is not well understood. In the hydration of tetracalcium aluminoferrite usually $C_3(A,F)H_6$ is formed and in the presence of sulfate AFt and/or AFm precipitate. Moreover, in the presence of silica, iron containing siliceous hydrogarnet will precipitate instead of $C_3(A,F)H_6$.

Taken into account which has been discussed previously, the general aim of this PhD Thesis has been to synthesize and characterize these single phases of ecocements to better understand their behavior during hydration. To do so, this PhD work is divided in two main blocks: i) structural studies of anhydrous phases and ii) hydration studies of selected phases. SXRPD, high-temperature LXPDP, NPD, DSC and permittivity measurements have been employed for the structural studies. On the other hand, XRPD is a powerful tool for material characterization in general, and for *in-situ* studies of hydration processes in particular. This technique has been extensively used for the characterization of pastes. Moreover, the use of an intense X-ray source, i.e. synchrotron X-rays, coupled with fast X-ray detectors permits time-resolved diffraction experiments allowing *in-situ* quantitative phase analysis during the early ages of cement hydration.

Firstly, for the study of β -dicalcium silicate samples, $Ca_2Si_{1-2x}Al_{2x}O_{4-x}\square_x$ (from $x=0$ to 0.03) solid solution was prepared and studied by LXPDP and the Rietveld method. The sample $Ca_2Si_{0.972}Al_{0.028}O_{3.986}\square_{0.014}$ which contained 99(1) wt% of β -polymorph was selected for further studies. Thermal analysis measurements of this sample in a wet atmosphere indirectly have confirmed that aluminum was incorporated into the framework of dicalcium silicate and stabilized the β -form by replacing the silicate units and generating oxygen vacancies. However, aluminum substitution at both calcium and silicon sites,

$\text{Ca}_{2-x}\text{Al}_x(\text{SiO}_4)_{1-x}(\text{AlO}_4)_x$, was not achieved, conversely to the aluminium doping in tricalcium oxysilicate.

Then, the coupled Na/B-doping of dicalcium silicate has also been investigated and $\text{Ca}_{2-x}\text{Na}_x(\text{SiO}_4)_{1-x}(\text{BO}_3)_x$ series have confirmed to exist for a large range of x values being $\alpha'_\text{H}\text{-C}_2\text{S}$ the main phase (for $x \geq 0.10$). In this case, the borate group was planar-triangular, BO_3^{3-} . Moreover, $\text{Ca}_{2-x}\text{B}_x(\text{SiO}_4)_{1-x}(\text{BO}_4)_x$ was also studied and in this case tetrahedral SiO_4^{4-} groups were replaced by tetrahedral BO_4^{5-} units. This solid solution also allowed to stabilize high amounts of α'_H -form. However, this series was not further studied as we were more interesting in the stabilization of $\alpha'_\text{H}\text{-C}_2\text{S}$ by borax for mimic the industrial conditions. The boron anion nature was determined by infrared studies. Other compositions $\text{Ca}_{2-x/2}\square_{x/2}(\text{SiO}_4)_{1-x}(\text{BO}_3)_x$, $\text{Ca}_2(\text{SiO}_4)_{1-x}(\text{BO}_3)_x\text{O}_{x/2}$ and $\text{Ca}_{2-3x}\text{B}_{2x}\text{Na}_x(\text{SiO}_4)_{1-x}(\text{BO}_4)_x$ were also tested but they were not achieved. Then, $\alpha'_\text{H}\text{-Ca}_{1.85}\text{Na}_{0.15}(\text{SiO}_4)_{0.85}(\text{BO}_3)_{0.15}$ was selected to perform a deep structural study, this was due to the fact that the sample presented sharp diffraction peaks and a high content of α'_H -phase (~90 wt%). Finally, a new revised structural description for $\alpha'_\text{H}\text{-Ca}_{1.85}\text{Na}_{0.15}(\text{SiO}_4)_{0.85}(\text{BO}_3)_{0.15}$ sample was obtained. The final refined unit cell parameters for $\alpha'_\text{H}\text{-Ca}_{1.85}\text{Na}_{0.15}(\text{SiO}_4)_{0.85}(\text{BO}_3)_{0.15}$ were $a=6.8432(2)$ Å, $b=5.4555(1)$ Å, $c=9.2346(2)$ Å and $V=344.76(2)$ Å³. The new revised crystal structure yielded to low disagreement values, $R_{\text{WP}}=6.5\%$ and $R_{\text{F}}(\alpha'_\text{H}\text{-C}_2\text{S})=2.4\%$ and fitted better this phase in active BCSA cements allowing more accurate Rietveld mineralogical analysis.

For ye'elimite, stoichiometric ($\text{Ca}_4\text{Al}_6\text{O}_{12}\text{SO}_4$) and doped ($\text{Ca}_{3.8}\text{Na}_{0.2}\text{Al}_{5.6}\text{Fe}_{0.2}\text{Si}_{0.2}\text{O}_{12}\text{SO}_4$) samples have been prepared in order to characterize the orthorhombic and pseudocubic polymorphs, respectively. Stoichiometric ye'elimite was successfully prepared but it contained small amount of impurities such as $\text{Ca}_3\text{Al}_2\text{O}_6$, CaAl_2O_4 and $\text{Ca}_{12}\text{Al}_{14}\text{O}_{33}$. Our structural study for stoichiometric ye'elimite by LXRPD and NPD joint Rietveld refinement

showed that this sample presents an orthorhombic symmetry with space group *Pcc2*. Final unit cell values were $a=13.0356(7)$ Å, $b=13.0350(7)$ Å, and $c=9.1677(2)$ Å. Moreover, several structures were determined by using density functional theory calculations being the lowest energy structure *Pcc2*, in agreement with our experimental result.

For doped ye'elimitite, $\text{Ca}_{3.8}\text{Na}_{0.2}\text{Al}_{5.6}\text{Fe}_{0.2}\text{Si}_{0.2}\text{O}_{12}\text{SO}_4$, dopants were added as Fe_2O_3 , Na_2CO_3 and SiO_2 obtaining a single crystalline phase. The structural model for this sample has been reported to be based on pseudocubic symmetry with $\bar{I}43m$ as space group. Final unit cell value was $9.1974(7)$ Å. The thermal behavior of the doped sample has been crucial for the determination of the pseudocubic symmetry. DSC measurements of this sample showed a phase transition at 525°C . Moreover, the high-temperature LXRPD studied showed a sharpening of the diffraction peaks over 500°C which is likely related with the dynamical disordering of the sulfate anions. Both results indicate that the RT form of doped ye'elimitite had a lower symmetry than cubic, consequently it can be assigned to a pseudocubic.

Thermodiffractometric studies of stoichiometric ye'emilite showed the transition of the orthorhombic form to a higher symmetry polymorph. Moreover, for stoichiometric ye'elimitite, DSC and permittivity measurements were used to measure the reversible phase transition from orthorhombic to cubic which was characterized to occur at 470°C .

In addition, an structural study for both samples at 800°C was carried out. The crystal structure of stoichiometric ye'elimitite was found to be cubic. For doped ye'elimitite, the structural study at 800°C also suggested a truly cubic structure at this temperature.

The motivation of revising the crystal structures of both polymorphs of dicalcium silicate and ye'elimitite was to use them to perform Rietveld quantitative phase analysis of sulfoaluminate cements. Our reported crystal structures enable

Ana María Cuesta García

more accurate mineralogical phase analysis of commercial calcium sulfoaluminate cements since lower disagreement values (R_F and R_{WP}) were obtained using these structures when compared to results achieved with the previous published ones.

After the initial characterization of anhydrous ye'elimite samples, orthorhombic and pseudocubic, hydration studies were carried out. Another important aim of this thesis has been to understand the early age hydration of stoichiometric (orthorhombic) and doped (pseudocubic) ye'elimite phases at early ages in order to understand “eco-cement” performances. Consequently, the influence of different water/cement ratios and the addition of different calcium sulfate sources on hydration kinetic and mechanism have been studied.

Hydration studies have been performed by using LXRPD with external standard methodology (G-factor) and/or by using SXRPD with internal standard methodology to determine the full phase assemblage including ACn contents. The internal standard method gives a total ACn value which includes FW. On the other hand, the external standard method was applied to stopped-hydration samples; consequently it enables to obtain only ACn contents. In this case FW was determined by the comparison of DTA-TG weight losses of stopped-hydration samples and the total added water. It is important to highlight that the results obtained by the internal standard method are in agreement with those obtained at later ages by external standard method, showing the consistence of both methodologies to follow hydration reactions with time. Calorimetry studies have also been carried out in order to complement the data obtained by XRPD.

The sample preparation was slightly different for each methodology. Samples for SXRPD were prepared in capillaries sealed with grease and for the *ex-situ* LXRPD study, pastes were prepared in a sealed cylinder shape mold and the hydration of the pastes were stopped after specific ages.

Firstly, stoichiometric ye'elimite was studied with different amount of water in order to check the influence on the hydration mechanism of ye'elimite of

this parameter. The main conclusion reached is that higher amounts of water enhanced ye'elimite reactivity, as expected. For stoichiometric ye'elimite, AFm was the main hydration product at all ages jointly with AFt. Higher w/s ratio favored the formation of larger amounts of AFm and less AFt. From the mass balance point of view the same AFm/AFt ratio should be present if the reaction is complete. Consequently, we speculate that the higher w/s ratio has yielded to almost complete reaction.

The role of ye'elimite polymorphism on the hydration mechanisms has also been established. Their reactivity was compared and it was found that doped ye'elimite (pseudocubic) presented a faster kinetics and yielded higher amounts of AFt than stoichiometric (orthorhombic) ye'elimite under the same experimental conditions. Calorimetric data also confirmed this behavior.

The hydration mechanisms of both ye'elimite compounds with a source of soluble sulfate, such as gypsum or anhydrite, were studied at very early ages using SXRPD. It is known that the presence of sulfate phases leads to the formation of AFt. Here, we showed that for a fixed gypsum and water content, AFt was the only crystalline hydrated product and AFm was not found at any hydration time. However, it is important to have in mind that there should be an amorphous phase with general formula, $AH_3 \cdot nH_2O$ which is formed jointly with AFt. The main difference between both ye'elimites was that the hydration kinetics of stoichiometric ye'elimite was faster than that of doped-ye'elimite at very early ages. Concretely, at 14 h of hydration ~100% of stoichiometric ye'elimite had reacted while only ~85% of doped ye'elimite was consumed after 14h. Moreover, the role of the addition of anhydrite was studied at early ages for the sake of comparison with the hydration behavior when gypsum is added to ye'elimite. It was found that both hydration mechanisms were very similar between both polymorphs but the reaction kinetics using anhydrite were slower due to the lower anhydrite solubility.

Hydration of cements can be summarized as a process of dissolution and crystallization/precipitation of different phases. Although ye'elimate is the main responsible of the hydration CSA cements, it is important to study the hydration of ye'elimate in combination with other phases. For this reason, another important target of this Thesis has been to study the hydration of both ye'elimites, stoichiometric and doped, in combination with other phases such as tetracalcium aluminoferrite, β -C₂S and α' _H-C₂S.

Firstly, the hydration of both ye'elimites in combination with C₄AF and gypsum has been studied by *in-situ* SXRPD. In the case of stoichiometric ye'elimate, AFt was firstly formed and then when gypsum was exhausted AFm started to precipitate. Moreover, this ye'elimate was also studied with different amount of w/s in order to determine the water influence on its hydration, obtaining that higher amounts of water enhanced the AFm precipitation and accelerated the reaction kinetic of stoichiometric ye'elimate. The ACn values have also been calculated for these samples. It can be observed that these values slightly diminished with time during the crystallization of AFt and they increased at the time that AFm started to appear.

In the case of the hydration of doped ye'elimate with C₄AF, the main difference after 46 hours was that this sample yielded much larger relative amounts of AFt (28.6(1) wt%) than with stoichiometric ye'elimate (15.5(3) wt%). So, here, we have proved that the differences in the hydration mechanisms between both ye'elimate polymorphs are exacerbated when tetracalcium aluminoferrite is in the reaction medium. In addition, SEM-EDS has been used in order to check if the iron which belongs to C₄AF phase is incorporated in the crystalline hydrated phases of these samples. It can be stated that AFm and AFt formed in the hydration of ye'elimate with gypsum and C₄AF does not contain appreciable iron content in their structures. Therefore, an iron-bearing amorphous phase should be present.

Hydration of ye'elimite has also been studied in combination with dicalcium silicate by LXRPD. Here we have reported the role of ye'elimite and dicalcium silicate polymorphisms on their hydration mechanisms. These studies will help to unravel the hydration mechanisms of BCSA.

It is known that BCSA cements which contain the α'_H -C₂S polymorphs develop higher mechanical strengths values than cements that contain β -C₂S polymorph. This behavior was previously proposed but not directly demonstrated. However, it is essential to establish the role of both-polymorphs of ye'elimite in these mixtures. Here, we have studied all the combinations between dicalcium silicate and ye'elimite until 6 months. Powder diffraction data at 28 days showed some small differences between samples. The sample which contained both α'_H -C₂S and doped-ye'elimite presented a higher degree of reaction and higher amounts of stratlingite at that age. However, important differences are expected at long ages. In the tested experimental conditions, both ye'elimite polymorphs yielded mainly crystalline ettringite. However, we have demonstrated that the hydration degree of α'_H -dicalcium silicate was much larger than that of β -C₂S in the investigated time range (up to six months). At that time, α'_H -dicalcium silicate was totally dissolved and, conversely, high amounts of β -C₂S were found in the samples. It is important to bear in mind that there were no differences between stoichiometric ye'elimite and doped ye'elimite in these samples due to the fact that studies were done from 7 days and ye'elimite hydration occurs earlier.

After the hydration studies of ye'elimite, the characterization of tetracalcium aluminoferrite hydration has also been carried out. The anhydrous sample was successfully prepared obtaining a phase assemblage of 98.1(1) wt% of C₄AF and 1.9(1) wt% of C₃A as an impurity.

Hydration behavior of C₄AF in selected experimental conditions has been thoroughly studied. C₄AF has been hydrated in the absence and presence of gypsum. C₄AF in the presence of water hydrated to form mainly a hydrogarnet-

Ana María Cuesta García

type phase, $C_3A_{0.845}F_{0.155}H_6$. This hydrated phase was measured by high resolution SXRPD in order to perform a structural study. In addition, TEM combined with EDS studies were used to confirm that iron was incorporated in the hydrogarnet phase, $C_3A_{0.845}F_{0.155}H_6$. A crystal structure for this phase is reported here.

The hydration of tetracalcium aluminoferrite in the presence of gypsum was different than the previous one and yielded a mixture of AFm and AFt. Firstly, AFt precipitated jointly with amorphous aluminum hydroxide and once gypsum was completely dissolved crystalline AFm started to precipitate. Calorimetric data showed a broad signal which correspond to the AFm formation. SEM-EDS studies have been used to corroborate that AFt and AFm phases incorporate some amount of iron.

Finally, new on-going research are being carried out using complementary techniques for the characterization of pure hydrated phases and for the study of some hydration mechanisms. Firstly, ptychographic X-ray computed tomography (PXCT) has been used here to study the hydration of ye'elimite samples. After different hydration times, the samples (cement pastes) were investigated at cSAXS beamline is SLS (Swiss Light source). The main goal is to characterize the microstructures of the pastes and to quantify the electron and mass densities of the phases present in these samples. Then, the densities were compared with the theoretical values in order to identify the phases. The measured mass densities matched well with the expected values. In order to obtain better results, the histograms of a VOI (volume of interest) were carried out for each sample excluding the capillaries.

Moreover, a high pressure SXRPD experiment has also been carried out. Hydrated samples were placed in DAC to determine their behavior under pressure. This technique enables to determine the bulk modulus and the stability of these cement phases. This pressure study has been carried out for an iron-hydrogarnet sample, $C_3A_{0.845}F_{0.155}H_6$, obtaining a bulk modulus of 54(2) GPa.

Resumen

Resumen

La producción de cementos de sulfoaluminato de calcio (CSA, del inglés Calcium SulfoAluminate) es más respetuosa para el medio ambiente que la de los cementos Portland ordinarios (OPC, del inglés Ordinary Portland Cement) ya que libera menos CO_2 . La reducción se debe a tres factores: i) Los cementos CSA requieren menos calcita que los OPC, lo cual disminuye las emisiones de CO_2 en el proceso de descarbonatación en el horno; ii) La temperatura de clinkerización del CSA es aproximadamente 1250°C , mientras que la de los OPC está en torno a 1450°C , dependiendo de la composición del cemento, por consiguiente se necesita menos cantidad de combustible y iii) los cementos tipo CSA son más fáciles de molturar lo cual implica una reducción energética y por tanto, una disminución de las emisiones de forma indirecta. Por ejemplo, en la producción de una tonelada de clínker OPC con una composición en peso del 65% de C_3S , 15% de C_2S , 10% de C_3A y 10% de C_4AF , se liberan 0.97 toneladas de dióxido de carbono. Sin embargo, una tonelada de clínker CSA compuesto por 65% de $\text{C}_4\text{A}_3\text{S}$, 20% de C_2S , 9% de CS y 6% C_4AF libera 0.61 toneladas de CO_2 . Teniendo en cuenta estas tres contribuciones se estima que en el proceso total hay una reducción del 37% en las emisiones de dióxido de carbono.

Los cementos CSA se preparan mezclando el clínker con diferentes cantidades de un sulfato de calcio como regulador de fraguado. Las principales prestaciones de los cementos CSA son un tiempo de fraguado rápido (acompañado por un endurecimiento rápido), buena resistencia química y, dependiendo de la cantidad de sulfato de calcio añadido pueden ser materiales controladores de la retracción.

Los cementos CSA presentan un amplio rango de ensamblaje de fases, pero todos contienen en torno a un 50% de ye'elimita además de belita, ferrito aluminato tetracálcico y otros componentes minoritarios como CA, CS y CSH_2 entre otros.

Ana María Cuesta García

La ye'elimita, también está incluida (25% en peso) en los cementos belíticos de sulfoaluminato de calcio (BCSA, del inglés Belite Calcium SulfoAluminate). La formulación más común de estos cementos consiste en β -C₂S, C₄A₃S̄ y C₄AF. La estabilización del polimorfo α' _H-C₂S, el cual es más activo hidráulicamente que los otros polimorfos del silicato dicálcico, juega un papel importante en la preparación de los cementos activados tipo BCSA en el laboratorio y en ensayos industriales.

Ca₂SiO₄ o silicato dicálcico (belita en nomenclatura de cementos) presenta cinco formas polimórficas: γ , β , α' _L, α' _H y α . El polimorfo estable a temperatura ambiente, γ -C₂S, es hidráulicamente inactivo por lo que su formación se evita en la producción de cementos. La forma β es la que se encuentra normalmente en un OPC y en la mayoría de cementos tipo CSA. Además, las fases α son más reactivas y éstas se encuentran en algunos cementos activados tipo BCSA. Durante muchos años se ha estudiado la estabilización de los polimorfos de alta temperatura dopando la estructura con otros elementos. Recientemente se ha publicado que la adición de B₂O₃ y Na₂O estabiliza el polimorfo α' _H del silicato dicálcico (Wesselsky and Jensen 2009). La hidratación del silicato dicálcico conduce a la formación de C-S-H y portlandita o de stratlingita siempre y cuando esté presente una fuente de aluminio y la portlandita no este presente. Sin embargo, la cinética de hidratación es muy lenta en comparación con la de otras fases presentes en los cementos.

La ye'elimita, Ca₄[Al₆O₁₂]SO₄, presenta una estructura tipo sodalita con una estequiometría general tipo M₄[T₆O₁₂]X. Sin embargo existe controversia en su estructura cristalina a temperatura ambiente, ya que se ha publicado que es ortorrómbica, tetragonal o cúbica. Recientemente se ha afirmado que no es posible que la ye'elimita presente una estructura cúbica a temperatura ambiente aunque se sabe que la presencia de Na⁺ y Fe³⁺ estabiliza el polimorfo cúbico. La ye'elimita es muy reactiva y la mayor parte del calor de hidratación se libera

durante las ocho primeras horas. Durante la hidratación a edades tempranas, el principal producto cristalino que se forma, debido a la disolución de la ye'elimita en presencia de sulfato, es la fase etringita (AFt). Sin embargo, la fase monosulfato o AFm se forma cuando no hay una fuente de sulfato soluble en el medio. En la hidratación de los cementos tipo CSA y BCSA ocurre un mecanismo similar a primeras edades ya que el proceso está dominado por la presencia de la fase ye'elimita. Debido a esto, los cementos comerciales que contienen grandes cantidades de fase ye'elimita tienen propiedades especiales como son el desarrollo de una alta resistencia a edades tempranas.

El ferrito aluminato tetracálcico, es la principal fase con hierro de los cementos OPC y está también presente en los cementos tipo BCSA. Sin embargo, la reactividad de esta fase durante su hidratación en los cementos es bastante más lenta que la hidratación de la fase ye'elimita y además no está bien definida. En la hidratación del C_4AF normalmente se forma $C_3(A,F)H_6$ (fase tipo hidrogranate) y en presencia de sulfato precipita AFt y/o AFm. Por otro lado, en presencia de sílica, precipita hidrogranate de silicio con hierro en lugar de $C_3(A,F)H_6$.

Teniendo en cuenta todo lo que se ha discutido anteriormente, el objetivo general de esta tesis doctoral ha sido sintetizar y caracterizar las fases individuales que están presentes en los ecocementos (cementos tipo CSA y BCSA) para comprender mejor su comportamiento durante la hidratación. Para ello, la tesis doctoral se ha dividido en dos bloques: i) estudios estructurales de fases anhidras y ii) estudios de hidratación de fases seleccionadas. Para llevar a cabo los estudios estructurales se han empleado diversas técnicas como son: difracción de rayos-X de laboratorio (LXRPD, del inglés Laboratory X-Ray Powder Diffraction), de sincrotrón (SXRPD, del inglés Synchrotron X-Ray Powder Diffraction) y de neutrones (NPD, del inglés Neutron Powder Diffraction) a temperatura ambiente. También se ha utilizado termodifracción de rayos-X de laboratorio, calorimetría diferencial de barrido (DSC, del inglés Differential Scanning Calorimetry) y medidas de permitividad.

El uso de una fuente intensa de rayos X, como es la radiación sincrotrón acoplada con detectores ultrarrápidos es muy útil para hacer experimentos de difracción que permiten un análisis cuantitativo de fases durante las primeras edades de hidratación en cementos. Es por ello que esta técnica ha sido ampliamente usada para la caracterización de las pastas hidratadas.

En primer lugar, para el estudio de la forma β del silicato dicálcico, se preparó la disolución sólida con fórmula general, $\text{Ca}_2\text{Si}_{1-2x}\text{Al}_{2x}\text{O}_{4-x}\square_x$ (con $0 < x < 0.03$). Los materiales se caracterizaron mediante LXRPD y el método de Rietveld determinándose el límite de la serie cercano a $x=0.014$, la composición con $x=0.03$ presenta pequeñas cantidades de C_3A como impureza. La muestra $\text{Ca}_2\text{Si}_{0.972}\text{Al}_{0.028}\text{O}_{3.986}\square_{0.014}$, que contiene 99(1)% en peso de polimorfo β , se seleccionó para realizar una caracterización más completa. Las medidas de análisis térmico en atmosfera húmeda confirmaron que el aluminio se incorpora en la red de silicato dicálcico y estabiliza la forma β debido a que se reemplazan unidades silicato por unidades aluminato generándose vacantes de oxígeno. Es importante destacar que a diferencia de lo que ocurre en el dopaje con aluminio del silicato tricálcico, la sustitución de aluminio en los sitios del calcio y del silicio de forma simultánea, $\text{Ca}_{2-x}\text{Al}_x(\text{SiO}_4)_{1-x}(\text{AlO}_4)_x$, no se logra.

Posteriormente, se investigó el dopaje conjunto de B/Na en la fase de silicato dicálcico, confirmándose que la disolución sólida de fórmula general $\text{Ca}_{2-x}\text{Na}_x(\text{SiO}_4)_{1-x}(\text{BO}_3)_x$ existe para un amplio rango de valores de x , siendo la fase principal el polimorfo $\alpha'_H\text{-C}_2\text{S}$ (para $x \geq 0.10$). En este caso, el grupo borato es triangular plano, BO_3^{3-} . También se estudió la serie $\text{Ca}_{2-x}\text{B}_x(\text{SiO}_4)_{1-x}(\text{BO}_4)_x$, en la que los grupos SiO_4^{4-} se reemplazan por unidades de BO_4^{5-} y para compensar las cargas, los cationes calcio se sustituyen por boro. Esta disolución sólida conduce a la estabilización de grandes cantidades de fase α'_H . Esta serie no se estudió en profundidad debido a que nuestro interés se centra en la estabilización de este polimorfo con bórax para imitar condiciones industriales, además el borax se ha

usado anteriormente para activar cementos tipo BCSA. La naturaleza del anión borato se elucidó por espectroscopía infrarroja ya que las bandas que aparecen cercanas a 1000 cm^{-1} se corresponden con unidades BO_4^{5-} tetraédricas mientras que la de los grupos BO_3^{3-} plano-triangular aparecen en torno a $1150\text{-}1350\text{ cm}^{-1}$. La ausencia de cal libre, CaO, demuestra que la reacción es completa y que las disoluciones sólidas se forman correctamente. También se intentaron, aunque sin éxito, otras formulaciones nominales, p.ej. $\text{Ca}_{2-x/2}\text{O}_{x/2}(\text{SiO}_4)_{1-x}(\text{BO}_3)_x$, $\text{Ca}_2(\text{SiO}_4)_{1-x}(\text{BO}_3)_x\text{O}_{x/2}$ y $\text{Ca}_{2-3x}\text{B}_{2x}\text{Na}_x(\text{SiO}_4)_{1-x}(\text{BO}_4)_x$ para confirmar los anteriores mecanismos de sustitución.

La muestra $\alpha'_H\text{-Ca}_{1.85}\text{Na}_{0.15}(\text{SiO}_4)_{0.85}(\text{BO}_3)_{0.15}$ se seleccionó para estudiar la estructura cristalina. Esta elección se basó en que la muestra es muy cristalina y presenta un alto contenido en fase α'_H , en torno al 90% en peso. Se obtuvo una nueva descripción estructural con una celda unidad de $a=6.8432(2)\text{ \AA}$, $b=5.4555(1)\text{ \AA}$, $c=9.2346(2)\text{ \AA}$ y $V=344.76(2)\text{ \AA}^3$. La estructura cristalina revisada condujo a unos valores de desacuerdo bajos, $R_{\text{WP}}=6.5\%$ y $R_{\text{F}}(\alpha'_H\text{-C}_2\text{S})=2.4\%$. Con este nuevo modelo, se pueden conseguir mejores ajustes en cementos activados tipo BCSA y análisis mineralógicos de fases más exactos.

Para el caso de la ye'elimita, se han preparado dos muestras: una estequiométrica ($\text{Ca}_4\text{Al}_6\text{O}_{12}\text{SO}_4$) y otra dopada ($\text{Ca}_{3.8}\text{Na}_{0.2}\text{Al}_{5.6}\text{Fe}_{0.2}\text{Si}_{0.2}\text{O}_{12}\text{SO}_4$) para caracterizar los polimorfos ortorrómbico y cúbico, respectivamente. La ye'elimita estequiométrica sintetizada contenía pequeñas cantidades de $\text{Ca}_3\text{Al}_2\text{O}_6$, CaAl_2O_4 y $\text{Ca}_{12}\text{Al}_{14}\text{O}_{33}$ como impurezas. El estudio estructural se ha realizado mediante un afinamiento de Rietveld combinado de LXRPD y NPD, demostrándose que presenta simetría ortorrómbica y grupo especial Pcc2. Los valores finales obtenidos de la celda unidad son $a=13.0356(7)\text{ \AA}$, $b=13.0350(7)\text{ \AA}$ y $c=9.1677(2)\text{ \AA}$. Además, a través de cálculos atómicos se determinó que la simetría que más baja energía presenta es la Pcc2, lo cual está de acuerdo con los resultados experimentales obtenidos.

Ana María Cuesta García

En el caso de la ye'elimita dopada, $\text{Ca}_{3.8}\text{Na}_{0.2}\text{Al}_{5.6}\text{Fe}_{0.2}\text{Si}_{0.2}\text{O}_{12}\text{SO}_4$, se obtuvo una única fase cristalina, en este caso los dopantes se añadieron como Fe_2O_3 , Na_2CO_3 y SiO_2 . Es importante destacar que esta composición se eligió basándose en un clínker tipo BCSA previamente preparado en el cual ya se había estabilizado la forma pseudocúbica de la ye'elimita. El modelo estructural se basa en una simetría pseudocúbica con grupo espacial $\bar{I}43m$. El valor final de la celda unidad es $9.1974(7)$ Å. El comportamiento térmico de la muestra dopada fue clave para determinar que su simetría es pseudocúbica. Las medidas de DSC muestran una transición de fase reversible a 525°C , y los estudios de LXRPD a alta temperatura mostraron un estrechamiento de los picos de difracción a partir de 500°C , que está relacionado con el desorden de los aniones sulfato. Ambos resultados indican que la forma de la ye'elimita dopada a temperatura ambiente tiene que presentar una simetría menor que la cúbica, consecuentemente se le puede asignar una simetría pseudocúbica.

Los estudios termodifracométricos de la ye'elimita estequiométrica muestran una transición de fase desde la forma ortorrómbica a un polimorfo de mayor simetría (cúbico). Mediante DSC y medidas de permitividad se determinó que la transición reversible está centrada a 470°C . Además, se llevó a cabo un estudio estructural para las dos muestras de ye'elimita a 800°C . A esta temperatura las dos presentaron una simetría cúbica real.

Después de la caracterización de la ye'elimita, se llevó a cabo la síntesis y caracterización de la fase ferrito aluminato tetracálcico. Esta muestra se preparó obteniéndose un ensamblaje de fases de $98.1(1)$ % de C_4AF y $1.9(1)$ % de C_3A como impureza (porcentajes en peso). Debido a la alta calidad del ajuste obtenido por SXRPD se han optimizado los factores de ocupación de Fe/Al de la estructura obteniéndose $0.746(2)$ de ocupación de Fe en el sitio octaédrico y por lo tanto, $0.254(2)$ de ocupación de Fe en el sitio tetraédrico.

Las estructuras cristalinas de ambos polimorfos de silicato dicálcico y de la ye'elimita se han revisado para utilizarlas en el análisis cuantitativo de fases de cementos de sulfoaluminato por el método de Rietveld. Las estructuras publicadas presentadas en la tesis doctoral permiten un análisis mineralógico de fases más exacto para cementos comerciales de sulfoaluminato de calcio y BCSA ya que con ellas se obtienen valores de desacuerdo más bajos (R_F y R_{WP}) que cuando se utilizan las estructuras publicadas anteriormente.

Tras la caracterización inicial de las muestras anhidras de ye'elimita, ortorrómbica y pseudocúbica, se llevaron a cabo los estudios de hidratación. Un objetivo muy importante de la tesis es correlacionar el mecanismo de hidratación a edades tempranas con las prestaciones de los “ecocementos”. Se ha estudiado la influencia en la cinética y en el mecanismo de hidratación de diferentes relaciones agua/sólido y de la adición de fuentes de sulfato.

Los estudios de hidratación se han realizado usando LXRPD con la metodología del estándar externo (factor-G) y/o usando SXRPD con la metodología del estándar interno para determinar el ensamblaje de fases incluyendo el material amorfo (ACn, del inglés Amorphous and Crystalline non-quantified). La metodología del estándar interno nos da un valor total de ACn, el cual incluye la cantidad de agua libre (FW, del inglés Free Water). Por otro lado, la metodología del estándar externo se aplicó a muestras donde la hidratación se detuvo a determinadas edades (más adelante “muestras con la hidratación parada”), por tanto esto permite obtener los valores individuales de ACn. El valor de FW se determinó por comparación entre el valor de las pérdidas de peso de las muestras con la hidratación parada obtenido por análisis térmico diferencial y termogravimétrico (DTA-TG, del inglés Differential Thermal Analysis-ThermoGravimetric) y el valor de la cantidad total de agua añadida. Es importante destacar que los resultados obtenidos por el método del estándar interno están de acuerdo con los obtenidos a altas edades usando el método del estándar externo, mostrando una consistencia entre ambas metodologías que permite entender las

reacciones de hidratación en función del tiempo. Para complementar los datos obtenidos por XRPD también se han realizado estudios calorimétricos.

La preparación de la muestra es ligeramente distinta para cada metodología: i) las muestras que se usaron para los estudios de SXPDP se prepararon en capilares sellados con grasa y, ii) en el caso de los estudios de hidratación *ex-situ* mediante LXPDP, las pastas se prepararon en moldes sellados con forma de cilindros y se pararon después a determinadas edades. El grado de cristalinidad y de hidratación de fases del tipo AFm depende de la metodología de preparación. En el caso de la muestra en capilar sellado la cristalinidad es mayor que aquellas en las que se ha parado la hidratación.

La ye'elimita estequiométrica se estudió con distintas cantidades de agua para comprobar su influencia en el mecanismo de hidratación. Como cabe esperar a mayor cantidad de agua se intensifica la reactividad de la ye'elimita. El producto principal de hidratación a todas las edades ha sido AFm y AFt. Mayores relaciones agua/sólido favorecen la formación de mayores cantidades de AFm y desfavorece la de AFt. Desde el punto de vista del balance de masas se debe mantener la misma proporción AFm/AFt si la reacción es completa. Por lo tanto, se puede especular que mayores relaciones agua/sólido han conducido a una reacción casi completa.

Se ha determinado el papel del polimorfismo de la ye'elimita en los mecanismos de hidratación comparándose la reactividad de ambos polimorfos. La ye'elimita dopada (pseudocúbica) presenta una cinética de hidratación más rápida y se forma una cantidad mayor de AFt que en el caso de la ye'elimita estequiométrica (ortorrómbica) en las mismas condiciones experimentales. Los datos de calorimetría también confirman este comportamiento.

Los mecanismos de hidratación a edades tempranas de ambas ye'elimitas se han estudiado en presencia de una fuente de sulfato (yeso o anhidrita) usando SXPDP ya que se sabe que cuando hay suficiente sulfato en el medio se forma exclusivamente AFt. En este estudio se demostró que para una cantidad

determinada de yeso y agua, la única fase cristalina que se obtiene es el AFt, no encontrándose AFm a ninguna edad. Por otro lado, es importante tener en cuenta que en la hidratación de las muestras se debería formar una fase amorfa con fórmula general, $AH_3 \cdot nH_2O$, la cual se obtiene en la reacción de hidratación junto con AFt. La principal diferencia que se encuentra entre ambos polimorfos de la ye'elimita es que la cinética de hidratación de la estequiométrica es más rápida que la de la dopada a edades tempranas. Exactamente, a 14 h de hidratación reacciona un 100% de la ye'elimita estequiométrica mientras que solo lo hace un 85% de la dopada. Además, se ha estudiado el papel de la adición de anhidrita a edades tempranas para hacer la misma comparación que con la adición de yeso. En este caso, se encontró que el mecanismo de hidratación es muy similar para ambos polimorfos pero la cinética de reacción usando anhidrita es mucho más lenta debido a su menor solubilidad.

La hidratación de los cementos se puede resumir como un proceso de disolución y cristalización/precipitación de diferentes fases. Aunque la ye'elimita es la principal responsable del mecanismo de hidratación de los cementos tipo CSA, es importante estudiar su hidratación en combinación con otras fases.

En primer lugar, se ha estudiado la hidratación en combinación con C_4AF y yeso usando *in-situ* SXRPD. En el caso de la ye'elimita estequiométrica, a primeras horas se formó AFt y después, cuando el yeso se consumió totalmente empezó a precipitar AFm. Además, se estudió también esta ye'elimita con diferentes cantidades de agua/sólido para poder determinar la influencia del agua. Se obtuvo que mayores cantidades de agua favorecen la precipitación de AFm y aceleran la cinética de hidratación para la ye'elimita estequiométrica. Como se explicó anteriormente, los valores de ACn para estas muestras se obtuvieron por SXRPD. En todos los casos, estos valores disminuyeron ligeramente con el tiempo durante la cristalización del AFt y se incrementaron en el momento que el AFm empezó a aparecer.

Ana María Cuesta García

Este mismo estudio se ha realizado en ausencia de yeso. Se ha comprobado que el único producto de hidratación es AFm. Se demuestra que el yeso es el principal responsable de la formación del AFt.

En el caso de la hidratación de la ye'elimita dopada en presencia de C_4AF y yeso, la principal diferencia que se encontró fue que a 46 horas esta muestra formaba mucha más cantidad de AFt (28.6(1) % en peso) que en el caso de la ye'elimita estequiométrica (15.5(3) % en peso). Debido a estos resultados se ha probado que las diferencias en la hidratación entre ambos polimorfos se intensifican cuando hay ferrito aluminato tetracálcico en el medio. Además, mediante microscopía electrónica de barrido acoplada con espectroscopia de energía dispersiva (SEM-EDS, del inglés Scanning Electron Microscopy- Energy Dispersive Spectroscopy) se ha comprobado que el hierro que pertenece al C_4AF no se incorpora de forma apreciable en las fases cristalinas hidratadas (AFm y AFt). Por lo tanto, se debe haber formado una fase amorfa con alto contenido en hierro.

Por último, se ha estudiado el papel de los polimorfos de la ye'elimita y del silicato dicálcico en sus mecanismos de hidratación mediante LXRPD. Se cree que estos estudios ayudaran a descifrar los mecanismos de hidratación de cementos tipo BCSA. Los cementos BCSA que contienen el polimorfo α'_H-C_2S desarrollan mayores resistencias mecánicas que aquellos cementos que contienen el polimorfo $\beta-C_2S$. Este comportamiento se propuso anteriormente pero no se demostró directamente, por tanto, es esencial establecer el papel de ambos polimorfos de la ye'elimita en estas muestras.

En la tesis se han estudiado todas las combinaciones entre el silicato dicálcico y la ye'elimita hasta edades de 6 meses. Los datos de difracción de polvo a 28 días muestran pequeñas diferencias. La muestra que contenía α'_H-C_2S y ye'elimita dopada presentó un mayor grado de hidratación y cantidad de stratlingita a esa edad. Sin embargo, se esperan aun mayores diferencias a largas

edades. En las condiciones experimentales estudiadas, ambos polimorfos de la ye'elimita formaron principalmente etringita. No obstante, se ha demostrado que el grado de hidratación del polimorfo α'_H del silicato dicálcico es mucho mayor que el del polimorfo β en el rango de tiempo estudiado. A los 6 meses, el α'_H -C₂S se disolvió totalmente, en cambio, se encontraron grandes cantidades de β -C₂S sin reaccionar en todas las muestras. Es importante destacar que no hubo diferencias importantes entre la ye'elimita dopada y la estequiométrica debido a que estos estudios se hicieron a partir de 7 días, y la hidratación de la ye'elimita ocurre mucho antes (en torno a 8 horas).

Se ha determinado el comportamiento de hidratación de la fase C₄AF en ausencia y presencia de yeso. En el caso de la hidratación del C₄AF en ausencia de yeso se formó una fase tipo hidrogranate con fórmula C₃A_{0.845}F_{0.155}H₆. Esta fase hidratada se estudió por SXRPD de alta resolución y microscopía electrónica de transmisión (TEM, del inglés Transmission Electron Microscopy) combinada con EDS para confirmar que el hierro se incorpora a la fase tipo hidrogranate, C₃A_{0.845}F_{0.155}H₆. Se obtuvo una descripción estructural muy precisa con una celda unidad de $a=12.60315(4) \text{ \AA}$ y $V=2001.88(2) \text{ \AA}^3$. La estructura cristalina revisada condujo a unos valores de desacuerdo de $R_{WP}=8.1\%$ y $R_F=4.8\%$.

La hidratación del C₄AF en presencia de yeso tuvo un comportamiento distinto. En este caso se formó una mezcla de AFm y AFt. En primer lugar, precipitó el AFt junto con hidróxido de aluminio amorfo y una vez que el yeso se disolvió totalmente empezó a precipitar el AFm. Los datos de calorimetría muestran una señal ancha que corresponde a la formación del AFm. De nuevo, los estudios de SEM-EDS se han utilizado para corroborar que las fases formadas, AFt y AFm, en este caso, sí incorporan hierro en su estructura.

Se ha comprobado que en presencia de ye'elimita, la hidratación del ferrito aluminato tetracalcico se inhibe. Concretamente, la ye'elimita dopada tiene un

Ana María Cuesta García

efecto de inhibición mucho más fuerte sobre el C_4AF haciendo que el principal producto de hidratación que se forma sea mayoritariamente AFt en lugar de AFm.

Actualmente se están llevando a cabo nuevas investigaciones con técnicas complementarias a las usadas en esta tesis para la caracterización de las fases hidratadas puras y para el estudio de los mecanismos de hidratación. En primer lugar, se ha usado ptycografía-tomografía de rayos-X computerizada (PXCT, del inglés ptychographic X-ray computed tomography) para estudiar la hidratación de muestras de ye'elimita. Se han investigado diferentes pastas con distintas edades de hidratación en la línea cSAXS del sincrotrón Swiss Light Source (Villigen, Suiza). El objetivo principal es caracterizar la microestructura de las pastas y cuantificar la densidad electrónica y másica de las fases presentes. Posteriormente, estas densidades experimentales se comparan con las teóricas lo que permite identificar las fases presentes. Se han obtenido acuerdos muy buenos comparándolos con los valores teóricos. Además, para obtener mejores resultados se estudiaron los histogramas seleccionando una región de interés para cada muestra eliminando la zona del capilar.

Por último, se ha realizado un experimento de SXRPD de alta presión. La muestras hidratadas se colocaron en celdas de diamante (DAC, del inglés Diamond anvil cell) para determinar su comportamiento bajo presión. Esta técnica permite determinar el módulo de compresibilidad y la estabilidad de estas fases del cemento. Este estudio a presión se realizó para diversas muestras, destacando la muestra de hidrogranate con hierro, $C_3A_{0.845}F_{0.155}H_6$, para la cual se obtuvo un módulo de compresibilidad de 54(2) GPa.

1. Introduction

1. Introduction to cements

OPC is the most used building material, which has become the dominant binder used in the preparation of concrete for construction applications. OPC is now prepared by heating a mixture of limestone and clay, or other materials of similar composition and sufficient reactivity, at a temperature of $\sim 1450^{\circ}\text{C}$ (Taylor 1997). Partial fusion occurs, and nodules of clinker are produced. The cement is finally prepared by grinding the clinker and mixing it with finely ground calcium sulfate, which will control the setting time. It is commonly described as gypsum, but this may be partly or wholly replaced by other forms of calcium sulfate. Some specifications allow the addition of other materials at the grinding stage. The main supplementary cementitious materials are fly ash, ground granulated blast furnace slag, silica fume, calcined clays and natural/industrial pozzolans. These materials are commonly blended with clinker to produce the different Portland cement types or used as a replacement for a portion of clinker in concrete mixtures (Juenger and Siddique 2015).

1.1. Ye'elinite-containing cements

Since 1970s commercial ye'elinite-containing cements known as CSA cements have been manufactured and used on a large scale in China (Zhang et al. 1999). CSA cements are/were known as “the third series cements of China” (the first series being OPC and the second series being CAC) with special applications such as high strength developments at early-ages used in precast concrete and at moderate curing temperatures (Glasser and Zhang 2001; Quillin 2001), self-stressing materials (Péra and Ambroise 2004; Georgin et al. 2008), with expansive properties for shrinkage compensating concrete (Klein 1963; Chen et al. 2012) or for radioactive element encapsulation in high-density cement pastes (Zhou et al. 2006; Cau Dit Coumes et al. 2009; Sun et al. 2011).

Ana María Cuesta García

These binders may have quite variable compositions, but all of them contain high amounts of ye'elinite (C_4A_3S), also called Klein's salt, calcium sulfoaluminate or tetracalcium trialuminate sulfate (Odler 2000). So, the main phases are C_4A_3S and C_2S and also they have minor amount of phases such as CA, C_4AF , CS, CSH_2 (Sahu and Majling 1993) and they are used due to their special applications. The properties and applications of this type of binder are strongly influenced by many factors: i) chemical and mineralogical composition of the clinker; ii) sulfate source (amount and type); iii) water to cement ratio (w/c); or iv) blending with other binders, for instance, OPC.

The interest in ye'elinite-containing cements is increasing as they are eco-friendly materials because their manufacture process releases less CO_2 into atmosphere than ordinary Portland cement (Gartner 2004; Barcelo et al. 2014; Gartner and Hirao 2015). This reduction depends on the composition, but it can release up to 40% less CO_2 emissions. This is described below.

These eco-cements can be classified according to the content of their main crystalline phase. Aranda and De la Torre (2013) proposed to unify the terminology used for these cements. However, only the most representative cements for this work are described below:

(i) Calcium Sulfo-Aluminate (CSA) cements which refer to those with high C_4A_3S contents, are prepared from CSA clinkers containing 50-80 wt% of C_4A_3S (Sahu and Majling 1993; Zhang et al. 1999; Older 2000; Glasser and Zhang 2001). These clinkers may also have minor phases such as C_2S , CT, C_4AF , CS and others. The calcium sulfate addition is very important as it may profoundly affect the properties of the resulting binder (Winnefeld and Barlag 2010; Berger et al. 2011; Chen et al. 2012; Bizzozero et al. 2014; García-Maté et al. 2015).

The calcium sulfate source and content have to be customized for a given application. These cements can be used alone or in combination with other cements to provide an improved early resistance (they can show mechanical strengths

1. Introduction

higher than 80 MPa at 7 days), low shrinkage, high impermeability, and a strong resistance to sulfate attack. Unfortunately due to the high amount of expensive aluminum source needed in their productions, CSA clinkers cannot replace OPC in massive constructions. Al_2O_3 and SO_3 contents in CSA usually range between 30-40 and 8-14 wt%, respectively.

(ii) Belite Calcium Sulfo-Aluminate (BCSA) term is reserved to the cements arising from clinkers containing C_2S (belite) as the main phase (40-50 wt %) and intermediate $\text{C}_4\text{A}_3\text{S}$ contents (20-30wt%). Due to the high amount of C_2S , these materials showed mechanical strengths up to 50 MPa at 28 days.

The most common formulation of BCSA clinkers consists on $\beta\text{-C}_2\text{S}$, $\text{C}_4\text{A}_3\text{S}$ and C_4AF (Janotka and Krajei 1999; Adolfsson et al. 2007; Janotka et al. 2007; Cuberos et al. 2010) and are also termed iron-rich BCSA (**BCSAF**). They are produced at temperatures close to 1250°C (Morin et al. 2011). To avoid confusion, it must be highlighted that BCSAF clinkers do not belong to “the third series cement of China” (CSA), which have much higher amounts of ye'elite. These cements are being studied with the final aim of replacing OPC as the aluminum demand is much smaller. Al_2O_3 and SO_3 contents in BCSAF usually range between 14-17 and 3.5-4.5 wt%, respectively (Aranda and De la Torre 2013).

In the last decade, the research in the preparation of BCSAF clinkers has increased considerably (Cuberos et al. 2011; Chen et al. 2011; De la Torre et al. 2011a,b; Morin et al. 2011; Álvarez-Pinazo et al. 2012). A HT-SXRPD study of a BCSAF clinker activated with boron was performed to clarify the formation mechanism of these types of clinkers (De la Torre et al. 2011a). The presence of minor elements such as alkaline oxide or boron in raw mixes decreases clinkering temperatures, as well as polymorphic transformation. For instance, the addition of 2 wt% of B_2O_3 to the raw materials decreased the minimum clinkering temperature, from 1300°C down to 1150°C (De la Torre et al. 2011a,b). In addition, the use of foreign elements promotes the decrease of the polymorphic transformation temperatures

Ana María Cuesta García

and produces the stabilization $\alpha'_H\text{-C}_2\text{S}$ polymorph, which yields higher mechanical strength developments. Active BCSAF materials were successfully prepared in the laboratory (Cuberos et al. 2010; Aranda et al. 2011; Álvarez-Pinazo et al. 2012; Ma et al. 2014). The main goal in these works, was the quantitative demonstration of $\alpha'_H\text{-C}_2\text{S}$ polymorph stabilization by borax addition to BCSAF clinkers, and cements containing α'_H -form of belite developed higher mechanical strengths than those without this polymorph. Moreover, Álvarez-Pinazo et al. (2014) reported an in-situ synchrotron X-ray powder diffraction study for the first hours of hydration of these materials concluding that the presence of the amount of ettringite and amorphous aluminum hydroxide strongly influences C_2S hydration. Concretely, non-active BCSAF which contains $\beta\text{-C}_2\text{S}$ and orthorhombic $\text{C}_4\text{A}_3\text{S}$ reacts at a higher pace than active BCSAF (with α'_H and pseudocubic $\text{C}_4\text{A}_3\text{S}$) to give stratlingite. However, active BCSAF, which contains $\alpha'_H\text{-C}_2\text{S}$, reacts a bit slower but it developed higher mechanical strengths.

A recent study (Bullerjahn et al., 2014) proved that iron-rich BCSA contains ye'elimite with significant amounts of iron stabilizing the cubic form and enhancing its hydration rates. Moreover, they stated that ternesite ($\text{C}_5\text{S}_2\text{S}$) was formed under certain clinkering conditions and it was found to be hydraulically active. This phase is only active in the presence of AH_3 .

CO₂ emission reduction in the manufacture of ye'elimite-containing cements

These types of cements are interesting because they release less CO₂ in their manufacture when compared to OPC production. The carbon dioxide emissions can be classified in two main categories: those coming from raw materials and those from the operation processes. Table 1.1. gives CO₂ emissions related to the production of cement components calculated according to the stoichiometry of chemical reactions, for example:



Reaction [1.1] is the main one in the OPC production. Therefore, the production of one ton of OPC clinker composed of 65 wt% of C_3S , 15 wt% of C_2S , 10 wt% of C_3A and 10 wt% of C_4AF released 0.54 tons of carbon dioxide. However one ton of CSA clinker composed by 65 wt% of $\text{C}_4\text{A}_3\text{S}$, 20 wt% of C_2S , 9 wt% of C_3S and 6 wt% C_4AF releases 0.26 tons of CO_2 (Figure 1.1). In this case the most important reaction is:



that gives CO_2 emissions from the formation of ye'elinite phase. Consequently, a reduction in carbon dioxide emissions of 49% is calculated due to raw material decomposition.

Table 1.1. CO_2 emissions per ton of component produced, considering CaCO_3 as calcium source.

Component	t CO_2 /t of component
C_3S	0.58
C_2S	0.51
C_3A	0.49
C_4AF	0.36
$\text{C}_4\text{A}_3\text{S}$	0.22

The second CO_2 emissions category comes from operation processes. However, this is not an easy task as it is directly related to the type of processing equipment and the specific chosen fuel. Gartner in 2004 published an estimation of 0.28 t of CO_2 per ton of clinker produced assuming that good quality of bituminous coal is used and taking into account energy efficiency of modern kilns. However, McCaffrey (2002) states that 0.34 t of CO_2 per ton of clinker produced is released into atmosphere due to the burning of coal in the kiln. The reduction in CO_2

emissions coming from the burning of the fuel can be achieved by different strategies (Gartner 2004; Juenger et al. 2011) including the reduction of clinkering temperature. This is the case of CSA clinker production where the operating temperature can be reduced down to $\sim 1250^{\circ}\text{C}$, $\sim 200^{\circ}\text{C}$ lower than that of OPC production (Phair 2006), with a concomitant reduction of up to approximately 0.04 t of CO_2 per ton of CSA clinker produced. Moreover, CO_2 emissions derived from electricity consumption for grinding in OPC clinker production are not negligible. In fact, 0.09 t of CO_2 per ton of clinker produced are calculated, assuming that fossil fuels are used to produce the electricity (McCaffrey 2002). Since the lower firing temperatures lead to a CSA clinker which is generally easier to be ground, hence energy savings also occur in the grinding of CSA clinker compared to OPC. Therefore, reduction on the electricity consumption yields a depletion of up to 0.02 t of CO_2 emissions.

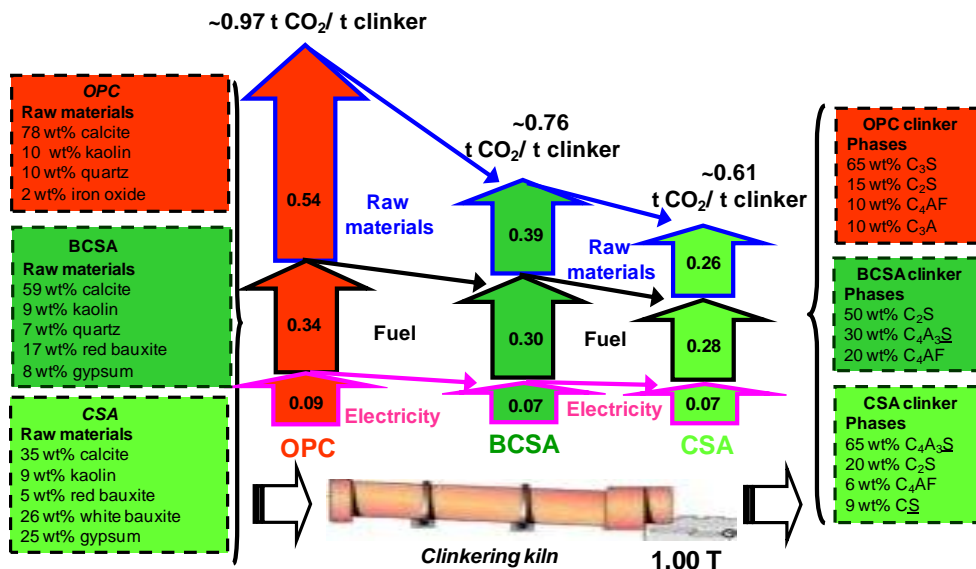


Figure 1.1. Comparison of OPC, BCSA and CSA CO₂ footprint.

Considering all together, the production of one ton of OPC clinker releases a maximum of 0.97 tons of CO₂, however the production of one ton of CSA clinker leads to a reduction, which will depend on the composition, but it can range

between 0.25 to 0.40 tons of CO₂. With the CSA composition shown in Figure 1.1, a reduction of 0.36 tons of CO₂ per ton of clinker is obtained which means a relative reduction of 37% of the CO₂ emission footprint when compared to OPC manufacturing.

The same calculation can be done for a BCSA clinker (50 wt% of C₂S, 30 wt% of C₄A₃S, and 20 wt% C₄AF), Figure 1.1. CO₂ emissions released during clinkering of 1 ton of BCSA are 0.39 tons. It implies a reduction of 0.15 tons of CO₂ for BCSA due to raw material decomposition. In BCSA clinkers, the operating temperature can be reduced down to 100°C with a concomitant reduction of up to 0.04 tons of CO₂ per ton of BCSA clinker produced. Moreover, as in CSA cements, the lower firing temperatures needed for BCSA clinkering make it easier to be ground, hence it yields a depletion of up to 0.02 t of CO₂ emissions. Considering all emissions together, the production of one ton of BCSA clinker leads to a reduction of ~22%, which will depend on the composition.

1.2. Pure phases of interest in calcium sulfoaluminate cements

1.2.1. Dicalcium silicate (Ca₂SiO₄, C₂S)

Dicalcium silicate with some substituting elements, belite in cement nomenclature, is the major constituent of Belite Portland and BCSA cements (with a weight percentage of about 60 wt%). Furthermore, belite is also the second most abundant constituent of OPC and CSA cements.

1.2.1.1. Dicalcium silicate chemical compositions and structures

Stoichiometric C_2S has five polymorphs (Mumme et al. 1995) γ , β , α'_L , α'_H and α , on heating, with β - C_2S being the form that commonly prevails in OPC and in BCSA without activation as it is stabilized by elements substitution(s). Its temperature evolution is shown in Figure 1.2. The structures of the polymorphs belong to a large family typified by that of glaserite, $K_3Na(SO_4)_2$ (Taylor, 1997) except the γ -phase, which is essentially nonreactive with water and stable at ambient temperature and it crystallizes in an orthorhombic olivine-type structure (Smith et al. 1965; Czaya 1971; Udagawa et al. 1980). The β -form is a metastable monoclinic phase at room temperature (Midgley 1952; Jost et al. 1977). This metastability has also been confirmed by the results of a structural simulation of possible hypothetical Ca_2SiO_4 phases (Yamnova et al. 2011). α'_L and α'_H orthorhombic phases are stable at higher temperatures (Susuki and Yamaguchi 1968). The α'_L -polymorph is generally considered a superstructure of the α'_H and it has been reported two possibilities for indexing: doubling the a and c parameters (Barnes et al. 1980) or tripling the b parameter (Saalfeld 1975; Jelenic and Bezjak 1982; Il'inets and Bikbau 1990). Finally, the highest-temperature polymorph is the α -form whose structure is still under discussion (Bredig 1950). It is noteworthy, that $\beta \rightarrow \gamma$ polymorphic transformation on cooling is disruptive with an important change in volume. The density of the γ -modification of 2.94 g/cm^3 is about 10% lower than the density of the β -modification of 3.20 g/cm^3 . As a result of this volume change an originally compact burning product cracks and rapidly disintegrates into dust (“dusting”) as soon as the temperature during cooling falls below about 500°C (Locher 2006) if the β -phase has not been stabilized.

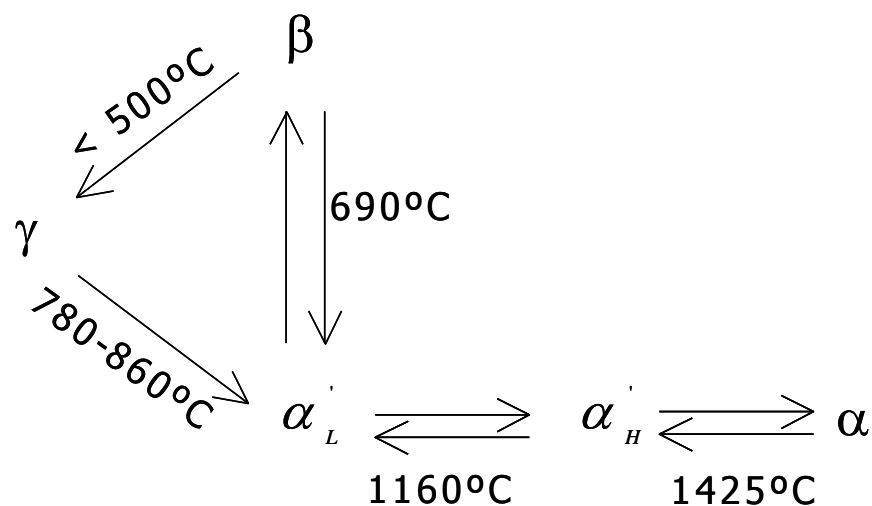


Figure 1.2. Dicalcium silicate polymorphic transformations with temperature.

The structures of all polymorphs are built from Ca^{2+} and SiO_4^{4-} ions. The arrangements of these ions are closely similar in the α , α'_H , α'_L and β polymorphs, but that in $\gamma\text{-C}_2\text{S}$ is somewhat different. The crystal structure of $\gamma\text{-C}_2\text{S}$ has two calciums in regular six-coordinated oxygen environments. Meanwhile, the crystal structure of $\beta\text{-C}_2\text{S}$ has two calciums surrounded by eight oxygens in distorted environments. Furthermore, the crystal structures of α'_H - and α - polymorphs have calcium cations in both eight and nine irregular coordinations (Midgley 1952; Smith et al. 1965; Regourd et al. 1968; Czaya 1971; Ghosh et al. 1979; Udagawa et al. 1980). It is worth noting that there are experimental evidences that an increase of the calcium coordination number seems to enhance the water reactivity (Kim and Hong 2004). Table 1.2 shows the crystallographic information of the corresponding dicalcium silicate polymorphs.

Table 1.2. Crystallographic data for dicalcium silicate “polymorphs” including temperature of stabilization or stabilizer.

Polymorph	Space group	Unit cell parameters			$\beta(^{\circ})$	V/Z (\AA^3)	T($^{\circ}\text{C}$)/ Stabilizer	ICSD
		a (\AA)	b (\AA)	c (\AA)				
α	P6 ₃ /mmc ^a	5.420	5.420	7.027	90.0	89.4	-	81099
	P6 ₃ /mmc ^b	5.532(9)	5.532(9)	7.327(11)	90.0	97.1	1545/-	82998
	P-3m1 ^b	5.532(9)	5.532(9)	7.327(11)	90.0	97.1	1545/-	82999
α' _H	Pnma ^a	6.7673(4)	5.5191(4)	9.3031(6)	90.0	86.9	-/5% (molar) Ca ₃ (PO ₄) ₂	81097
	Pnma ^b	6.871(0)	5.601(0)	9.556(1)	90.0	92.0	1250/-	82997
	Pmnb ^c	5.647(1)	7.037(1)	9.644(2)	90.0	95.8	-/Ca _{1.8} Sr _{0.2} SiO ₄	49662
α' _L	Pna2 ₁ ^b	20.527(2)	9.496(1)	5.590(1)	90.0	90.8	1060/-	82996
	Pna2 ₁ ^d	20.863(2)	9.5000(8)	5.6005(5)	90.0	92.5	-/ Ca _{0.84} Sr _{1.16} SiO ₄	39203
	P2 ₁ cn ^e	5.566	9.355	20.569	90.0	89.3	-	39100
β	P2 ₁ /n ^a	5.512(0)	6.758(0)	9.314(0)	94.6	86.5	-/0.5 wt% Cr ₂ O ₃	81096
	P2 ₁ /n ^f	5.48(2)	6.76(2)	9.28(2)	85.5	85.7	-	24640
	P2 ₁ /n ^g	5.502(1)	6.745(1)	9.297(1)	94.6	86.0	-	963
γ	Pbnm ^a	5.082(0)	11.224(0)	6.764(0)	90.0	96.5	-	81095
	Pbnm ^h	5.081(2)	11.224(5)	6.778(10)	90.0	96.6	-	200707

(a) Mumme et al. 1995; (b) Mumme et al. 1996; (c) Catti et al. 1984; (d) Il'inets and Bikbau 1990; (e) Udagawa et al. 1979; (f) Midgley 1952; (g) Jost et al. 1977 (h) Udagawa et al. 1980.

Physical and chemical properties of phases can be altered by introducing within the defects or strains crystalline structures. The different type of defects can be introduced during the material preparation by the formation of solid solutions or by specific thermal treatments (Fukuda and Ito 1999). Moreover, these defects can even stabilize high-temperature forms of C₂S at room temperature (Ghosh et al. 1979; Nettleship et al. 1992). Depending on the nature and concentration of the foreign substance or mixture it is possible to selectively produce certain modifications. There are many studies concerning the chemical-stabilization of β -C₂S by foreign ions such as SO₃, Cr₂O₃, Na₂O, K₂O, BaO, MnO₂ and Al₂O₃ (Pritts and Daugherty 1976; Kantro and Weise 1979; Matkovic et al. 1981; Fierens and Tirlocq 1983; Ziemer et al. 1984; Benarchid et al. 2004; Zhao et al. 2013). Also, the presence of Fe₂O₃ can stabilize the β polymorph by sol-gel method using microwave and conventional heating (Gajbhiye and Singh 2010). The stabilization

1. Introduction

of α' -forms by introduction of foreign oxides, such as MgO, P₂O₅, K₂O, BaO and SO₃ has also been studied (Bensted 1979; Fukuda et al. 2001; Park 2001; Zhao et al. 2013). These works stated that hydraulic properties were increased when compared to the materials without foreign ions. B₂O₃ has also been studied in order to stabilize β and α' -forms at room temperature (Jelenic et al. 1978; Wesselsky and Jensen 2009). Some authors (Park 2001; Kim and Hong 2004; Wesselsky and Jensen 2009) have demonstrated that the effectiveness of addition of B₂O₃, with no other co-dopants, for stabilizing the α' -forms, is poor. On the other hand, the addition of a combination of dopants, for instance B₂O₃ and Na₂O, succeeds to stabilize α' -C₂S (Wesselsky and Jensen 2009) although these authors did not state which α' -form, α'_L or α'_H , was stabilized. Moreover, previous studies reported that the stabilization of α' -belite forms in a cement matrix can be attained by introducing minor elements, such as alkaline oxide, boron or phosphor, in raw materials (Morsli et al. 2007a,b; Li et al. 2007; Wesselsky and Jensen 2009; Cuberos et al. 2010; Morin et al. 2011; Álvarez-Pinazo et al. 2012).

Figure 1.3 shows the simulated laboratory X-ray powder diffractograms of different C₂S polymorphs. The stabilization of the high temperature polymorph is due to both ionic substitutions and quenching. Moreover, Remy and Andrault (1997) established new formulas which represent the variation of molar volume as a function of temperature for the dicalcium silicate polymorphs (see Table 1.3).

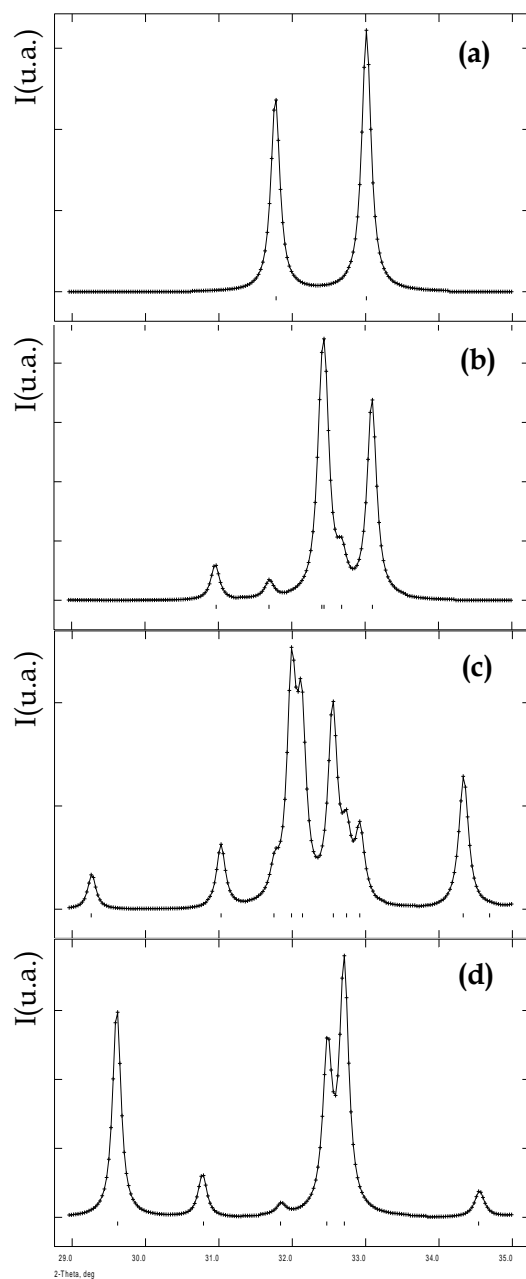


Figure 1.3. Range from 29 to 35° (2θ $\text{CuK}\alpha$) of the theoretical diffractograms at RT of: (a) $\alpha\text{-C}_2\text{S}$ (Mumme et al. 1995), (b) $\alpha'\text{-C}_2\text{S}$ (Mumme et al. 1996), (c) $\beta\text{-C}_2\text{S}$ (Mumme et al. 1995) y (d) $\gamma\text{-C}_2\text{S}$ (Udagawa et al. 1980).

Table 1.3. Molar volume data as a function of temperature for dicalcium silicate.

Polymorphs	$V_{\text{mol}} (\text{cm}^3) = f(T(^{\circ}\text{C}))$	$\Delta T (^{\circ}\text{C})$
γ	$58.085 + 0.00137(T) + 5.205 \times 10^{-7}(T)^2$	25-800
β	$51.827 + 0.00191(T) + 4.527 \times 10^{-7}(T)^2$	25-700
α'_{L}	$51.212 + 0.00326(T) + 1.377 \times 10^{-7}(T)^2$	800-1100
α'_{H}	$44.842 + 0.01466(T) - 4.899 \times 10^{-6}(T)^2$	1200-1420
α	$51.117 + 0.00466(T)$	1500 -1700

The belite grains in Portland cement clinkers frequently show complex striated structures. These have been studied over a long period by workers using optical microscopy; Yamaguchi and Takagi(1969) and Ono et al. (1969) who also used XRPD and other methods, gave the first substantially complete interpretation.

A very common type of belite grain in production clinkers, called Type I belite, is rounded, typically 20-40 μm in mean dimension, and shows at least two sets of parallel striations (Taylor 1997). Type I belite grains are those which have crystallized from the liquid at temperatures above 1420 $^{\circ}\text{C}$. The primary striations arise on cooling through the α to α'_{H} transition, in which the symmetry decreases from hexagonal to orthorhombic, each set of these striations is representing a different orientation of the α'_{H} structure. The transition to α'_{L} -C₂S that occurs on further cooling does not increase the number of orientations, but that from α'_{L} to β , in which the symmetry falls to monoclinic, causes each orientation to split into two (Figure 1.4.a)

Type II belites are irregular grains with one set of distinct parallel striations (lamellae). This is not a common variety in normal clinker. Parallel striations in Type II belite from the α' to β transformation are polysynthetic twins, observed in clinkers produced at a very low temperature or cooled very slowly (Ono 1995), see Figure 1.4.b.

Type III belite, which does not present lamellae, is uncommon in normal plant clinkers and is a merely single crystal with a uniform internal microstructure (Campbell 1999).

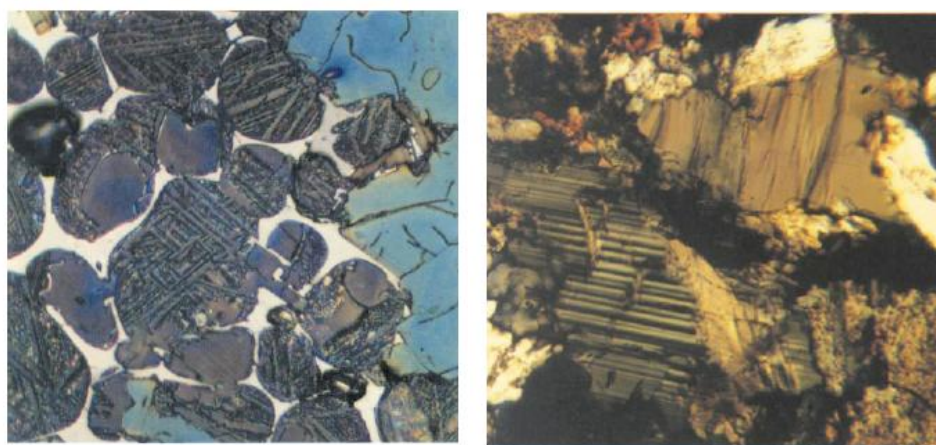


Figure 1.4. a) Type I belite (Insley 1936). Belite crystals exhibit relatively large areas which are either nonlamellar or show a single set of parallel lamellae b) Type II belite (Insley 1936). Polysynthetically twinned belite in lower left and slightly splintery gamma belite (upper right) in matrix of coarsely microcrystalline ferrite and aluminates (Campbell (1999)).

1.2.1.2. Hydration mechanisms of dicalcium silicate

The C_2S hydration is of special interest in BCSA. However, the hydration kinetic is slow when compared to other phases, i.e. ye'elinite. Some efforts are being performed to enhance the hydration kinetic, for instance, by adding minor elements during clinkering to obtain high temperature polymorphs of C_2S (Gartner and Li 2006; Li et al. 2007; Cuberos et al. 2010; Álvarez-Pinazo et al. 2012). Thus, α -forms of belite are considered more reactive than β - C_2S . The way the polymorphs are stabilized can have a significant influence on its reactivity (Gartner et al. 2002). Jost and Ziemer (1984) argue that the sharing faces of CaO_x polyhedral is an important feature controlling reactivity. Both α' and β -forms have distorted CaO_7 polyhedra, while γ -polymorph has a relatively symmetrical closed-

1. Introduction

packed CaO_6 octahedra which do not share faces (Jost and Ziemer 1984). Nevertheless, the hydration reaction could be the same independently of the rate of reaction of α - and β - polymorphs, where calcium silicate hydrate gel and portlandite are formed.



Calcium silicate hydrates (C_ySH_x) are produced with a crystalline order which, according to X-ray diffraction investigations, is very low. They are extremely fine-grained, so they are also designated like a gel. The hydration of belite to form the amorphous gel C_ySH_x and portlandite corresponds to reaction [1.3]. In the C-S-H, the Ca/Si molar ratio lies between 1.2 and 2.3 with an average value of about 1.75 (Taylor 1986; Richardson 1999; Scrivener 2015). The inner C-S-H is produced as a dense mass at the place of the original cement grain. The outer C-S-H forms fibers in the water-filled interstitial spaces between the cement grains. The outer C-S-H is richer in CaO than the inner gel and also contains more amounts of Al_2O_3 , K_2O and SO_3 (Taplin 1959; Rodgers and Aldrige 1977). However, only few authors have found the presence of portlandite and C-S-H in their hydration studies, as reaction 1.3 shows (El-Didamony et al. 2012).

It is important to highlight that if belite coexists with aluminum rich amorphous hydrates ($\text{AH}_3 \cdot n\text{H}_2\text{O}$), the formation of stratlingite (AFm-type) will be favored (Palou et al. 2005; Cuberos et al. 2010; Gartner and Macphee 2011; Álvarez-Pinazo et al. 2013).



Reaction [1.4] consumes the amorphous AH_3 formed by the hydration reactions of aluminum-rich phases. The presence of stratlingite has been

Ana María Cuesta García

confirmed, for example, in BCSAF and CSA pastes by XRPD and DTA techniques by numerous independent investigations (Cuberos et al. 2010; Aranda et al. 2011; Morin et al. 2011; Álvarez-Pinazo et al. 2013; Ioannou et al. 2014).

Other reactions need to be taken into account. Some studies have confirmed the presence of katoite phases (see section 1.2.6), also known as siliceous hydrogarnet (Taylor 1997). It can be formed according to the following chemical equation [1.5].



Reaction [1.5] requires the formation of portlandite, which is not detected by XRPD or DTA, through the consumption of ferrite. Consequently, it is speculated that this portlandite may be consumed by stratlingite, producing larger quantities of katoite, see reaction [1.6]:



1.2.2. Ye'elimite ($\text{Ca}_4[\text{Al}_6\text{O}_{12}]\text{SO}_4$, $\text{C}_4\text{A}_3\text{S}$)

Ye'elimite was introduced as a cementitious phase in the 1960s, when it was patented by Alexander Klein (Klein 1963) as an expansive or shrinkage compensating addition to cementitious binders ("Klein compound"). The interest in the ye'elimite structure (Klein's salt or tetracalcium trialuminate sulfate ($\text{C}_4\text{A}_3\text{S}$)) has recently increased because it is the major component in calcium sulfoaluminate cements, CSA, (Odler 2000; García-Maté et al. 2012, 2013; Telesca et al. 2014), and the second most relevant phase in sulfobelite cements, BCSA, (~25 wt%) (Cuberos et al. 2010; Morin et al. 2011; Álvarez-Pinazo et al. 2013; Bullerjahn et al. 2014).

1.2.2.1. Ye'elimité chemical compositions and structures

Ye'elimité, $\text{Ca}_4[\text{Al}_6\text{O}_{12}]\text{SO}_4$, crystallizes in a sodalite type structure which has a tetrahedral framework and it is built from all-corner-connected tetrahedra. Sodalites of the general composition $\text{M}_4[\text{T}_6\text{O}_{12}]\text{X}$ have been known for many years as both naturally-occurring minerals and as synthetic compounds (Hurlbut and Klein 1985). This general formula refers to a structure that is (ideally) a body-centered cubic unit cell with a lattice parameter of 9 Å and where M is a relatively low-charged caged cation such as Na^+ , Ca^{2+} or Sr^{2+} (Depmeier 1988); T occupies tetrahedral site(s) and is typically Si or Al; and X is the caged anion which is either spherical (in the case of Cl^-) or tetrahedral (in the case of SO_4^{2-} , WO_4^{2-} , and CrO_4^{2-}).

Therefore, stoichiometric ye'elimité is a tectoaluminosilicate sodalite with $\text{M}=\text{Ca}$, $\text{T}=\text{Al}$ and $\text{X}=\text{SO}_4$. This sodalite forms from CaO , Al_2O_3 and CaSO_4 at around 1350°C, a temperature at which CaSO_4 decomposes. Consequently, the sulfate group is trapped in the sodalite cages, without being able to escape (Depmeier 2005). Figure 1.5 shows a perspective view of a pseudocubic sodalite cage along the (100) direction, where the sulfate group is in the center of the cage. The cage is formed by Al-O bonds and the cations (Ca^{2+}) tend to locate in the center of the six-member rings. In general, these cages are about 4-4.5 Å wide. The guest species in adjacent cages are isolated from each other and interact only weakly and indirectly (Depmeier 2005).

Depending on the Si/Al ratio and the type of cage ions, different sodalite compounds can be produced with a range of interesting properties and features such as negative thermal expansion (Leardini et al. 2012), ferroelectric behaviour (Setter et al. 1984), F centers (Barrer and Coler 1968), *s*-electron antiferromagnetism (Monnier et al. 1994), catalytic activity (Ogura et al. 2008), tunable electronic properties (Moran et al. 1996) and optical emission (Borgmann et al. 1999), to mention just a few.

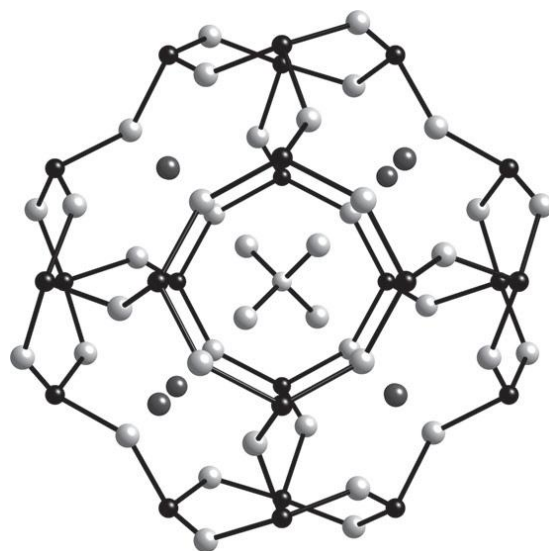


Figure 1.5. Pseudocubic sodalite cage (ye'elinite) viewed along the (100) direction. Al (black), Ca (dark grey), O (medium grey), and S (small ball in the center of the cage, light grey). (Reprinted from Hargis et al. 2014a, Copyright (2014), with permission from John Wiley and Sons).

Members of the aluminate sodalite family, with XO_4 anions, undergo reversible structural phase transitions at moderate temperatures (Depmeier and Bührer 1991; Smaalen et al. 1997; Antao et al. 2004). The temperatures, crystal structure evolution and associated enthalpies of the transitions have been reviewed (Depmeier 1988). The phase transitions are ferroic and occur at the boundary of the Brillouin zone, a fact that accounts for the formation of complicated superstructures and for frequently-found pseudomerohedral twinning (Depmeier 1987).

The fine details of the crystal structure of stoichiometric ye'elinite at room temperature are controversial, as has been reported to be cubic (Saalfeld and Depmeier 1972), tetragonal (Peixing et al. 1992) and orthorhombic (Calos et al. 1995).

This structure was first analyzed in 1962 by Halstead and Moore using X-ray powder diffraction. They suggested the cubic space group $I4_132$ bases on

1. Introduction

systematic absences in their powder patterns. In 1965, it was ascribed the cubic group I23 to ye'elimite (Kondo 1965). In 1972, Saalfeld and Depmeier produced a crystal structure for the subcell based on the cubic space group $I\bar{4}3m$ with $a=9.195\text{\AA}$ (Saalfeld and Depmeier 1972). Later, Feng et al. (1991) chose the same cubic space group but their atomic positions and calcium occupancy factors differ in some regards. These authors also reported two cubic, an orthorhombic, and a tetragonal superstructure in their data. Peixing et al. (1992) proposed a tetragonal structure using infrared spectroscopy. They determined the space group to be $P\bar{4}c2$ and gave a full set of atomic positions. In 1995, Calos et al. (1995) published an orthorhombic crystal structure using space group Pcc2 and lattice parameters $a=13.028(3)\text{\AA}$, $b=13.037(3)\text{\AA}$ and $c=9.161(2)\text{\AA}$. Recently, the disordered crystal structure of cubic stoichiometric ye'elimite at 800°C has been satisfactorily studied in the $I\bar{4}3m$ space group using a split-atom model (Kurokawa et al. 2014). They have suggested that the Pcc2-to- $I\bar{4}3m$ transformation of ye'elimite on heating would be accompanied by the statistical disordering in orientation of the SO_4 tetrahedral.

Hargis et al. (2014a) published that it was improbable that a pure-stoichiometric ye'elimite would have a cubic structure at room temperature and pressure but the substitutions of Ca^{2+} by Na^+ and Al^{3+} by B^{3+} , Si^{4+} or Fe^{3+} seems to restore the cubic symmetry. However, some authors tested a solid solution with Fe^{3+} , with nominal formula, $\text{Ca}_4\text{Al}_{5.7}\text{Fe}_{0.3}\text{O}_{12}\text{SO}_4$, and they did not obtain a cubic cell under their synthesis conditions, the structure for this solid solution was determined as orthorhombic (Schmidt and Poellmann 1999). In the case of iron, its maximum substitution degree may depend on the crystal structure of ye'elimite, due to the competition between aluminum and iron. The polymorphism of ye'elimite and its solid solutions in the presence of different amounts of Na^+ and Fe^{3+} were also investigated (Andac and Glasser 1994). It is also known that the incorporation of Fe_2O_3 into the crystal structure of ye'elimite in a CSA clinker promotes the formation of the cubic ye'elimite (Bullerjahn et al. 2014).

The structure of stoichiometric ye'elimité has been recently evaluated using a high-pressure synchrotron XRPD experiment. Orthorhombic and cubic unit cells were used to determine the isothermal bulk modulus (Hargis et al. 2014a).

Table 1.4 shows the published crystallographic data of ye'elimité up to this work.

Table 1.4. Ye'elimité polymorphs crystallographic data.

Polymorph	Space Group	Unit cell parameters				V/Z (Å ³)	Ref. bibl.	ICSD
		a (Å)	b (Å)	c (Å)	β (°)			
Cubic	I $\bar{4}3m$	9.205	9.205	9.205	90.0	390	(a)	9560
Orthorhombic	Pcc2	13.028	13.037	9.161	90.0	389	(b)	80361
Tetragonal	P $\bar{4}c2$	13.031	13.031	9.163	90.0	389	(c)	-
Cubic (800°C)	I $\bar{4}3m$	9.243	9.243	9.243	90.0	395	(d)	-

(a) Saalfeld y Depmeier 1972; (b) Calos et al. 1995; (c) Zhang et al. 1992; (d) Kurokawa et al. 2014.

1.2.2.2. Ye'elimité hydration mechanisms

Hydration can be summarized as a process of dissolution and precipitation/crystallization of different phases. During early age hydration of ye'elimité in the presence of a sulfate source such as gypsum, bassanite or anhydrite, i.e. up to 3 days, ettringite phase is the main crystalline hydration product being an exothermic process. Immediately after wetting, the reaction [1.7] takes place (Winnefeld and Barlag 2010; Hargis et al. 2013; Álvarez-Pinazo et al. 2014). Once the sulfate source is depleted or in absence of that and if there is enough free water available, monosulfate, is formed (Winnefeld and Barlag 2010) according to reaction [1.8]. In both reactions amorphous aluminum hydroxide is also formed. Amorphous aluminum hydroxide (known as AH₃, see section 1.2.6) is initially an amorphous phase as it is not be directly detected by XRPD, but its

occurrence may be confirmed by DTA-TG techniques (Cuberos et al. 2010; Martín-Sedeño et al. 2010; Morin et al. 2011; Song et al. 2015).



A similar hydration mechanism can be found in the early age hydration of CSA and BCSA cements because the hydration procedure is mainly dominated by the ye'elimite phase. Very recently, many authors (Telesca et al. 2014; Song et al. 2015) have followed the hydration of ye'elimite in these kinds of cements obtaining as main crystalline hydrates AFm and AFt. It is known that the ratio between both phases strongly depend on the amount and type of the added calcium sulfate.

Figure 1.6 shows a thermogravimetric analysis of ye'elimite paste hydrated after 18 hours with and without gypsum (Winnefeld and Barlag 2010) in order to show the main phases which are present after ye'elimite hydration. The hydration kinetics not only depends on the w/s ratio and the solubility of the additional sulfate source, but also on the polymorphism of ye'elimite. Moreover, there are some contradictory results concerning the reactivity of ye'elimite with water in the absence of another sulfate source. Some authors stated that only reaction [1.8] takes place, Figure 1.6, (Winnefeld and Barlag 2010) while others have published that mixtures of AFt and AFm phases are produced (Berger et al. 2011; Álvarez-Pinazo et al. 2014). From a stoichiometric point of view only monosulfate and aluminum hydroxide could be formed (reaction [1.8]), but ettringite may precipitate when (i) AFm occurs as a solid solution including hydroxide, which makes some sulfate available to form ettringite or (ii) some CAH₁₀ forms, which as well makes sulfate available for ettringite formation. The latter is observed for some commercial CSA cements.

Recently, Hargis et al. (2014b) studied the influence of gypsum, calcite, and vaterite (CaCO_3) during the ye'elimite hydration in six calcium sulfoaluminate-based cementitious systems. They concluded that vaterite and calcite improved the mortar mechanical properties. Moreover, vaterite was more effective than calcite in mitigating the compressive strength loss. The expansion was reduced by calcite and vaterite, irrespective of the presence of gypsum.

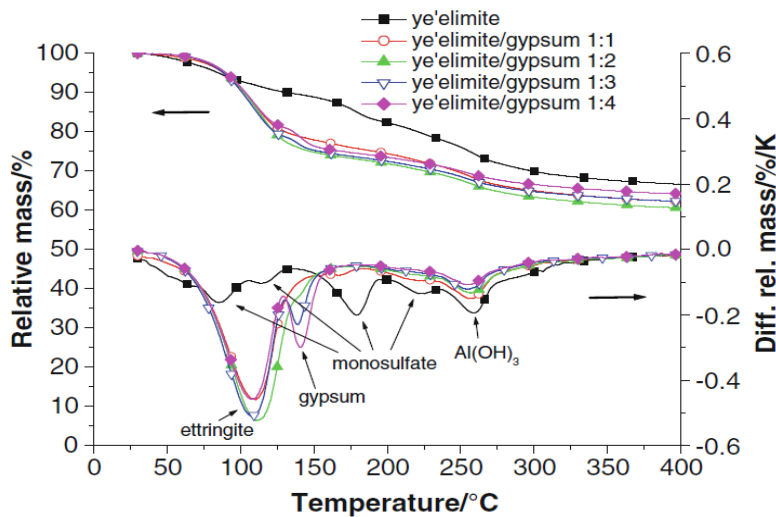


Figure 1.6. Thermogravimetric analyses of ye'elimite pastes after 18 hours of hydration (reprinted from Winnefeld and Barlag (2010), Copyright (2010), with permission from Springer).

1.2.3. Tetracalcium aluminoferrite ($\text{Ca}_4\text{Al}_2\text{Fe}_2\text{O}_{10}$, C_4AF)

C_4AF in cement nomenclature, also called brownmillerite or ferrite, is the major iron-containing phase in Ordinary Portland Cement and is also present in sulfoaluminate cements. Nevertheless, C_4AF is not a stoichiometric compound, but part of a solid solution series called the ferrite phase.

1.2.3.1. C_4AF chemical compositions and structures

The term “ferrite” usually refers to a solid solution with a wide range of composition of the general formula $\text{Ca}_2(\text{Al}_y\text{Fe}_{2-y})\text{O}_5$, where y can vary from 0 to about 1.33 (Touzo et al. 2013). The ferrite phase has been much investigated (Colville and Geller 1971, 1972; Touzo et al. 2013) and crystal structures and chemical compositions are well known. Due to the occupation of iron and aluminum in tetrahedral and octahedral sites within the solid solution, a change of space group from Pcmn to Ibm2 takes place at a high Al contents $y > 1.14$ (Colville and Geller 1971, 1972). Table 1.5 gives the crystallographic data of C_4AF structures. In cement chemistry the ideal composition C_4AF ($4\text{CaO} \cdot \text{Al}_2\text{O}_3 \cdot \text{Fe}_2\text{O}_3$), is used to describe the ferrite phase in Portland cement, in full awareness that major impurities may be present and that the A/F ratio is commonly not unity (Ectors et al. 2013). Compared with pure C_4AF , typical clinker ferrites have smaller values of a and c , but larger values of b . The XRPD powder patterns of clinker ferrites are affected by the cooling rate as this can change Fe/Al distributions (Ichikawa et al. 1994). The ferrite in the quenched samples was poorly crystalline, many peaks other than the three most intense (200, 141 and 202) disappear.

Table 1.5. Crystallographic data of ferrite phase polymorphs ($\text{Ca}_2\text{Al}_y\text{Fe}_{2-y}\text{O}_5$).

Space Group	Z	Unit cell parameters			V/Z (\AA^3)	y	ICSD
		a (\AA)	b (\AA)	c (\AA)			
Pcmn^a	4	5.559	14.771	5.429	111.5	0.0	14296
Ibm2^b	4	5.584	14.600	5.374	109.5	1.0	9197

(a) Colville 1970 y (b) Colville y Geller 1971.

The coexistence of $\text{C}_4\text{A}_3\text{S}$ and ferrite solid solution was investigated in CSA cements (Juenger and Chen 2011; Touzo et al. 2013) and some iron content, up to 4.3 mol% (8.8 wt%), was found in the $\text{C}_4\text{A}_3\text{S}$ phase which coexists with melt and ferrite phase. However, at high overall iron contents, it is difficult to avoid several problems: (i) formation of excessive amounts of liquid phase, (ii) rather

rapid development of a very fluid melt over a short range of temperatures, (iii) formation of other iron bearing phases such as monocalcium ferrite in iron-rich compositions, (iv) progressive replacement with increasing iron content of C_4A_3S by $CaSO_4$ as sulfate-containing solid phase. These factors, taken together, suggest that the control of the Al/Fe ratio may well be a key parameter in optimizing sulfoaluminate clinker production.

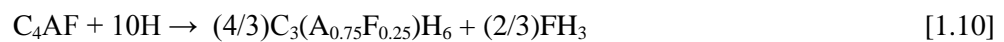
1.2.3.2. C_4AF hydration mechanisms

In the absence of any other phases, the hydration of brownmillerite appears to be similar to the hydration of the iron-free C_3A , in which a C-A-H gel first coats the C_3A grains from which metastable hexagonal C-A-H plates (Jupe et al. 1996; Meredith et al. 2004). Finally, these plates convert to the stable cubic hydrate, C_3AH_6 . It has been reported that iron does not form separate phases in the hydration of ferrite, but the hydration products of this phase are (more often than not) assumed to incorporate some iron (Rogers and Aldridge 1977; Fukuhara et al. 1981; Meller et al. 2004a). The hydration of pure brownmillerite with water initially forms metastable C-(A,F)-H hydrates (hydroxy-AFm), possibly in a C-(A,F)-H gel (Meredith et al. 2004). The C-(A,F)-H hydrates convert to a hydrogarnet phase $C_3(A,F)H_6$ (also called katoite) over time (Ectors et al. 2013). The exact Al/Fe ratios of the hydrogarnets are as yet debatable but these crystalline phases have a higher A/F ratio than does the unhydrated material (Meyer et al. 2004b). Thus, to maintain stoichiometry an iron-rich hydroxide must be formed (or FH_3). This phase is amorphous to X-rays (there is a lack of order in the large scale), but has been detected by SEM (Rogers and Aldridge 1977) and Mossbauer spectroscopy (Teoreanu et al. 1979).

The hydration of brownmillerite (Meller et al. 2004a) in the absence of sulfates may be written formally as:

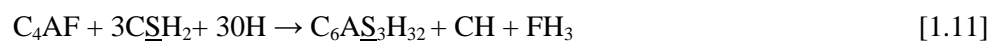


If Fe is incorporated into the hydrogarnet product by consumption of the CH produced:

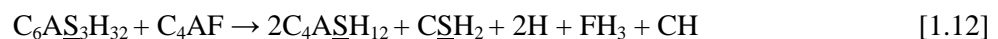


The addition of calcium sulfates to C_4AF inhibits the direct hydration of C_4AF to hydroxy-AFm or $\text{C}_3(\text{A},\text{F})\text{H}_6$. The hydration product that is formed rapidly on first contact with water is most commonly ettringite. There are some theories about the exact mechanism governing the retardation process (Ectors et al. 2013).

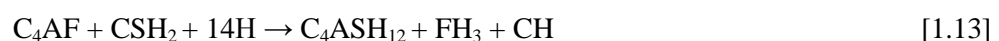
In the presence of sulfate the simplest (i.e. no Fe-solid solution) scheme is (Meller et al. 2004a):



where again $\text{C}_6\text{AS}_3\text{H}_{32}$ is the AFt trisulfoaluminate mineral ettringite. Successively, ettringite can decompose to form an AFm monosulfoaluminate hydrate in the presence of C_4AF as stated next:



The gypsum released in [1.12] can react with any remaining C_4AF to form further AFm ($\text{C}_4\text{ASH}_{12}$). Meller et al. (2004a) reported that small amounts of gypsum are seen to remain in the paste even after AFm forms and for this reason a transient increase in gypsum accompanies the AFt to AFm transformation (Meyer et al. 2004a).



It is known that a partial series of solid solutions can be formed between C_3AH_6 and C_3FH_6 ; hence all the formulae in the above equations can be written as $C_x(A,F)_yH_z$ or $C_x(A,F)_yS_wH_z$. However, no simple crystalline iron oxides, hydroxides or hydrous reaction products are observed in any system studied (Meller et al. 2004a). Moreover, the hydration process involving iron-containing phases may be more complex, as the formation of solid solutions between Fe and Al-containing hydrates may stabilize mixed solids, such as Fe-AFt (Möschner et al. 2009) and Fe-AFm (Dilnesa et al. 2012).

1.2.4. Ettringite or AFt ($Ca_6Al_2(OH)_{12}(SO_4)_3 \cdot 26H_2O$, $C_6AS_3H_{32}$).

Ettringite is a mineral which rarely occurs in nature but is widely present in the mineralogy of hydrated cements. This phase is known in cement nomenclature as $C_6AS_3H_{32}$ ($6CaO \cdot Al_2O_3 \cdot 3SO_3 \cdot 32H_2O$). Ettringite, commonly named AFt, is calcium sulfoaluminate hydrate and have the general formula $[Ca_3(Al,Fe)(OH)_6 \cdot 12H_2O]_2 \cdot X_3 \cdot nH_2O$, where n is, normally at least, ≤ 2 and X represents one formula unit of a doubly charged, or with reservations, two formula units of a singly charged anion. The term AFt refers to the three units of CX in an alternative way of writing the formula, $C_3(A,F) \cdot 3CX \cdot yH_2O$ [or $C_6(A,F)X_3 \cdot yH_2O$], where $y = x + 30$. In case of ettringite, the anion $X = SO_4^{2-}$. The crystal structure can be described as a compact columns of $[Ca_3Al(OH)_6 \cdot 24H_2O]^{3+}$ composition, running parallel to the c-axis, with the X anions and, usually, H_2O molecules in the intermediate channels (Taylor, 1997). It was proved that ettringite could be thermally unstable for temperatures higher than $80^\circ C$, depending on the water pressure (Zhou and Glasser 2001). During the dehydration process, the removal of hydroxyls and water molecules from the structure occurs (Hartmann et al. 2006).

The structural model for ettringite was proposed by Moore and Taylor (1970) by single-crystal X-ray examination with a naturally specimen. However, no consideration was given to hydrogen atoms. For this reason, the crystalline structure of ettringite was revised by Goetz-Neunhoeffer and Neubauer (2006) to obtain a more complete structure model for this phase. The symmetry of ettringite is trigonal, with $a=11.229(1) \text{ \AA}$, $c=21.478(3) \text{ \AA}$ and $Z=2$, the space group is $P31c$, apparent higher symmetry being due to twinning or disorder. At the same time, Hartman and Berliner (2006) proposed a similar structure using time-of-flight neutron powder diffraction techniques. In addition, ettringite crystallizes in the form of needles or strips. Figure 1.7 shows a SEM micrograph where needles of ettringite are observed.

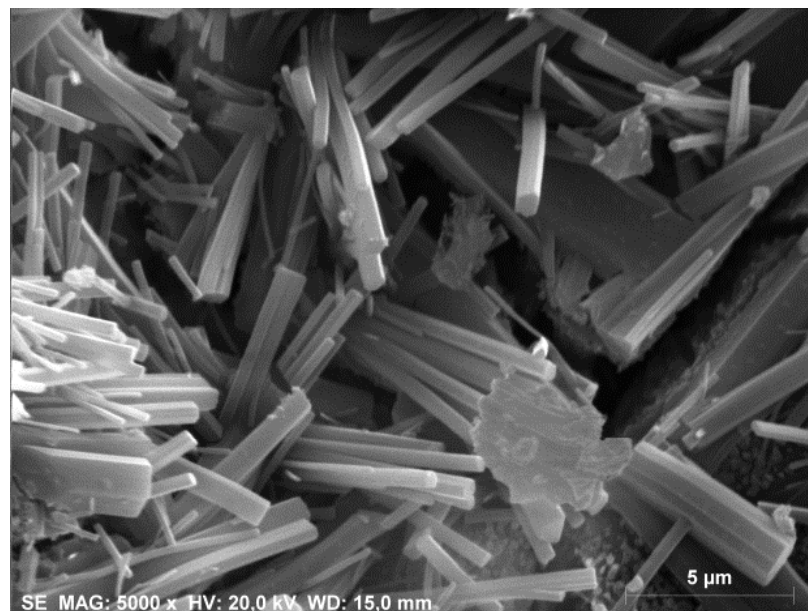


Figure 1.7. SEM micrograph of the fracture surface of a CSA with gypsum after 1 day of hydration (Reprinted from García-Maté et al. 2015, Copyright (2015), with permission from Elsevier).

1.2.5. AFm-type phases

AFm phases have a layer structure with the general formula $[\text{Ca}_2\text{Al}(\text{OH})_6]\text{X}\cdot n\text{H}_2\text{O}$ ($n=8-14$) where X denotes an exchangeable singly charged (e.g. OH^- or chloride) or half a formula unit of a doubly charged anion (for instance sulfate, carbonate and aluminosilicate) placed in the interlayer space jointly with water molecules. Some Fe(III) may also substitute aluminum. The AFm compounds crystallize in the form of hexagonal plates. The most ordinary AFm-type phases are kuzelite (Allmann 1977), Stratlingite (Rinaldi et al. 1990) and C_2AH_8 . There are other AFm-type phases such as monocarbonates (François et al. 1998) or monochlorides (Renaudin et al. 1999) that used to appear in chemically aggressive environments.

(i) The typical AFm which crystallizes in cements ($[\text{Ca}_2\text{Al}(\text{OH})_6](\text{SO}_4)_{1/2}\cdot 3\text{H}_2\text{O}$), whose formula is $\text{C}_4\text{A}\underline{\text{S}}\text{H}_{12}$ in cement nomenclature, is called AFm-12. This phase is formed when the sulfate source (gypsum, bassanite or anhydrite) is depleted and there is enough free water available (Winnefeld and Lothenbach 2010). However, in the presence of carbonates hemi- and/or monocarbonate are formed instead of $\text{C}_4\text{A}\underline{\text{S}}\text{H}_{12}$. The crystal structure of AFm-12 was determined by Allman (1977) as it occurs naturally as the mineral kuzelite. The presence of related AFm-phases with different layer spacing is justified twofold: i) by the partial anion replacement $\text{OH}^-/\text{SO}_4^{2-}$ within the layers; and ii) depending on the supply of available water from the surroundings the intermediate layer contains not only anions but also a variable number of water molecules. The AFm phase has proven a difficult subject for analysis because of its low crystallinity, polytypic and changes to the position and intensity of reflections in their diffraction patterns (Matschei et al. 2007). Figure 1.8 shows a SEM micrograph of AFm.

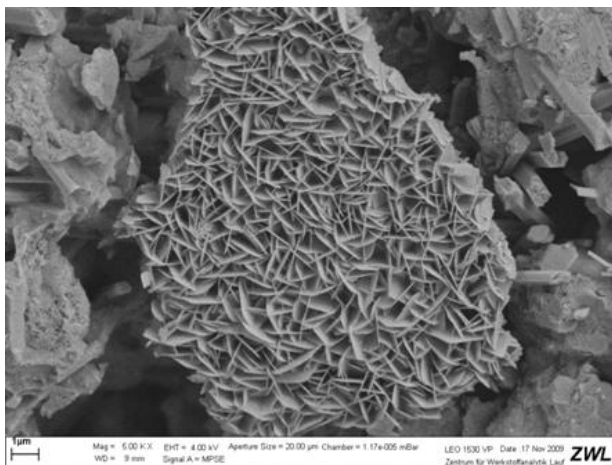


Figure 1.8. SEM micrograph of a BCSAF cement paste which displays AFm particles (Reprinted from Cuberos et al. 2010, Copyright (2010), with permission from American Chemical Society).

(ii) Stratlingite, $\text{Ca}_2\text{Al}(\text{OH})_6[\text{AlSiO}_2(\text{OH})_4]\cdot 3\text{H}_2\text{O}$, C_2ASH_8 in cement nomenclature, appears as hydration product of aluminium-rich cements, such as calcium aluminate, calcium sulfoaluminate and also belite calcium sulfoaluminate cements. It appears as a consequence of the reaction of C_2S with $\text{AH}_3\cdot n\text{H}_2\text{O}$. The structure of stratlingite is known from single crystal studies of mineral fragments from Mayern and Montalto di Castro (Rinaldi et al. 1990). It is formed by a principal octahedral or brucite-type layer, $[\text{Ca}_2\text{Al}(\text{OH})_6\cdot 2\text{H}_2\text{O}]^+$ with a full occupancy, and a double tetrahedral layer, $[(\text{T}, \square)_4(\text{OH}, \text{O})_8\cdot 0.25\text{H}_2\text{O}]^-$, where T can be Si or Al and \square represents a vacant tetrahedral site. This vacancies are around 45 % . The symmetry of stratlingite is R3m. The structure analysis (Kwan et al. 1995; Rinaldi et al. 1990) indicates that the octahedral layer shows an ordered scheme where each Al-octahedron is linked to 6 edge-sharing CaO_7 polyhedra (2 out 3 positions are then occupied by the seven coordinated Ca-type cation). The structure also contains hydration water. Most of the water is located in the aluminum octahedral layer projecting towards the centre of the 6-membered rings of the double tetrahedral layers (Santacruz et al. 2015). Figure 1.9 shows the crystal

structure of stratlingite where selected atoms are labeled (Santacruz et al. 2015). In this work not only the structure but also the microstructure of stratlingite is discussed.

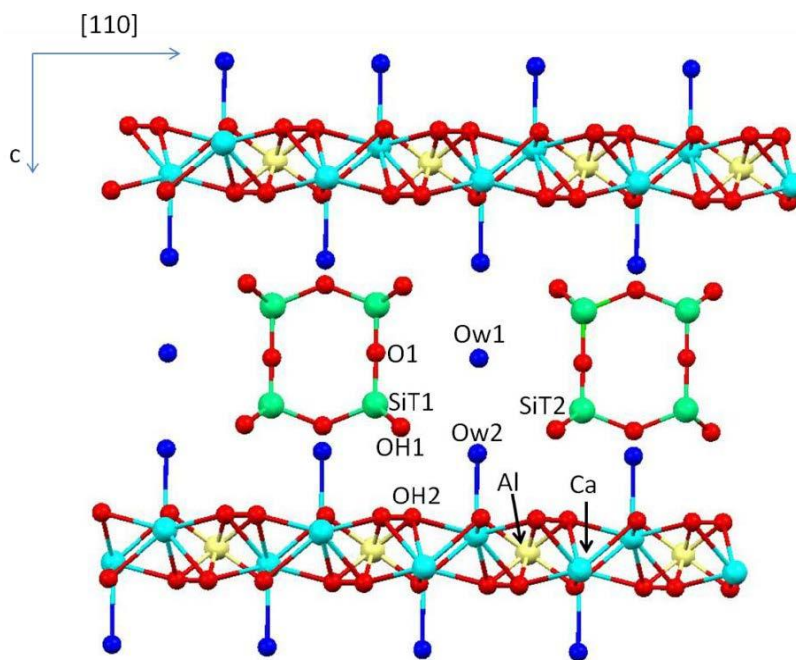


Figure 1.9. Layered crystal structure of stratlingite. (Reprinted from Santacruz et al. 2015, Copyright (2015), with permission from ICE Publishing).

(iii) C_2AH_8 is the main hydration product in CAC. It belongs to the group of AFm-type phases consisting of a main layer with the following composition $[Ca_2Al(OH)_6 \cdot 2H_2O]^+$ and the interlayer containing the $[Al(OH)_4 \cdot nH_2O]^-$ groups. The interlayer has variable water content depending on temperature, relative humidity and pressure. Therefore, the formula C_2AH_{8+x} is generally used. The degree of reaction of this hydrated phase can be unravel by analyzing the first (0 0 1) peak, which correlates with the main layer distance (Raab and Pöllmann 2011).

1.2.6. Other hydrated phases: hydrogarnet phases and amorphous aluminum hydroxide, $\text{Al}(\text{OH})_3 \cdot n\text{H}_2\text{O}$

Hydrogarnet phases have a cubic structure related to that of grossular or garnet ($\text{Ca}_3\text{Al}_2\text{Si}_3\text{O}_{12}$) with the general formula $\text{X}_3\text{Y}_2(\text{SiO}_4)_3$. The X site is usually occupied by divalent cations (Ca^{2+} , Mg^{2+} , and Fe^{2+}) and the Y site by trivalent cations (Al^{3+} , Fe^{3+} and Cr^{3+}) in an octahedral/tetrahedral framework with $[\text{SiO}_4]^{4-}$ occupying the tetrahedral positions. Hydrogarnet ($\text{Ca}_3(\text{Al,Fe})_2(\text{SiO}_4)_y(\text{OH})_{4(3-y)}$; $0 < y < 3$) includes a group of minerals where the $[\text{SiO}_4]^{4-}$ tetrahedra are partially or completely replaced by OH^- (Dilnesa et al. 2014). The Al-containing hydrogarnet includes hydrogrossular ($\text{Ca}_3\text{Al}_2(\text{SiO}_4)_y(\text{OH})_{4(3-y)}$; $0 < y < 3$) with the end member katoite ($\text{Ca}_3\text{Al}_2(\text{OH})_{12}$ or C_3AH_6). This katoite is reported to be the only thermodynamically stable calcium aluminate hydrate formed in calcium aluminate cements (Rivas-Mercury et al. 2007) and is a quaternary compound that crystallizes in the space group Ia3d and displays the cubic unit cell $a=12.55695(3)$ Å and $z=8$ (Lager et al. 1987). Moreover, Fe-katoite ($\text{Ca}_3\text{Fe}_2(\text{OH})_{12}$ or C_3FH_6) also belongs to this group. In the mineralogical nomenclature recommended by Passaglia and Rinaldi (1984), phases in the C_3AH_6 - C_3AS_3 series are collectively called hydrogrossular, and the names katoite and hibschite are used more specifically to denote those with $\text{SiO}_2/\text{Al}_2\text{O}_3$ molar ratios below and above 1.5, respectively, see Figure 1.10.

It has been reported an empirical equation which gives better agreement for hydrated compositions which appears in cement chemistry with the formula $\text{C}_3\text{A}_{1-x}\text{F}_x\text{S}_{3-y/2}\text{H}_y$:

$$a = 11.71 + 0.16\text{Fe}_2\text{O}_3 + 0.144\text{H}_2\text{O} \quad (1.1)$$

where a is the cell parameter in Å and Fe_2O_3 and H_2O are the values of x and y , respectively (Taylor 1997). In order to determine the composition of a phase of this general composition from the XRPD pattern, the intensity ratio of the 022 peak to

the 116 peak has been previously used. Table 1.6 gives some values of a and of this ratio, calculated from equation 1.1 and from the XRPD pattern respectively (Taylor 1997).

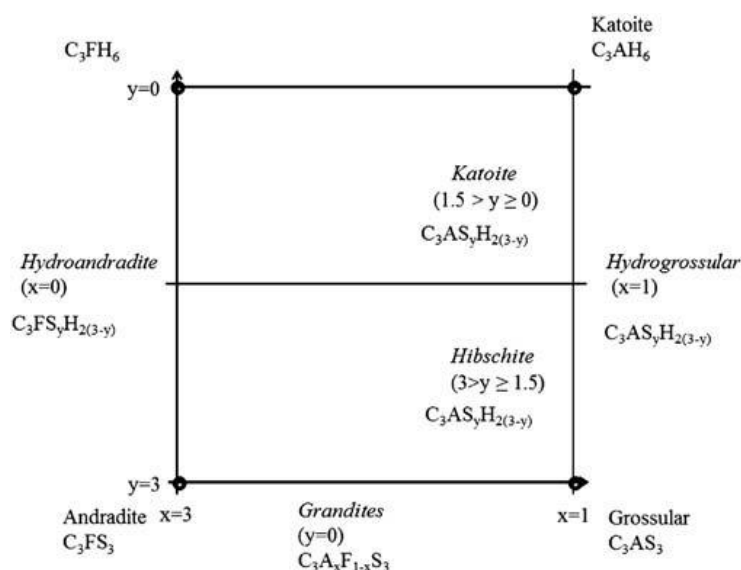


Figure 1.10. Nomenclature of minerals of the hydrogarnet group $\text{Ca}_3(\text{Al}_x\text{Fe}_{1-x})_2(\text{SiO}_4)_y(\text{OH})_{4(3-y)}$ (Reprinted from Dilnesa et al. 2014, Copyright (2014), with permission from Elsevier).

Table 1.6. Calculated values of the cell parameters a and ratio of intensities of the 022 to the 016 XRPD powder reflections for some hydrogarnet phases (Adapted from Taylor 1997).

x (moles Fe_2O_3 in formula)	$\text{C}_3\text{A}_{1-x}\text{F}_x\text{H}_6$		$\text{C}_3\text{A}_{1-x}\text{F}_x\text{SH}_4$		$\text{C}_3\text{A}_{1-x}\text{F}_x\text{S}_2\text{H}_2$	
	a (Å)	I_{022}/I_{016}	a (Å)	I_{022}/I_{016}	a (Å)	I_{022}/I_{016}
1.0	12.73	2.22	12.45	1.77	12.16	1.36
0.5	12.65	1.15	12.37	0.78	12.08	0.43
0.0	12.57	0.41	12.29	0.17	12.00	0.03

The amorphous aluminum hydroxide, $\text{Al}(\text{OH})_3 \cdot n\text{H}_2\text{O}$ is incorrectly known as AH_3 , which represents its crystalline form, gibbsite. However, this crystalline gibbsite never appears as ye'elimite hydration product. $\text{Al}(\text{OH})_3 \cdot n\text{H}_2\text{O}$ is the main

1. Introduction

amorphous hydration product of ye'elimite containing cement and has been proposed by many researchers (Pelletier et al. 2010; Winnefeld and Barlag 2010; Winnefeld and Lothenbach 2010; Pelletier-Chaignat et al. 2011; Chen et al. 2012; Song et al. 2015). This phase is formed during the first hours of hydration along with AFt and/or AFm (see reactions [1.7] and [1.8]). However, it is very difficult to quantify because it is amorphous or ill crystalline nature. This phase occurs as an X-ray amorphous form, showing ones some very broad signals in the XRPD pattern, centered where crystalline gibbsite main reflections are placed. On the other hand, TGA analysis is a suitable tool to identify amorphous gibbsite type-gel, which loses its bound water around 250-280°C (Winnefeld and Barlag 2010), see Figure 1.6. However, the presence of some free water molecules in the structure of aluminum hydroxide gel cannot be excluded, which could lead to an additional water loss around 100°C during the TGA analysis (Pelletier et al. 2010). It appears that slightly less $\text{Al}(\text{OH})_3 \cdot n\text{H}_2\text{O}$ is produced in the hydration of ye'elimite with gypsum when compared to the hydration of the former in the absence of other sulfates (Winnefeld and Barlag 2010).

Some studies (Wu 1995; Song et al. 2015) of the microstructure of amorphous aluminum hydroxide prepared by a special method in CSA pastes reveals that $\text{Al}(\text{OH})_3 \cdot n\text{H}_2\text{O}$ has a spherical morphology.

Finally, it is important to highlight that other phases can appear during the hydration of sulfoaluminate cements. Table 1.7 lists a summary of additional hydrated phases that may be present in cement pastes.

Table 1.7. Structural and crystallographic details for hydrated phases in cements.

Phase	Formula	s.g.	μ (cm ⁻¹)	a (Å)	b (Å)	c (Å)	α (°)	β (°)	γ (°)	V (Å ³)	Z	ρ (g/cm ³)	ICSD codes	PDF codes	Ref
Portlandite	Ca(OH) ₂	P-3m	211.4	3.5653		4.895				54.49	1	2.26	15471	01-072-0156	[1]
Gibbsite	Al(OH) ₃	P2 ₁ /in	57.1	8.664	5.078	9.736	94.54			427.98	8	2.42	6162	01-070-2038	[2]
Clinotobermorite	Ca ₈ (SiO ₃) ₅ H ₂ O	C1	168.6	11.274	7.344	11.468	99.18	97.19	90.02	929.78	2	2.61	90034	01-074-2595	[3,2]
Tobermorite-14A	Ca ₈ Si ₁₀ (OH) ₂ 7H ₂ O	Bb	135.6	6.735	7.425	27.987			123.25	1170.43	2	2.23	152489	00-029-0331	[9]
Tobermorite-11A	Ca ₈ Si ₁₀ (OH) ₂ 5H ₂ O	B11m	144.3	6.735	7.385	22.487			123.25	935.35	2	2.46			[3,1]
Tobermorite-9A	Ca ₈ Si ₁₀ (OH) ₂ 8H ₂ O	P-1	164.3	10.576	7.265	10.931	101.30	96.98	109.65	759.50	1	2.32	151413	00-018-1206	[4]
Dicalcium silicate hydrate	Ca ₂ (SiO ₃) ₂ H ₂ O	P2 ₁ /c2 ₁	225.6	9.467	9.179	10.666				928.81	8	2.72	73404	01-081-1987	[4,1]
Hydrogarnet / C ₂ AH ₆	Ca ₂ Al ₂ (OH) ₁₂	la-3d	163.7	12.565						1983.75	8	2.53	202316	01-084-1354	[5]
Katoite	Ca ₂ Al ₂ (OH) ₁₂ (SiO ₃) ₁	la-3d	187.8	12.270						1847.28	8	2.88	172077	00-038-0368	[6]
Katoite	Ca _{2.93} Al _{1.97} (OH) ₁₂ (SiO ₃) _{0.84}	la-3d	185.5	12.38						1887.41	8	2.73	49772	01-077-1713	[6,1]
'CAH' ₁₀	Ca ₂ Al ₂ (OH) ₁₂ (H ₂ O) ₂ ·1.84H ₂ O	P6 ₃ /m	16.387			8.279				1925	6	1.55	407150	01-088-1410	[6,2]
AFI															
Etringite	Ca ₆ Al ₂ (OH) ₁₂ (SO ₄) ₂ ·26H ₂ O	P31c	84.4	11.229		21.478				2345.34	2	1.78	155395	00-041-1451	[7]
Etringite-CO ₂	Ca ₆ Al ₂ (OH) ₁₂ (CO ₃) ₂ ·26H ₂ O	No structure	77.6	10.8344		21.250				2160.23	2	1.76	-	00-036-1465	[7,2]
Etringite-BO ₃	Ca ₆ Al ₂ (OH) ₁₂ (B(OH) ₃) ₂ (OH) ₂ ·22H ₂ O	P3c	11.0296			10.6992				1127.2	1	1.72			[7,1]
Thaumasite	Ca ₆ Si ₂ (OH) ₁₂ (CO ₃) ₂ (SO ₄) ₂ ·24H ₂ O	P6 ₃	85.7	11.030		10.396				1095.34	2	1.89	31247	01-075-1688	[8]
AFm															
Kuzelite / C ₂ ASH ₁₂	Ca ₂ Al(OH) ₄ (SO ₄) _{0.5} ·3H ₂ O	R-3	115.8	5.7586		26.7946				789.5	3	2.02	100138	01-083-1289	[9]
Friedel's salt	Ca ₂ Al(OH) ₄ (Cl)·2H ₂ O	R-3c	146.7	5.724		46.689				1324.78	3	2.11	88617	01-089-8294	[10]
Friedel's salt	Ca ₂ Al(OH) ₄ (Cl)·2H ₂ O	R-3	141.7	5.7487		23.492				672.34	3	2.08	51890	01-072-4773	[11]
Friedel's salt	Ca ₂ Al(OH) ₄ (Cl)·2H ₂ O	R-3	259.1	5.873		23.362				697.85	3	2.21	51892	01-072-4775	[11]
Kuzel's salt	Ca ₂ Al(OH) ₄ (Cl) _{0.5} (SO ₄) _{0.5} ·2.5H ₂ O	R-3	124.0	5.7508		50.4185				909.73	1	2.09	63250	00-019-0203	[12]
Hydroxaluminite	Ca ₂ Al(OH) ₄ (Cl) _{0.5} (CO ₃) _{0.5} ·2.4H ₂ O	C2/c	130.1	10.020	5.751	16.286		104.22		1333.7	6	2.054	-	-	[15,2]
Chloro-carboaluminite	Ca ₂ Al(OH) ₄ (Cl) _{0.5} (CO ₃) _{0.5} ·2.27H ₂ O	R-3c	5.7400			46.7402				1453.01	6	2.22	59327	01-087-0493	[13]
Monocarb- aluminite	Ca ₂ Al(OH) ₄ (CO ₃) _{0.5} ·2.5H ₂ O	P1	124.7	5.7747		9.923	64.77	82.75	81.43	1410.1	3	1.9	263124		[15,1]
Hemicarb- aluminite	Ca ₂ Al(OH) ₄ (CO ₃) _{0.5} (OH) _{0.5} ·2H ₂ O	R-3c	113.9	5.7757		48.812							-	-	[14]
Monocarb- Ferrite	Ca ₂ Fe(OH) ₄ (CO ₃) _{0.5} ·3.1H ₂ O	R-3c	222.1	5.9196		47.8796				1431.8	3	1.92	-	00-045-0564	[7,1]
Borale-AFm	Ca ₂ Al(OH) ₄ (HBO ₃) _{0.5} ·3.1H ₂ O	R-3c	106.4	5.7764		49.5499				1878.76	6	1.89	-	-	
C ₂ AH ₆	Ca ₂ Al(OH) ₄ (Al(OH) ₃)·3H ₂ O	No structure	107.1	5.7907		64.6960				1079.59	3	2.05	69413	01-080-1579	[16]
Stratlingite/C ₂ ASH ₆	Ca ₂ Al(OH) ₄ (AlSO ₄ (OH)) _{0.5} ·3H ₂ O	R-3m	98.8	5.7445		37.770				492.55	1	2.07	280171	01-089-6723	[17]
Nitroaluminite	Ca ₂ Al(OH) ₄ (NO ₃)·2H ₂ O	P-3c	111.2	5.7445		17.2350				703.4	3	2.303	280087		[18]
Bromoaluminite	Ca ₂ Al(OH) ₄ (Br)·2H ₂ O	R-3	163.8	5.758		24.4990				765.69	3	2.421	280150		[19]
Iodoaluminite	Ca ₂ Al(OH) ₄ (I)·2H ₂ O	R-3	353.1	5.772		26.5380									
Bromochoaluminite	Ca ₂ Al(OH) ₄ (Br _{0.5} Cl _{0.5})·2H ₂ O	R-3c	153.5	5.7537		48.1080				1379.25	6	2.182	280444		[20]

[1] Patch 1961; [2] Saelefield and Weide 1974; [3] Bonaccorsi et al. 2005; [3,1] Merino et al. 2000; [4] Bonaccorsi et al. 2004; [4,1] Yano et al. 1987; [6] Ferro et al. 2003; [6,1] Sacerdoti and Passaglia 1985; [6,2] Curato et al. 1998; [7] Goetz-Neunhoeffer and Neubauer 2006; [7,1] Champenois et al. 2012; [7,2] Moore and Taylor 1970; [8] Effenberger et al. 1983; [9] Almann 1977; [10] Renaudin et al. 1998; [11] Rousselle et al. 2002; [12] Mesbah et al. 2011; [13] François et al. 1998; [14] Dinesa et al. 2011; [15] Sacerdoti and Passaglia 1988; [15,1] Runčevski et al. 2012; [16] Rinaldi et al. 1990; [17] Renaudin and François 1999; [18] Rapin et al. 1999a; [19] Rapin et al. 1999b; [20] Rapin and François 2001.

1.3. Methodologies

1.3.1. Laboratory X-Ray Powder Diffraction (LXRPD) and Rietveld Method

Powder diffraction patterns, are obtained by the interaction of X-rays (or neutrons or electrons) with crystalline compounds. Crystalline compounds have long range periodic order. The position, height and even width of these reflections may be used to determine many aspects of the sample structure and microstructure (Pecharsky and Zavalij 2005; Dinnebier and Billinge 2008).

The Rietveld method is a technique devised by Hugo Rietveld in late sixties (Rietveld 1967; Rietveld 1969) for a deeper characterization of polycrystalline compounds by treating in a ‘better/different’ way the powder diffraction patterns. The very original contribution of the Rietveld method to powder diffraction was its conceptual breakthrough: ‘To use measured powder pattern intensities instead of reflection (peak) intensities’. This conceptual breakthrough, together with the coming of computers, allowed to properly dealing with strongly overlapping reflections. The introduction of this technique was a key step forward in the diffraction analysis of polycrystalline samples.

The Rietveld method was originally devised for the refinement of crystal and magnetic structures from powder neutron data. However, today the uses of the Rietveld method are numerous and help extracting the maximum information already present in a powder diffraction pattern. This information is listed just below. From the position of the diffraction peaks: i) lattice parameters, ii) space group determination, iii) phase identification and iv) macro-strain; from the intensities of the diffraction peaks: v) crystal (nuclear) structure (including atomic positions, occupation factors and atomic displacement parameters), vi) magnetic structure, vii) texture (preferred orientation), and viii) quantitative phase analysis;

from the widths/shapes of the diffraction peaks: ix) micro-strains (mainly in solid solutions), and x) coherent diffraction domain size(s) (Aranda et al. 2012).

Focusing on Rietveld quantitative phase analysis (RQPA), several steps have to be fulfilled. Initially, sample has to be properly prepared and this will depend upon the nature of the sample itself and the diffractometer where the data will be taken. Secondly, the diffractometer should be well aligned and maintained. Different optical configurations are possible in modern diffractometers and the optimal set-up should be used. For example, LXRPD studies can be performed mainly by two different geometry modes: i) Transmission geometry (Debye-Scherrer), and ii) Reflection geometry (Bragg-Brentano).

In this Thesis, LXRPD studies were performed in reflection geometry. LXRPD data were recorded in on an X'Pert MDP PRO diffractometer (PANalytical) equipped with a Ge (111) primary monochromator, using strictly monochromatic $\text{CuK}\alpha_1$ radiation ($\lambda=1.54059 \text{ \AA}$) and an X'Celerator detector. An overall measurement time between 2h and 4h per pattern, depending of the sample, was required for good statistics with a 0.017° step size.

Once a proper powder diffraction pattern has been taken, a third step follows: qualitative phase identification. Every crystalline phase in the sample should be identified. Then a possible strategy follows, we compute the RQPA with the phases which are clearly present in the pattern and, from the net intensity in the difference curve, the remaining low-content phases are determined. In addition to the main, clearly-observed phases, dubious phases are added to the Rietveld calculation and its absence/presence can be individually estimated.

In any case, when the main (all) phases are identified, the fourth step is to carry out the RQPA with the appropriate software. In this Thesis, we have used GSAS (Larson and von Dreele 1994; Toby 2001) and HighScore Plus software by PANalytical. The fit is carried out by optimizing all appropriate variables such as: i) scale factor of every crystalline phase; ii) background parameters for the chosen

function; iii) unit cell parameters for every crystalline phase; iv) peak shape parameters for every computed phase; and finally, v) correction parameters which may be phase-dependent (such as preferred orientation, extinction, etc.) or pattern-dependent (zero-shift, absorption correction when working in transmission geometry, etc.).

The application of RQPA to clinkers/cements/pastes is not an easy task for the following reasons (Aranda et al. 2012; Aranda et al. 2015): i) there are many phases, usually more than five, which increases the diffraction peak overlapping and so the correlations; ii) each phase has its own mass absorption coefficient which may yield the micro-absorption problem; iii) the small irradiated volume ($\sim 2 \text{ mm}^3$) for Cu $K\alpha$, which may lead to poor particle statistics; iv) some phases, for instance alite or gypsum, crystallise as plaques which show preferred orientation, increasing the errors; v) phases can crystallise as several polymorphs that must be identified a priori; vi) the diffraction peak broadening for some phases may be anisotropic and it must be properly modelled; and vii) the atomic impurities inside each phase are not known and their scale factors are computed for ideal/stoichiometric phases. In any case, RQPA shows several advantages over other methods based on powder diffraction and other technologies (microscopy, thermal analysis, etc.).

As stated above, conventional RQPA requires all crystal structures to be known. Aranda et al. (2012) reported the main hydrated and anhydrous cement standards phases. There are alternative whole-pattern quantitative phase analysis methods for crystalline phases with unknown structures (Smith et al. 1987; Taylor and Zhu 1992; Scarlett and Madsen 2006; Snellings et al. 2014). Currently, three ways to derive the phase content, from the Rietveld refined scale factor, S_α , can be used to determine the RQPA (Madsen et al. 2011; Gualtieri et al. 2014):

I) Normalization to full crystalline phase content method. The simplest approach is the approximation that the sample is composed only of crystalline

phases with known structures. However, the method normalizes the sum of the analyzed weight fractions to 1.0. Thus, if the sample contains amorphous phases, and/or some amounts of unaccounted for crystalline phases, the analyzed weight fractions will be overestimated.

II) Internal standard method. A second, more experimentally-demanding, approach is to mix the sample with a crystalline standard in a known amount. This standard must be free of amorphous content or at least its non-diffracting content must be known. The weight value, W_{st} , of the standard is compared to the obtained value from RQPA, R_{st} to obtain a quantification of amorphous phases (De la Torre et al. 2001). The obtained value accounts for any amorphous phase(s), but also any misfitting problems of the analyzed crystalline phases, and any crystalline phases may not be included in the control file (due to the lack of crystal structure or because the phase was not identified, etc.). This overall content is hereinafter named ACn which stands for Amorphous and Crystalline not-quantified, to highlight that not only an amorphous fraction but any not-computed crystalline phase and any misfit problem may contribute to this number.

III) External standard method (G-factor approach). To avoid complications that may arise from mixing an internal standard with the sample, it is possible to use an external standard method. This approach requires the recording of two patterns in identical diffractometer configuration/conditions for Bragg-Brentano $\Theta/2\Theta$ reflection geometry. The method was proposed several years ago (O'Connor and Raven 1988) and consists in determining the diffractometer constant, with an appropriate standard (for instance silicon powder from Si-single crystal). This method is also known as G-method as the standard allows to calculate the G-factor of the diffractometer in the operating conditions.

The calculated G-factor represents a calibration factor for the whole experimental setup and comprises the diffractometer used, radiation, optics, and all data acquisition conditions, (f.i. detector configuration, integration time, etc.). This

G-factor is used to determine the mass concentration of each phase of the sample under study by using a diffractometer constant that must be previously determined. From the difference between 100 and the sum of the crystalline phase contents, an overall unaccounted/left-out weight percentage, ACn, can be derived.

This methodology has been recently applied to anhydrous cements (Jansen et al. 2011; Álvarez-Pinazo et al. 2012) and to cement pastes (Jansen et al. 2012a, b; Álvarez-Pinazo et al. 2013; García-Maté et al. 2013). In any case, the external standard method is experimentally more demanding but it may have the brightest future for the study of hydration reactions. This statement is based on the lack of need of spiking an internal standard.

In this PhD Thesis, all the errors are the mathematical errors from the Rietveld fits, not the standard deviations derived from three measurements.

1.3.2. Synchrotron X-Ray Powder Diffraction (SXRPD) (BL04 – MSPD, ALBA)

The use of an intense and monochromatic X-ray source, such as synchrotron X-rays, coupled with a fast X-ray detection system permits the collection of powder diffraction patterns with excellent counting statistics. In addition, it is also possible to collect patterns with short collection times enabling time-resolved analysis of rapid reaction sequences such as *in-situ* measurements during the hydration process of cements (Merlini et al. 2007, Álvarez-Pinazo et al. 2014). X-rays, which are generated by a synchrotron facility, are at least 5 orders of magnitude more intense than the best X-ray laboratory source. The high brilliance of the synchrotron radiation drastically improves the structural characterization and level of detection of mixture components.

In this Thesis, SXRPD patterns were collected using the X-ray powder diffraction station of ALBA in the Materials Science and Powder Diffraction

Ana María Cuesta García

Beamline (BL04-MSPD), the Spanish Synchrotron Radiation Facility (Barcelona, Spain). Patterns were collected in Debye-Scherrer (transmission) mode synchrotron (Fauth et al. 2013). The wavelengths, 0.61975(1) Å and 0.62020(1), were selected with a double-crystal Si (111) monochromator and determined from Si640d NIST standard ($a=5.43123$ Å). The diffractometer is equipped with two different detectors: i) a MYTHEN detector especially suited for time-resolved experiments and ii) a detector system based on crystal analyzers in the diffracted beam especially suited for high-resolution experiments giving also a flat background.

Raw SXRPD patterns were normalized taking into account the loss of X-ray beam flux with time due to the electron beam current decline in the storage ring. Normalized SXRPD patterns were analyzed by using the Rietveld methodology in order to obtain Rietveld Quantitative Phase Analysis (RQPA). Internal standard methodology has been also used with SXRPD data using quartz as internal standard.

1.3.3. Isothermal conduction calorimetry

The isothermal (heat conduction) calorimetry is an efficient tool to study the stages related by the hydration of cement pastes or mortars at constant temperature. The calorimeter continuously measures and displays the heat flow related by the hydration reactions (and chemical processes in general) taking place in the cement paste after mixing. At least for a single process, the thermal power is proportional to the rate of a reaction and the produced heat is proportional to the extent of the reaction (Lawrence 2003).

This methodology allows understanding the chemical origin of different regions/features (hydration reactions), the changes in reaction kinetics (Winnefeld and Barlag, 2010; Jansen et al. 2012b; Hargis et al. 2014b) and also supports the accuracy of RQPA (Hesse et al. 2011; Jansen et al. 2012a). X-ray diffraction data

on the hydration pastes allow an assignment of chemical reactions to the different peaks in heat evolution over periods of hydration approaching 250 h (Lawrence 2003).

For instance, Winnefeld and Barlag (2010) studied the hydration kinetics of ye'elinite pastes in different conditions using conduction calorimetry. They observed that without gypsum, the pure ye'elinite phase showed two maxima in the calorimetry curve. The first peak appears directly when the water is added due to the very early reactions (see Figure 1.11). After that, a dormant period occurs with a low heat flow during about 10 hours. Later, it can be appreciated a second maximum after about 15 hours of hydration, this second peak covers the main part of the hydration reactions. In the ye'elinite with gypsum sample, the first peak appears to be a little more intense indicating a higher intensity of the reactions (see Figure 1.11).

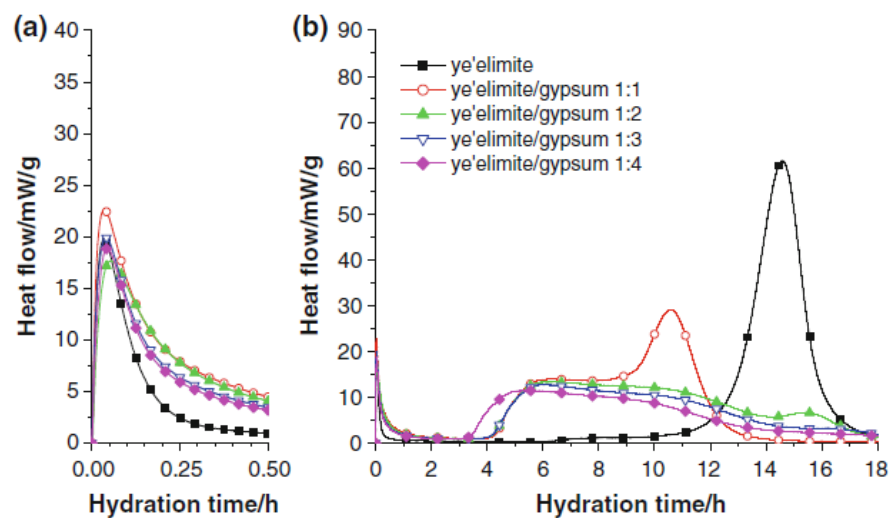


Figure 1.11. Conduction calorimetry of ye'elinite hydrated samples without and with different amounts of gypsum a) at short times and b) up to 18 hours (reprinted from Winnefeld and Barlag (2010), Copyright (2010), with permission from Springer).

In this work, the isothermal calorimetric study was performed in an eight channel Thermal Activity Monitor (TAM) instrument. Pastes were prepared ex-situ by mixing the sample with the appropriated amount of water. A stabilization period of 45 minutes was needed to start the measurements.

1.3.4. Thermal measurements

DTA-TGA have been used to identify hydration phases in cement pastes and to determine chemically bounded water. The TGA analyses are usually performed to confirm the mineralogical observations made by XRPD. It is also possible to determine the free water content by the difference between the added water (theoretical) and the chemically combined water. Although the use of this analysis is straightforward, it allows the determination of different phases (f.i. calcium silicate hydrate, ettringite, gypsum, monosulfate, amorphous aluminum hydroxide and calcium hydroxide in a CSA cement paste) through the corresponding dehydration endothermic peaks (Telesca et al. 2014). It is important to highlight that in contrary to the XRPD, TGA is suitable to identify amorphous phases, which have associated a loss of water, such as $\text{Al}(\text{OH})_3 \cdot n\text{H}_2\text{O}$ (Winnefeld and Barlag 2010), see Figure 1.6.

In this Thesis, differential thermal analysis and thermogravimetric (TGA) measurements were performed in a SDT-Q600 analyzer from TA instruments for stopped-hydration pastes. The temperature was varied from RT to 1000°C at a heating rate of 10 °C/min. Measurements were carried out in open platinum crucibles under nitrogen flow.

1.3.5. Scanning electron microscopy (SEM)

SEM is a type of electron microscope that produces images of a sample surface by scanning it with a focused beam of relatively high-energy electrons. The

signals that derive from the interactions between electrons and atoms of the sample contain information about the sample surface topography, chemical composition, microstructure and other properties such as electrical conductivity. The resolution depends on the probe size and the information volume that contributes to the signal, and thus on the specimen and the mode of operation.

SEM–BSE (backscattered electron imaging) has been extensively used to study the microstructure of cement and cementitious materials and in combination with EDS (energy dispersive X-ray spectroscopy) to determine the elemental compositions of the hydrate assemblage (Winnefeld and Lothenbach 2010, Bizzozero et al. 2014). This technique can also allow to quantify the different phases (unreacted cement pastes and hydration products) and to follow the evolution of the porosity (Pelletier et al. 2010). A recent investigation using SEM–BSE showed that using this technique is possible to establish connections between the modeled porosity and the compressive strength (Le Saoût et al. 2013). Moreover, SEM is a good complementary technique to XRPD in order to follow the hydration product development with the time (Winnefeld and Lothenbach 2010, Chen et al. 2012).

In this Thesis, prior to SEM observation, the hydration reactions of selected samples were stopped by immersing them in isopropanol for 3 days and then heated at 40 °C for 24 h (Le Saoût et al. 2013). Microscopic characterization of samples was performed in a JEOL JSM-6490LV electron microscope. Samples were impregnated with low viscosity resin and polished down. Energy dispersive spectroscopy measurements were carried out with the OXFORD INCA Energy 350 attachment.

2. Objectives

2. Objectives

The main aim of this PhD thesis is to synthesize and characterize some of the most important phases of interest in sulfoaluminate cements and belite sulfoaluminate cements, such as dicalcium silicate, ye'elite and tetracalcium aluminoferrite. After the initial characterization of these anhydrous phases, the study of their hydration mechanisms (including some mixtures) have been also carried out. The specific objectives can be described as follow:

- To investigate the stabilization mechanisms of β and α'_H -dicalcium silicate at room temperature by adding different dopants and to obtain a new revised crystal structure for α'_H -dicalcium silicate.
- To synthesize and characterize stoichiometric and doped ye'elimites in order to revise their crystal structures.
- To understand the thermal behavior of both polymorphs of ye'elite.
- To understand the hydration mechanisms of ye'elite as a function of its polymorphism, amount of water and type and content of sulfate source.
- To study the hydration of both polymorphs of ye'elite jointly with tetracalcium aluminoferrite or dicalcium silicate phases.
- To study the hydration of tetracalcium aluminoferrite phase in different chemical environments: in the presence and absence of gypsum and under the influence of ye'elite.
- To understand and characterize the amorphous gibbsite (or aluminum oxide hydrated) that is formed in these hydration reactions.

3. Articles section

a#1: “Mechanism of stabilization of dicalcium silicate solid solution with aluminium”

Cuesta A, Aranda M A G, Sanz J, De la Torre A G and Losilla E R (2014), *Dalton Trans*, 43, 2176-2182.

doi: 10.1039/c3dt52194j

Abstract

Stoichiometric dicalcium silicate, Ca_2SiO_4 , displays a well-known polymorphism with temperature. When this phase is doped by a range of elements generates belite, one of the main phases of cements. Here, we thoroughly study the aluminum doping of dicalcium silicate. This type of study is important for cement characterization and also from a basic point of view. $\text{Ca}_2\text{Si}_{1-2x}\text{Al}_{2x}\text{O}_{4-x}\square_x$ ($x=0, 0.010, 0.014, 0.03$.) has been prepared and studied by X-ray powder diffraction and the Rietveld method. The limiting composition has been established as $\text{Ca}_2\text{Si}_{0.972}\text{Al}_{0.028}\text{O}_{3.986}\square_{0.014}$. ^{27}Al MAS NMR band located close to ~ -70 ppm is ascribed to tetrahedral environments, in agreement with the proposed alivalent Si/Al atomic substitution mechanism. Thermal analysis measurements in a wet atmosphere indirectly confirm the increase of oxygen vacancies as the amount of incorporated protons increases with the aluminium content. A thorough electrical characterization has been carried out including overall conductivity measurements in wet and dried atmospheres and conductivity as a function of the oxygen partial pressure. The samples show oxide anion conductivity with a small p-type electronic contribution under oxidizing conditions. These compounds display a very important proton contribution to the overall conductivities under humidified atmospheres.

Ana María Cuesta García

a#2: “Reactive belite stabilization mechanisms by boron-bearing dopants”

Cuesta A, Losilla E R, Aranda M A G, Sanz J and De la Torre A G (2012), *Cem Concr Res*, 42, 598-606.

doi:10.1016/j.cemconres.2012.01.006

Abstract

Belite-rich cements hold promise for reduced energy consumption and CO₂ emissions, but their use is hindered by the slow hydration rates of ordinary belites. This drawback may be overcome by activation of belite by doping. Here, the doping mechanism of B and Na/B in belites is reported. For B-doping, three solid solutions have been tested: $\text{Ca}_{2-x/2}\text{B}_{x/2}(\text{SiO}_4)_{1-x}(\text{BO}_3)_x$, $\text{Ca}_2(\text{SiO}_4)_{1-x}(\text{BO}_3)_x\text{O}_{x/2}$ and $\text{Ca}_{2-x}\text{B}_x(\text{SiO}_4)_{1-x}(\text{BO}_4)_x$. The experimental results support the substitution of silicate groups by tetrahedral borate groups with the concomitant substitution of calcium by boron for charge compensation, $\text{Ca}_{2-x}\text{B}_x(\text{SiO}_4)_{1-x}(\text{BO}_4)_x$. Otherwise, the coupled Na/B-doping of belite has also been investigated and $\text{Ca}_{2-x}\text{Na}_x(\text{SiO}_4)_{1-x}(\text{BO}_3)_x$ series is confirmed to exist for a large range of x values. Along this series, $\alpha'_H\text{-C}_2\text{S}$ is the main phase (for $x \geq 0.10$) and is single phase for $x = 0.25$. Finally, a new structural description for borax doping in belite has been developed for $\alpha'_H\text{-Ca}_{1.85}\text{Na}_{0.15}(\text{SiO}_4)_{0.85}(\text{BO}_3)_{0.15}$, which fits better borax activated belite cements in Rietveld mineralogical analysis.

a#3: “Structure, Atomistic Simulations, and Phase Transition of Stoichiometric Yeelimité”

Cuesta A, De la Torre A G, Losilla E R, Peterson V K, Rejmak P, Ayuela A, Frontera C and Aranda M A G (2013), *Chem Mater*, 25, 1680-1687.

doi: 10.1021/cm400129z

Abstract

Yeelimité, $\text{Ca}_4[\text{Al}_6\text{O}_{12}]\text{SO}_4$, is outstanding as an aluminate sodalite, being the framework of these type of materials flexible and dependent on ion sizes and anion ordering/disordering. On the other hand, yeelimité is also important from an applied perspective as it is the most important phase in calcium sulfoaluminate cements. However, its crystal structure is not well studied. Here, we characterize the room temperature crystal structure of stoichiometric yeelimité through joint Rietveld refinement using neutron and X-ray powder diffraction data coupled with chemical soft-constraints. Our structural study shows that yeelimité has a lower symmetry than that of the previously reported tetragonal system, which we establish to likely be the acentric orthorhombic space group $Pcc2$, with a $\sqrt{2}a \times \sqrt{2}a \times a$ superstructure based on the cubic sodalite structure. Final unit cell values were $a = 13.0356(7) \text{ \AA}$, $b = 13.0350(7) \text{ \AA}$, and $c = 9.1677(2) \text{ \AA}$. We determine several structures using density functional theory calculations, with the lowest energy structure being $Pcc2$ in agreement with our experimental result. Yeelimité undergoes a reversible phase transition to a higher-symmetry phase which has been characterized to occur at $470 \text{ }^\circ\text{C}$ by thermodiffraction. The higher-symmetry phase is likely cubic or pseudocubic possessing an incommensurate superstructure, as suggested by our theoretical calculations which show a phase transition from an orthorhombic to a tetragonal structure. Our theoretical study also predicts a pressure-induced phase transition to a cubic structure of space group $I\bar{4}3m$. Finally, we show that our reported crystal structure of yeelimité enables better mineralogical phase analysis of commercial calcium sulfoaluminate cements, as shown by R_F values for this phase, 6.9% and 4.8% for the previously published orthorhombic structure and for the one reported in this study, respectively.

Ana María Cuesta García

a#4: “Pseudocubic crystal structure and phase transition in doped ye'elinite”

Cuesta A, De la Torre A G, Losilla E R, Santacruz I and Aranda M A G (2014), *Cryst Growth Des*, 14, 5158–5163.

doi: 10.1021/cg501290q

Abstract

Sodalites are tridimensional alumino-silicate materials containing cages where loosely bonded anions are located. Ye'elinite, $\text{Ca}_4[\text{Al}_6\text{O}_{12}]\text{SO}_4$, is outstanding as an aluminate sodalite with a flexible framework accepting several type of dopants with important structural consequences. Moreover, ye'elinite is also important from an applied perspective as it is the most relevant phase in calcium sulfoaluminate cements. The crystal structure of stoichiometric ye'elinite has recently been unraveled, but the structure of dopant-containing ye'elinite, which is present in cements, is not well studied. Here, we report the pseudocubic crystal structure of doped ye'elinite, $\text{Ca}_{3.8}\text{Na}_{0.2}\text{Al}_{5.6}\text{Fe}_{0.2}\text{Si}_{0.2}\text{O}_{12}\text{SO}_4$, from high-resolution synchrotron powder diffraction data. The powder pattern is indexed with a cubic cell, and a structural model is reported based on the $I\bar{4}3m$ space group. However, this compound displays diffraction peak narrowing on heating. Furthermore, some high-angle split peaks become a single peak on heating, and a phase transition is measured at 525 °C. Therefore, it is concluded that the crystal structure at room temperature has a lower symmetry, although it can be described as cubic. The structural study at 800 °C suggests a truly cubic structure, and we speculate that this phase transition, on heating, is likely related to the dynamical disordering of the sulfate anions. Finally it is concluded that the high temperature cubic state was not quenchable to ambient, even when the tested chemical substituents are introduced into the structure.

a#5: “Hydration mechanisms of two polymorphs of synthetic ye'elinite”

Cuesta A, Álvarez-Pinazo G, Sanfélix S G, Peral I, Aranda M G A and De la Torre A G (2014), *Cem Concr Res*, 63, 127-136.

doi:10.1016/j.cemconres.2014.05.010

Abstract

Ye'elinite is the main phase in calcium sulfoaluminate cements and also a key phase in sulfobelite cements. However, its hydration mechanism is not well understood. Here we reported new data on the hydration behavior of ye'elinite using synchrotron and laboratory powder diffraction coupled to the Rietveld methodology. Both internal and external standard methodologies have been used to determine the overall amorphous contents. We have addressed the standard variables: water-to-ye'elinite ratio and additional sulfate sources of different solubilities. Moreover, we report a deep study of the role of the polymorphism of pure ye'elinites. The hydration behavior of orthorhombic stoichiometric and pseudo-cubic solid-solution ye'elinites is discussed. In the absence of additional sulfate sources, stoichiometric-ye'elinite reacts slower than solid-solution-ye'elinite, and AFm-type phases are the main hydrated crystalline phases, as expected. Moreover, solid-solution-ye'elinite produces higher amounts of ettringite than stoichiometric-ye'elinite. However, in the presence of additional sulfates, stoichiometric-ye'elinite reacts faster than solid-solution-ye'elinite.

a#6: “Ye’elimite: structures and hydration mechanisms”

Cuesta A, Garcia-Mate M, Leon-Reina L, De la Torre A.G, Santacruz I, Aranda M. A. G (2015), *Proceedings of the 14th International Congress on the Chemistry of Cement*, Beijing, Spain.

Abstract

Belite calcium sulfoaluminate, aka BCSA or sulfobelite, cements are environmentally friendly building materials, as their production may have up to 25% lower CO₂ footprint than OPC fabrication. They are prepared by mixing the clinker with different amounts of a calcium sulfate set regulator. Hereafter cement nomenclature will be used: C=CaO, S=SiO₂, A=Al₂O₃, F=Fe₂O₃, S=SO₃, T=TiO₂ and H=H₂O. BCSA cements are based on belite (C₂S), ye’elimite (also called Klein’s salt or tetracalcium trialuminate sulfate (C₄A_{3S)) and other minor phases, such as ferrite (C₄AF) or calcium aluminates (C₁₂A₇). Additionally, calcium sulfoaluminate cements, CSA, contain ye’elimite as the main phase with belite being the second phase in terms of content. The phase composition variability in CSA cements is much larger than in BCSA cements.}

During early age hydration, i.e. up to 3 days, ettringite phase is the main crystalline hydration product formed in CSA and BCSA cement pastes arising from the dissolution and reaction of ye’elimite and calcium sulfate(s). Subsequently, and mainly in BCSA pastes, belite may yield stratlingite, amorphous C-S-H gel and portlandite. Minor phases present in the anhydrous cement may provoke the precipitation of other hydration products such as monosulfoaluminate, hydrogarnet or katoite. The reactivity of ferrite during hydration in these cements is slower than that of C₄A_{3S and it is still not well understood.}

Stoichiometric and doped ye’elimite crystal structures, including their polymorphisms, with temperature, have been studied and reported very recently. Furthermore, the reactivity of stoichiometric and doped ye’elimite has also very recently reported by us.

The aim and originality of this work is to better understand the hydration of stoichiometric (orthorhombic) and doped (pseudo-cubic) ye’elimite phases in combination with belite crystallized as both polymorphs (α'_H and β) at different

ages to improve “ecocement” performances. This work has allowed establishing kinetics and mechanisms for hydration of ye’elinite with belite samples using ex-situ laboratory X-ray powder diffraction (LXRPD) in combination with the external standard method, G-factor, up to 6 months. This strategy has allowed quantifying the amorphous content, including free water (the latter determined through thermogravimetric measurements (TGA), for stopped-hydration pastes).

It is known that active BCSA cements which contain the $\alpha'_{\text{H}}\text{-C}_2\text{S}$ polymorphs have a faster hydration reaction than related cements containing the $\alpha_{\text{H}}\text{-C}_2\text{S}$ polymorph. However, it is essential to establish the role of both ye’elinite polymorphs in the hydration behavior of these mixtures. Here, we study all the combinations between belite and ye’elinite. To simplify the problem, we prepare these artificial mixtures without aluminates. Powder diffraction data at 56 days show some small differences between samples. Chiefly, the sample which contains both $\alpha'_{\text{H}}\text{-C}_2\text{S}$ and doped-ye’elinite presents a higher degree of reaction and higher amounts of stratlingite at that age.

Moreover, the hydration of tetracalcium aluminoferrite (ferrite) in combination with ye’elinite (stoichiometric and doped) has also been studied by in-situ SXRPD (synchrotron X-ray powder diffraction) to understand the dissolution/crystallization processes that take place during hydration processes at early-ages. The main difference after 46 hours is that the sample with doped-ye’elinite yields much larger relative amounts of AFt.

Ana María Cuesta García

a#7: “Hydration of C₄AF in the presence of other phases: a synchrotron X-ray powder diffraction study”

Cuesta A, Santacruz I, Sanf elix S G, Fauth F, Aranda M G A and De la Torre A G (2015), *Constr Build Mater*, in press.

doi: 10.1016/j.conbuildmat.2015.10.114

Abstract

Hydration behaviour of C₄AF in selected experimental conditions has been determined. C₄AF has been hydrated in the absence and presence of gypsum, two polymorphs of ye’elinite and different water/solid ratios. C₄AF in the presence of water hydrates to form mainly a hydrogarnet-type phase. The crystal structure of C₃A_{0.845}F_{0.155}H₆ is reported from the Rietveld analysis of its synchrotron X-ray powder diffraction pattern. The hydration of C₄AF in the presence of gypsum gives AFt. However, the mixture tetracalcium aluminoferrite/gypsum/ye’elinite gives both AFt and AFm phases. C₄AF hydrated with ye’elinite in the absence of gypsum gives only AFm. Ye’elinite has inhibited tetracalcium aluminoferrite hydration.

4. Results and discussion

4. General results and discussion

This PhD Thesis is focused on the preparation and characterization of single phases of interest in calcium sulfoaluminate cements. After the characterization of the anhydrous samples, the hydration mechanisms of some pure samples and mixtures pastes have been profoundly studied.

This work has been organized in two main blocks: i) structural studies of anhydrous phases such as β and α'_H dicalcium silicate; stoichiometric and doped ye'elinite and finally a characterization of tetracalcium aluminoferrite and ii) hydration studies of selected phases and mixtures.

The writing up of this Thesis has ended by July 20th, 2015.

4.1. Dicalcium silicate.

4.1.1. Synthesis and sample characterization of dicalcium silicate.

Stoichiometric C_2S has five polymorphs, see Figure 1.2, (Mumme et al. 1995), γ , β , α'_L , α'_H and α . An important aim of this thesis has been to prepare and to study high temperature polymorphs of dicalcium silicate metastabilized at room temperature.

Some solid solutions were tested for the stabilization of the high temperature polymorphs in the dicalcium silicate samples by using different dopants (articles #1 and #2). However, some compositions were not achieved.

Firstly, $Ca_{2-x}Al_xSi_{1-x}Al_{2x}O_4$ and $Ca_2Si_{1-2x}Al_{2x}O_{4-x}\square_x$ compositions were tested in order to stabilize the β polymorph (article #1) using aluminum as dopant. It was reported that for tricalcium silicate, C_3S , (Porrás-Vázquez et al. 2007) the aluminum doping was achieved by substitution of calcium and silicon sites by

Ana María Cuesta García

aluminum, $\text{Ca}_{3-x/2}\text{Al}_{x/2}(\text{Si}_{1-x/2}\text{Al}_{x/2}\text{O}_4)\text{O}$. However, for the C_2S samples, the similar mechanism was not achieved as all attempts to synthesize $\text{Ca}_{2-x}\text{Al}_x\text{Si}_{1-x}\text{Al}_{2x}\text{O}_4$ series were not successful. Nevertheless, $\text{Ca}_2\text{Si}_{1-2x}\text{Al}_{2x}\text{O}_{4-x}\square_x$ solid solution was successfully prepared. Table 1 in article #1 gives weight fractions of all phases as well as the refined unit cell volumes of the series. The volume increases along the series as expected, as Al^{3+} has a larger ionic radius than Si^{4+} . So, this result confirms the partial substitutions of silicon by aluminum. In addition, the limit of the series has to be close to $x=0.014$ because the $x=0.030$ sample presented some amount of C_3A phase.

Then, for stabilizing the α'_H -polymorph (article #2), boron oxide and sodium oxide were used as dopants due to the fact that previous studies reported that borax stabilized α'_H -form in a cement matrix (Cuberos et al. 2010). The first issue to be clarified in the following boron-containing solid solutions was to unravel if the borate group was tetrahedral BO_4^{5-} or planar-triangular BO_3^{3-} . Firstly, $\text{Ca}_{2-x}\text{Na}_x(\text{SiO}_4)_{1-x}(\text{BO}_3)_x$ solid solution ($x=0.00-0.25$) was successfully prepared. This series was designed for stabilizing dicalcium silicate with planar BO_3^{3-} anions. Figure 3b (in article #2), shows the intensities of their vibration bands, close to 1250 cm^{-1} that confirmed the presence of BO_3^{3-} units in this sample. Moreover, Table 2 (in article #2) gives RQPA of this series. The first result shown in this table is the absence of free calcium oxide along this series. A second very relevant result is that high temperature polymorphs of C_2S , i.e. β - and α'_H - C_2S , are stabilized as x increases, as expected. For instance, β - C_2S was present between $x=0.00$ and $x=0.20$. Otherwise, α'_H - C_2S appeared from $x=0.025$ up to $x=0.25$, being the last composition a single phase. Finally, it can be seen that samples with larger x values presented higher FWHM values (Figure 7 in article #2). This behavior may be due to small (variable) particle sizes and/or microstrain evolution.

Moreover, $\text{Ca}_{2-x}\text{B}_x(\text{SiO}_4)_{1-x}(\text{BO}_4)_x$ ($0\leq x\leq 0.20$) series was also prepared. In this case only boron oxide was added as dopant. This mechanism was based on

4. Results and discussion

substitution of tetrahedral SiO_4^{4-} groups by tetrahedral BO_4^{5-} units with the boron substitution of calcium for charge compensation. ATR-FTIR infrared spectra were also performed and Figure 3a (article #2) shows the ATR-FTIR infrared spectra of all the members of this series (up to $x=0.10$). These measurements show bands close to 1000 cm^{-1} which correspond to BO_4^{5-} stretching vibrations. Furthermore, tiny signals from 1150 to 1350 cm^{-1} , corresponding to BO_3^{3-} (or similar) units, are also observed (Heyns et al. 1990, Tukia et al. 2005). However, this could be due to the fact that BO_3^{3-} units can be locally formed where boron cations substitute calcium atoms as boron is much smaller than calcium. In addition, a large displacement within the site was expected which might have led to the formation of a BO_3^{3-} -type groups. Taking all these results into account, it can be affirmed that boron stabilizes high temperature polymorphs by substituting silicon units as BO_4^{5-} and calcium cations by B^{3+} at the same time. Moreover, Table 2 (in article #2) gives RQPA for all members.

Finally, $\text{Ca}_{2-x/2}\square_{x/2}(\text{SiO}_4)_{1-x}(\text{BO}_3)_x$, $\text{Ca}_2(\text{SiO}_4)_{1-x}(\text{BO}_3)_x\text{O}_{x/2}$ and $\text{Ca}_{2-3x}\text{B}_{2x}\text{Na}_x(\text{SiO}_4)_{1-x}(\text{BO}_4)_x$ compositions were also tested in order to check other possible substitution mechanisms for the case of boron and, in some cases, sodium. However, all members of these series contained large amounts of free calcium oxide and/or other secondary phases which indicated that these solid solutions were not formed (see Table 2 in article #2).

$\text{Ca}_2\text{Si}_{0.972}\text{Al}_{0.028}\text{O}_{3.986}\square_{0.014}$ and $\text{Ca}_{1.85}\text{Na}_{0.15}(\text{SiO}_4)_{0.85}(\text{BO}_3)_{0.15}$ were selected to further study of β and α'_H polymorphs, respectively.

On the one hand, $\beta\text{-C}_2\text{S}$ with formula (article #1), $\text{Ca}_2\text{Si}_{0.972}\text{Al}_{0.028}\text{O}_{3.986}\square_{0.014}$, was synthesized by sintering reaction using high purity oxides and carbonates as starting materials: CaCO_3 (99.95%-100.05% from Alfa Aesar), SiO_2 (99.7% from ABCR) and $\gamma\text{-Al}_2\text{O}_3$ (99.999% from Alfa Aesar). Raw mixtures were ground during 30 min in a planetary ball mill and preheated at 1050°C for 4 hours. The resulting powders were reground, pelletized and a second

thermal treatment was carried out at 1500°C for 6 hours before being slowly cooled.

On the other hand, $\alpha'_H\text{-C}_2\text{S}$, $\text{Ca}_{1.85}\text{Na}_{0.15}(\text{SiO}_4)_{0.85}(\text{BO}_3)_{0.15}$, was prepared using a similar experimental procedure (article #2). Dopants were added as $\text{Na}_2\text{B}_4\text{O}_7 \cdot 10\text{H}_2\text{O}$ (100% from Aldrich) and Na_2CO_3 (99.999% from Aldrich). Raw mixtures were ground for 10 min in an agate mortar, and preheated at 1000°C for 4 hours. After cooling, the mixtures were milled during 1 h in a planetary ball mill. The resulting powders were pelletized and a second thermal treatment was carried out at 1300°C for 30 min and quenched from high temperature with an air flow.

In a second stage, a similar synthetic method was employed to obtain 100 g of each sample for the hydration studies. In this case, the raw material was ground in a Micro-deval machine with a cylinder container and steel balls and was pelletized (600 mm diameter and 1000 MPa). The heating and cooling conditions were those described above.

The Rietveld quantitative phase analyses for both samples are shown in Table 4.1. It is important to underline that these thermo-mechanical treatments at high temperature ensured the absence of free lime, CaO, showing that both reactions were complete. After this initial characterization it is important to confirm that these solid solutions have been properly formed.

Table 4.1. Rietveld quantitative phase analyses for $\text{Ca}_{1.85}\text{Na}_{0.15}(\text{SiO}_4)_{0.85}(\text{BO}_3)_{0.15}$ and $\text{Ca}_2\text{Si}_{0.972}\text{Al}_{0.028}\text{O}_{3.986}\square_{0.014}$

	$\gamma\text{-C}_2\text{S}(\text{wt}\%)$	$\beta\text{-C}_2\text{S}(\text{wt}\%)$	$\alpha'_H\text{-C}_2\text{S}(\text{wt}\%)$
$\text{Ca}_{1.85}\text{Na}_{0.15}(\text{SiO}_4)_{0.85}(\text{BO}_3)_{0.15}$	-	9.9(2)	90.1(1)
$\text{Ca}_2\text{Si}_{0.972}\text{Al}_{0.028}\text{O}_{3.986}\square_{0.014}$	1.0(1)	99.0(1)	-

The β -form was synthesized with nominal formula $\text{Ca}_2\text{Si}_{0.972}\text{Al}_{0.028}\text{O}_{3.986}\square_{0.014}$ where \square stands for vacancies in the structure. The most

4. Results and discussion

important point was to check the presence of those vacancies. In order to do that, both samples $\text{Ca}_2\text{Si}_{0.972}\text{Al}_{0.028}\text{O}_{3.986}\square_{0.014}$ and $\text{Ca}_{1.85}\text{Na}_{0.15}(\text{SiO}_4)_{0.85}(\text{BO}_3)_{0.15}$, the later without vacancies, were studied by thermogravimetric analysis to evaluate the influence of Al-substitution. In this study, the increase in vacancy concentration due to the incorporation of water in the structure was checked. Water uptake depends on the available oxygen vacancies in the structure and the differences are expected depending on the vacancy contents. The thermogravimetric measurements recorded under humidified air showed reproducible curves on both cooling and heating cycles, see Figure 4.1. The curve of $\text{Ca}_2\text{Si}_{0.972}\text{Al}_{0.028}\text{O}_{3.986}\square_{0.014}$ shows the typical behavior of a proton conducting material with weight increase upon cooling due to water uptake and the formation of protonic defects. For these samples the water uptake increases with the oxygen vacancies content from 0.09 wt% for $\text{Ca}_{1.85}\text{Na}_{0.15}(\text{SiO}_4)_{0.85}(\text{BO}_3)_{0.15}$ (no vacancies) to 0.22 wt% for $\text{Ca}_2\text{Si}_{0.972}\text{Al}_{0.028}\text{O}_{3.986}\square_{0.014}$ due to the large concentration of oxygen vacancies. Consequently, these results confirmed that Si was being substituted by Al in the dicalcium silicate framework and that this substitution induced the presence of oxygen vacancies.

Finally, an impedance spectroscopy study was carried out for the $\text{Ca}_2\text{Si}_{0.972}\text{Al}_{0.028}\text{O}_{3.986}\square_{0.014}$ sample. This study finally confirmed the existence of proton conductivity in this material due to the presence oxygen vacancies in comparison with $\text{Ca}_{1.85}\text{Na}_{0.15}(\text{SiO}_4)_{0.85}(\text{BO}_3)_{0.15}$, as standard (no vacancies). See Figures 6 and 7 in article #1.

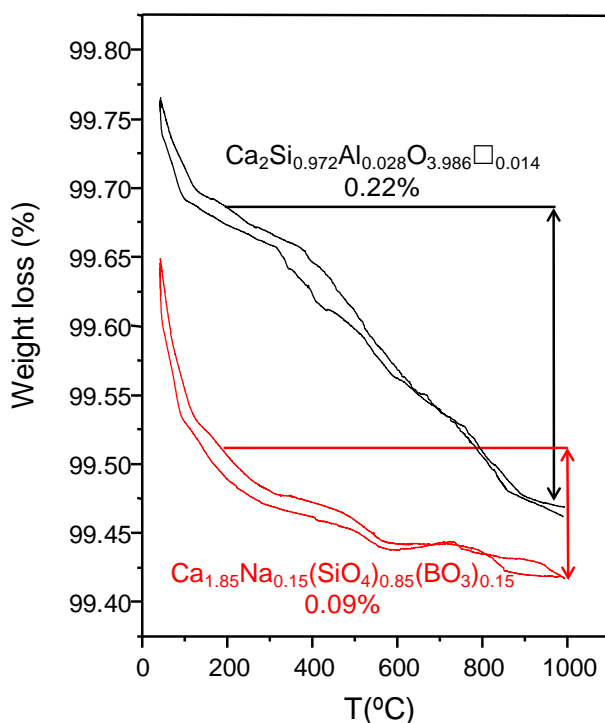


Figure 4.1. Thermogravimetric curves for $\text{Ca}_2\text{Si}_{0.972}\text{Al}_{0.028}\text{O}_{3.986}\square_{0.014}$ and $\text{Ca}_{1.85}\text{Na}_{0.15}(\text{SiO}_4)_{0.85}(\text{BO}_3)_{0.15}$ samples performed under humidified air from RT to 1000°C.

On the other hand, the nature of boron anion in $\alpha'_H\text{-C}_2\text{S}$ sample, which belongs to $\text{Ca}_{2-x}\text{Na}_x(\text{SiO}_4)_{1-x}(\text{BO}_3)_x$ series, was firstly studied. Concretely, as it has been explained previously for this solid solution, we wanted to unravel if the borate group was tetrahedral BO_4^{5-} or planar-triangular BO_3^{3-} . Figure 3b (in article #2), shows the intensities of their vibration bands, close to 1250 cm^{-1} that confirmed the presence of BO_3^{3-} units in this sample. Moreover, Figure 4.2 displays the ^{11}B ($I = 3/2$) MAS-NMR spectra for $\text{Ca}_{1.85}\text{Na}_{0.15}(\text{SiO}_4)_{0.85}(\text{BO}_3)_{0.15}$. This figure also shows, as an inset, the ^{11}B MAS-NMR spectra (experimental and calculated) for crystalline $\text{B}(\text{OH})_3$ standard taken from Klochko et al. (2009). The $\text{Ca}_{1.85}\text{Na}_{0.15}(\text{SiO}_4)_{0.85}(\text{BO}_3)_{0.15}$ spectrum shows three maxima arising from a unique trigonal-planar BO_3^{3-} group due to the quadrupolar splitting (Silver and Bray

1958). The ^{11}B MAS-NMR spectra for $\text{Ca}_{1.85}\text{Na}_{0.15}(\text{SiO}_4)_{0.85}(\text{BO}_3)_{0.15}$ sample is very similar to that of $\text{B}(\text{OH})_3$ and fully consistent with the presence of trigonal BO_3^{3-} groups. The central signal is formed by two maxima at 19 and 8 ppm and a small shoulder at -2 ppm, see Figure 4.2.

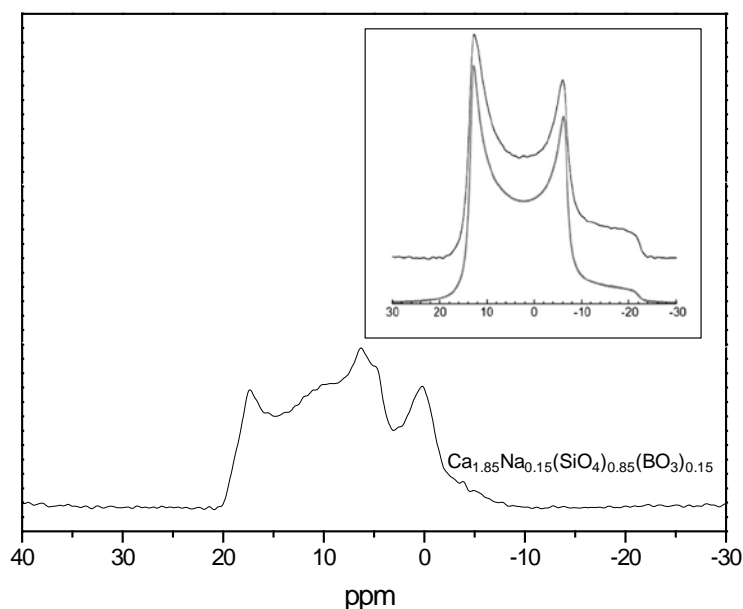


Figure 4.2. ^{11}B ($I = 3/2$) MAS-NMR spectra for $\text{Ca}_{1.85}\text{Na}_{0.15}(\text{SiO}_4)_{0.85}(\text{BO}_3)_{0.15}$. Inset: ^{11}B MAS-NMR spectra (experimental and calculated) for crystalline $\text{B}(\text{OH})_3$ (adapted from Klochko et al. 2009, Copyright (2009), with permission from Elsevier).

4.1.2. Dicalcium silicate structural study.

To study, $\beta\text{-C}_2\text{S}$ polymorph, $\text{Ca}_2\text{Si}_{0.972}\text{Al}_{0.028}\text{O}_{3.986}\square_{0.014}$, was selected as it contains 99.0(1) wt% of β -dicalcium silicate (see Table 4.1). Rietveld refinements were performed by refining only the overall parameters including scale factors. However, atomic parameters were not finally optimized and the powder pattern were analyzed using the crystal structure reported by Mumme et al. (1995) due to the fact that the final Rietveld disagreement factors were low enough ($R_F = 2.2\%$). Figure 4.3(a) gives the Rietveld fit of this sample. The final refined unit cell

parameters were $a=5.5127(1)$ Å, $b=6.7586(1)$ Å, $c=9.2366(2)$ Å, $\beta=346.42^\circ$ (2) and $V=346.42(2)$ Å³.

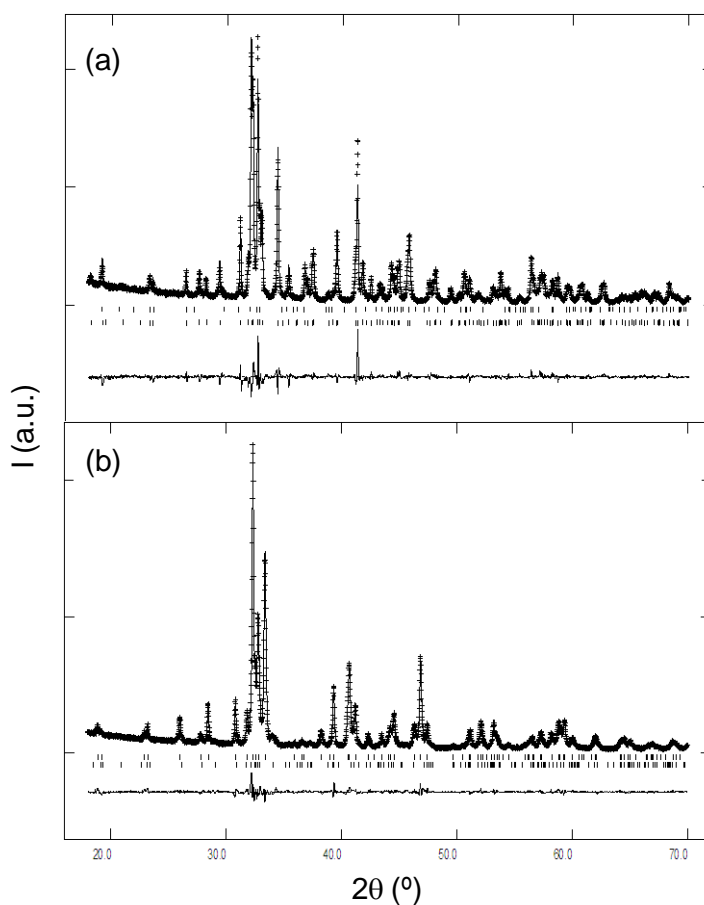


Figure 4.3. LXPDP Rietveld plots ($\lambda=1.5406$ Å) for (a) $\text{Ca}_2\text{Si}_{0.972}\text{Al}_{0.028}\text{O}_{3.986}\square_{0.014}$ using the crystal structure reported by Mumme et al. (1995) for $\beta\text{-C}_2\text{S}$ and (b) $\text{Ca}_{1.85}\text{Na}_{0.15}(\text{SiO}_4)_{0.85}(\text{BO}_3)_{0.15}$ sample using the crystal structure reported here for $\alpha'_\text{H}\text{-C}_2\text{S}$.

$\text{Ca}_{1.85}\text{Na}_{0.15}(\text{SiO}_4)_{0.85}(\text{BO}_3)_{0.15}$ composition was selected to further study the crystal structure of room-temperature stabilized $\alpha'_\text{H}\text{-C}_2\text{S}$. This choice was based on the trade off both sharp diffraction peaks and the highest content of α'_H -polymorph (article #2). This sample contains 90.1(1) wt% of the α'_H polymorph (see Table 4.1)

4. Results and discussion

determined by Rietveld method. The crystal structure description reported by Mumme et al. (1995) was used as a starting model for the Rietveld refinement. After that, the atomic position parameters and ADPs were optimized and the nominal cation stoichiometry was included by substitution of Ca^{2+} by Na^+ and Si^{4+} by B^{3+} . Refined atomic positional parameters and isotropic ADPs are given in Table 4.2. As a result, the improvement of the quality of the fit was significant with a reduction of R_{WP} from 10.8% to 6.5% and $R_{\text{F}}(\alpha'_{\text{H}}\text{-C}_2\text{S})$ from 4.1% to 2.4%. Figure 4.3(b) gives the Rietveld plot for the final refinement. The final refined unit cell parameters were $a=6.8432(2)$ Å, $b=5.4555(1)$ Å, $c=9.2346(2)$ Å and $V=344.76(2)$ Å³.

Table 4.2. Final (refined) atomic parameters (positional coordinates and isotropic ADPs) for $\text{Ca}_{1.85}\text{Na}_{0.15}(\text{SiO}_4)_{0.85}(\text{BO}_3)_{0.15}$

Atom	Wyckoff position	Occupation factors	x	y	z	ADPs / Å ²
Ca1	8d	0.4625	0.3270(2)	0.2850(8)	0.5702(2)	0.0260(7)
Na1	8d	0.0375	0.3270(-)	0.2850(-)	0.5702(-)	0.0260(-)
Ca2	8d	0.4625	0.9912(2)	0.2709(9)	0.2938(1)	0.0107(6)
Na2	8d	0.0375	0.9912(-)	0.2709(-)	0.2938(-)	0.0107(-)
O1	8d	0.5000	1.0027(7)	0.3247(11)	0.5427(5)	0.0374(22)
O2	8d	0.5000	0.7555(8)	0.0258(10)	0.7086(7)	0.0055(20)
O3	8d	0.5000	0.6517(7)	0.1838(13)	0.4439(5)	0.0279(19)
O4	8d	0.5000	0.6973(9)	0.4868(13)	0.6600(7)	0.0182(23)
Si1	4c	0.8500	0.7745(3)	0.2500	0.5901(3)	0.0175(7)
B	4c	0.1500	0.7745(-)	0.2500	0.5901(-)	0.0175(-)

4.2. Ye'elimité.

4.2.1. Ye'elimité synthesis.

$\text{Ca}_4[\text{Al}_6\text{O}_{12}]\text{SO}_4$, stoichiometric ye'elimité, was synthesized following a similar methodology reported by Winnefeld and Barlag (2010) using CaCO_3 (99.95%, Alfa Aesar), Al_2O_3 (99.997%, Alfa Aesar) and $\text{CaSO}_4 \cdot 2\text{H}_2\text{O}$ (ground

Ana María Cuesta García

natural single-crystal from Málaga). The raw mixture was prepared with the amounts of starting materials needed for obtaining approximately 8 g of ye'elimite. This mixture was ground for 1 hour in an agate mortar with ethanol. The resulting powders were pelletized (20 mm diameter) and heated at 1300°C for 4 hours. The sample was cooled by turning off the furnace (article #3).

Doped ye'elimite, with a nominal composition of $\text{Ca}_{3.8}\text{Na}_{0.2}\text{Al}_{5.6}\text{Fe}_{0.2}\text{Si}_{0.2}\text{O}_{12}\text{SO}_4$ was synthesized with the same methodology. Dopants were added as Fe_2O_3 (99.945%, Alfa Aesar), SiO_2 (99.56%, ABCR) and Na_2CO_3 (99.999%, Sigma Aldrich). This composition was chosen based on a previous work (Alvarez-Pinazo et al. 2012) focused on belite calcium sulfoaluminate clinkers. They prepared active BCSA clinkers doping with B and Na and by SEM-EDX and they determined the composition of the pseudocubic ye'elimite stabilized in their clinkers. It is important to highlight that the temperature was reduced 50°C in comparison to the synthesis temperature for stoichiometric ye'elimite, due to the presence of mainly iron oxide in the reaction medium. The heating procedure of this sample was followed by quenching from high temperature with an air flow (article #4)

Moreover, these synthetic procedures were adapted to obtain around 120 g of each sample for the hydration studies, calorimetric studies and so on. In this case, the raw material was ground in a Micro-deval machine with a cylinder container and steel balls and was pelletized (600 mm diameter and 1000 MPa). The heating and cooling conditions were the same described above.

On the one hand, for stoichiometric ye'elimite, the synthesis yielded a sample consisting of 90.3(1) wt% ye'elimite with minor amounts impurities: 1.2 wt% of $\text{Ca}_3\text{Al}_2\text{O}_6$ (C_3A), 4.4(2) wt% of CaAl_2O_4 (CA), and 4.0(2) wt% of $\text{Ca}_{12}\text{Al}_{14}\text{O}_{33}$ (C_{12}A_7). Furthermore, the thermodiffraction study in open atmosphere showed the crystallization on heating of a small amount of CaCO_3 . For that reason, a minor amount of amorphous calcium compound such as $\text{Ca}(\text{OH})_2$,

CaO or CaCO₃, could also be present in the sample. On the other hand, the synthesis for doped or solid solution ye'elime yielded a single phase sample. Figure 4.4 shows the raw powder patterns of both polymorphs.

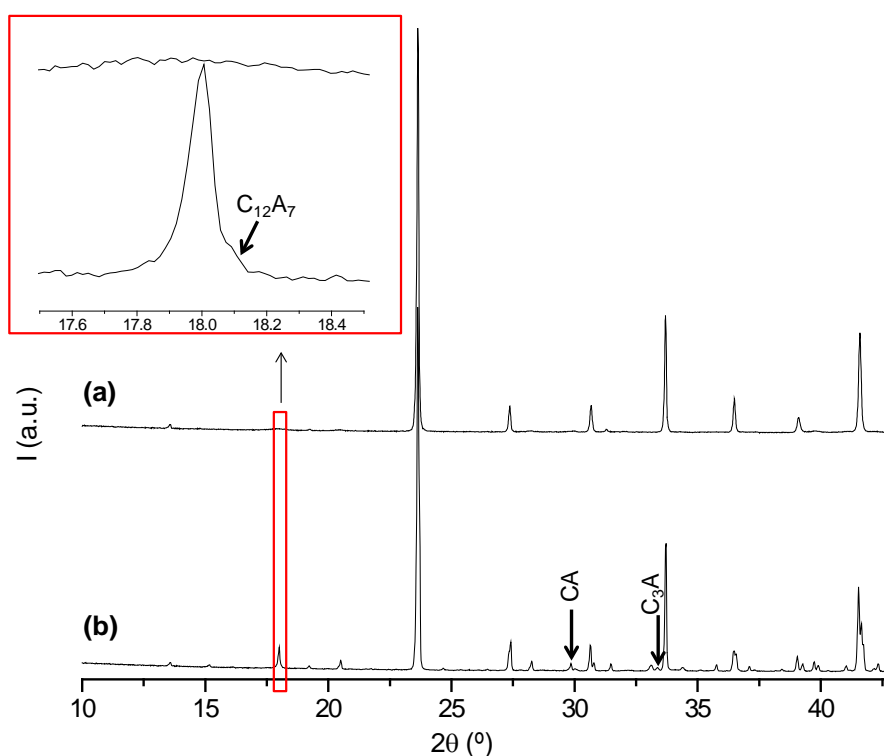


Figure 4.4. Selected range of the LXRPD ($\lambda=1.5406 \text{ \AA}$) raw patterns for (a) $\text{Ca}_{3.8}\text{Na}_{0.2}\text{Al}_{5.6}\text{Fe}_{0.2}\text{Si}_{0.2}\text{O}_{12}\text{SO}_4$ and (b) $\text{Ca}_4[\text{Al}_6\text{O}_{12}]\text{SO}_4$. Main peaks of minor phases have been labeled. Inset details enlarged the low-angle range.

4.2.2. Ye'elime structural study.

The first step in the study of ye'elime samples has been the determination of their crystal structures because as we have discussed in the introduction section (1.2.2.1) there was controversy about the crystal structure of stoichiometric ye'elime at room temperature. It is important to highlight that due to the difficulty of this study a joint refinement was performed by using Cu-K α_1 LXRPD and NPD

data for the stoichiometric sample, $\text{Ca}_4[\text{Al}_6\text{O}_{12}]\text{SO}_4$. Firstly, as the recorded pattern clearly contains splitted diffraction peaks the cubic sodalite structure was not tested here. Then, the tetragonal structural description reported by Peixing et al. (1992) was used but the fits were so poor that this symmetry choice had to be dismissed. For this reason, orthorhombic crystal structure description reported by Calos et al. (1995) was finally used as a starting model for the Rietveld refinement. Table 4.3. gives the starting and final disagreement values for the joint Rietveld refinements. Moreover, Figure 1 in article #3 shows the final LXRPD and NPD Rietveld plots using the refined orthorhombic structure. Finally, the following unit cell parameters were obtained, $a=13.0356(7)$ Å, $b=13.0350(7)$ Å and $c=9.1677(2)$ Å, yielding a cell volume of $1557.78(6)$ Å³. Table 4.4 shows the final refined atomic parameters and the isotropic ADPs which were refined independently.

Table 4.3. Disagreement factors for the Rietveld refinements of LXRPD, NPD, SXRPD and HT-LXRPD patterns for stoichiometric and doped ye'elimite samples by using previously-reported structures and after atomic parameter refinement.

	T/°C	Orthorhombic		Cubic Structure		Revised	
		Structure (a)		(b)		Structure	
		R _{WP} /%	R _F /%	R _{WP} /%	R _F /%	R _{WP} /%	R _F /%
Stoichiometric(LXRPD)*	26	17.1	14.6			13.6	5.5
Stoichiometric (NPD)*	26	6.5	8.3			5.4	4.7
Doped (SXRPD)	26			15.4	16.9	11.0	7.9
Stoichiometric (LXRPD)	800			11.4	6.5	9.9	3.2
Doped (LXRPD)	800			6.6	4.4	5.8	3.0

(a) Calos et al. 1995; (b) Kurokawa et al. 2004

*joint refinement

It is important to bear in mind that this study was corroborated by using atomistic calculations and several conclusions could be deduced. Firstly, the most stable found phase was the orthorhombic Pcc2 structure, in agreement with our experimental results (see article #3). Secondly, the ideal cubic structure is less stable than the orthorhombic phase at room temperature. Finally, it is possible that a pressure-induced transition of ye'elimite from orthorhombic to cubic polymorph

4. Results and discussion

may occur. The phase transition with temperature for ye'elimite has been also studied in this work and it will be discussed in the next section.

Table 4.4. Refined positional coordinates and isotropic ADPs for stoichiometric ye'elimite at room temperature in the *Pcc2* space group.

Atom	x	y	z	ADPs/ Å ²
S1	0.2691(7)	0.2693(7)	0.9654(10)	0.028(3)
O1	0.6790(12)	0.2645(16)	0.6111(12)	0.099(8)
O2	0.8260(8)	0.2042(9)	0.4666(15)	0.033(4)
O3	0.7590(15)	0.3781(7)	0.4296(22)	0.103(8)
O4	0.6598(10)	0.2280(14)	0.3507(17)	0.073(7)
Ca1	0.0627(11)	0.2495(14)	0.1554(17)	0.020(4)
Ca2	0.2549(14)	0.9417(12)	0.2945(16)	0.011(4)
Ca3	0.2591(16)	0.5301(11)	0.2196(13)	0.035(4)
Ca4	0.4910(9)	0.2548(13)	0.2196(13)	0.013(3)
Al1	0.5000	0.5000	0.2242(15)	0.005(4)
Al2	0.5000	0.0000	0.2466(12)	0.016(8)
Al3	0.0000	0.0000	0.2292(15)	0.021(5)
Al4	0.0000	0.5000	0.2011(11)	0.026(8)
Al5	0.6269(7)	0.1202(7)	0.0036(10)	0.005(5)
Al6	0.1238(6)	0.6282(7)	0.9519(8)	0.007(6)
Al7	0.3708(6)	0.6293(7)	0.9760(13)	0.012(3)
Al8	0.1233(7)	0.8793(7)	0.9787(13)	-0.001(3)
O5	0.3983(10)	0.2439(6)	0.4338(11)	0.027(6)
O6	0.5628(6)	0.4028(5)	0.1320(13)	0.013(5)
O7	0.5457(8)	0.1035(5)	0.1446(11)	0.032(5)
O8	0.7546(5)	0.5910(9)	0.5102(9)	-0.004(3)
O9	0.5957(5)	0.4375(6)	0.8201(13)	0.011(5)
O10	0.8984(5)	0.4459(7)	0.7976(8)	0.08(3)
O11	0.7539(6)	0.9027(10)	0.5520(10)	0.018(4)
O12	0.8916(5)	0.0345(7)	0.8323(14)	0.013(4)
O13	0.6069(5)	0.0378(8)	0.8490(11)	0.024(5)
O14	0.1050(11)	0.2433(6)	0.4026(11)	0.027(6)
O15	0.9646(7)	0.1066(5)	0.1224(14)	0.014(4)
O16	0.9571(7)	0.3947(5)	0.0996(8)	-0.001(3)

For the doped sample, $\text{Ca}_{3.8}\text{Na}_{0.2}\text{Al}_{5.6}\text{Fe}_{0.2}\text{Si}_{0.2}\text{O}_{12}\text{SO}_4$, the cubic crystal structure recently reported for stoichiometric ye'elimite at 800°C (Kurokawa et al.

2014), space group $I\bar{4}3m$, was used as a starting model for the Rietveld refinement due to the fact that the recorded pattern clearly contains the diffraction reflections of the cubic sodalite structure. The cubic crystal structure reported by Saalfeld and Depmeier (1972) was previously tested but was rejected since the disagreement values were much higher than those obtained with the structure reported by Kurokawa et al. (2014), see Table 2 in article #4. SXRPD data, obtained in the X-ray powder diffraction station of ALBA with a MAD detector system, which is especially suited for high-resolution experiments, were used to revise the structure of the doped sample. The final Rietveld disagreement factors of SXRPD data of doped ye'elimite are also shown in Table 4.3. Moreover, Figure 1 in article #4 shows the SXRPD Rietveld plot using the refined cubic structure.

For the doped ye'elimite, the refined unit cell parameter was $a=9.1970(1)$ Å and the cell volume was $777.93(2)$ Å³. The anisotropic ADPs were also optimized. Table 4.5 shows the refined atomic parameters (positional coordinates and anisotropic ADPs) for the RT cubic structure of doped ye'elimite. It is important to point out that foreign elements were excluded from the crystal structural study as they did not make any improvement in the refinement due to their high degree of disorder.

Table 4.5. Final (refined) atomic parameters (positional coordinates and anisotropic ADPs) for doped ye'elimite at room temperature.

Atom	Ca1	Al1	S1*	O1	O2*
Wyckoff position	8c	12d	2a	24g	24g
occupation factor	1	1	1	1	0.3333
x	0.2944(1)	0.2500	0.0000	0.3479(2)	0.1129(5)
y	0.2944 (1)	0.5000	0.0000	0.3479(2)	0.1129(5)
z	0.2944 (1)	0.0000	0.0000	0.0533(3)	0.0136(16)
u ₁₁	0.096(1)	0.007(1)	0.087(2)	0.028(1)	0.139(7)
u ₂₂	0.096(1)	0.015(1)		0.028(1)	
u ₃₃	0.096(1)	0.015(1)		0.034(2)	
u ₁₂	0.069(2)	0.000		0.009(1)	
u ₁₃	0.069(2)	0.000		0.007(1)	
u ₂₃	0.069(2)	0.000		0.007(1)	

*isotropic displacement parameters

It is important to highlight that there are some issues which point towards a pseudocubic structure for this sample instead of cubic. That fact will be better explained with the thermodiffractometric study.

4.2.3. Thermodiffractometric study and phase transition

A thermodiffractometric study, up to 800°C, has been performed for both ye'elimites. Firstly, for stoichiometric ye'elimitite, we have studied in detail the low- to high-symmetry phase transition on heating previously reported by Depmeier (1983) without specific details. Figure 4.5 gives a selected view of the patterns at different temperatures. This figure clearly shows the transition of the orthorhombic form to a higher symmetry polymorph the latter being cubic above 400°C. The unit cell parameter behavior observed during the phase transition, given in Figure 7 in article #3, is that expected for the evolution of a lower-symmetry phase due to long-range sulfate ordering to a higher-symmetry phase where sulfate anions display disorder, likely due to rotation.

Furthermore, a thermodiffractometric study for doped ye'elemite was also performed (article #4) up to 800°C. It is important to have in mind that doped ye'elimitite is cubic at room temperature and for this reason no phase transition would be expected. Moreover, all attempts to index the low temperature patterns with symmetry lower than cubic were unsuccessful as the observed splitted peaks at high angles were very small and only observable for some diffraction reflections. Figure 4.6 shows a selected range of the high temperature LXRPD patterns of doped ye'elimitite. However, although no phase transition was observed, Figure 4.6 display the sharpening of one of the cubic reflection (622) with temperature as an example. Moreover, changes in the widths of the diffraction peaks with temperature were clearly measured and were compared with silicon as cubic standard (see Figure 3, article #4). Those results showed that variation of FWHM of silicon peaks was negligible while the FWHM values of ye'elimitite peaks were

decreasing with increasing temperature. This behavior indicates that the symmetry of the RT form has to be lower than cubic, i.e. pseudocubic.

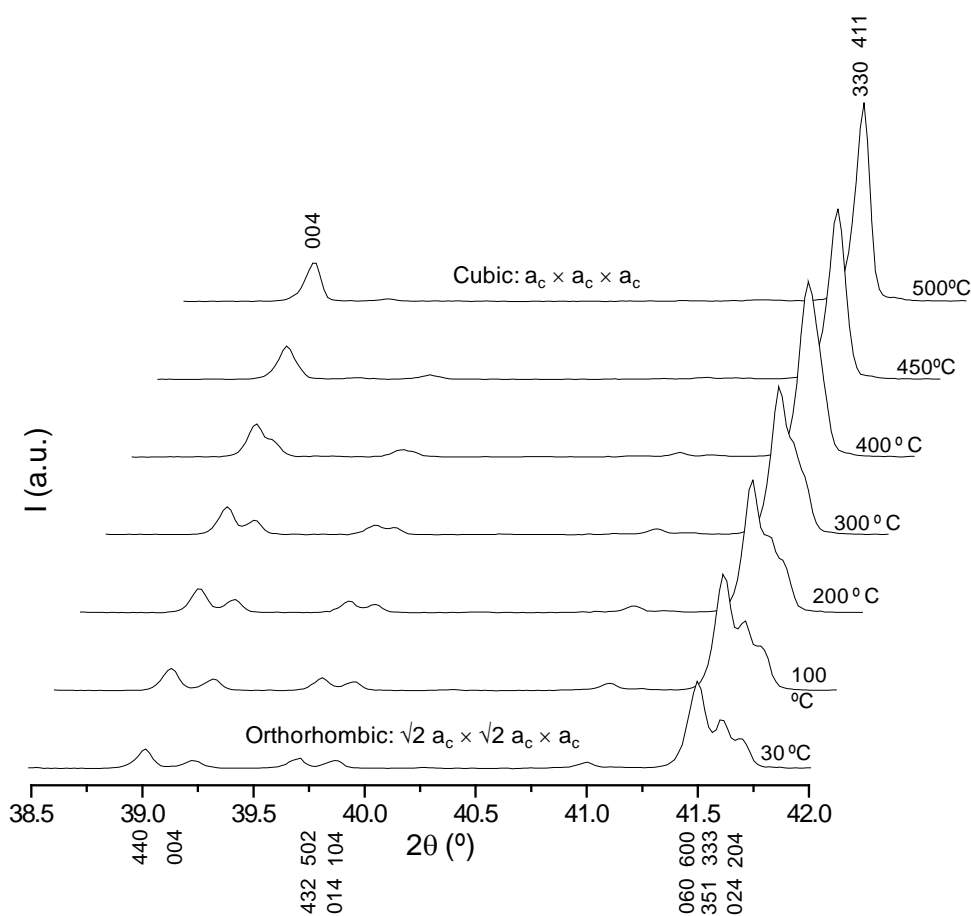


Figure 4.5. Temperature-dependence LXRPD ($\lambda=1.5406 \text{ \AA}$) patterns for stoichiometric ye'elimites shown over a selected range with Miller indexes displayed for the orthorhombic (bottom) and cubic (top) phases.

Both ye'elimites have also been studied by DSC and permittivity measurements. The phase transition for stoichiometric ye'elimites takes place close to 470 °C on cooling determined by DSC and permittivity studies. These results agree quite well with the reported value of 464°C (Depmeier 1988). Figure 4.7 shows a comparative of the permittivity study for both ye'elimites. The permittivity

4. Results and discussion

curve for doped ye'elimitite shows a phase transition close to 525°C, Figure 4.7. This result was not expected if the RT form is truly cubic. However, this signal in the DSC curve shows that RT form has a symmetry lower than cubic, i.e. pseudocubic, in full agreement with HT-LXRPD study.

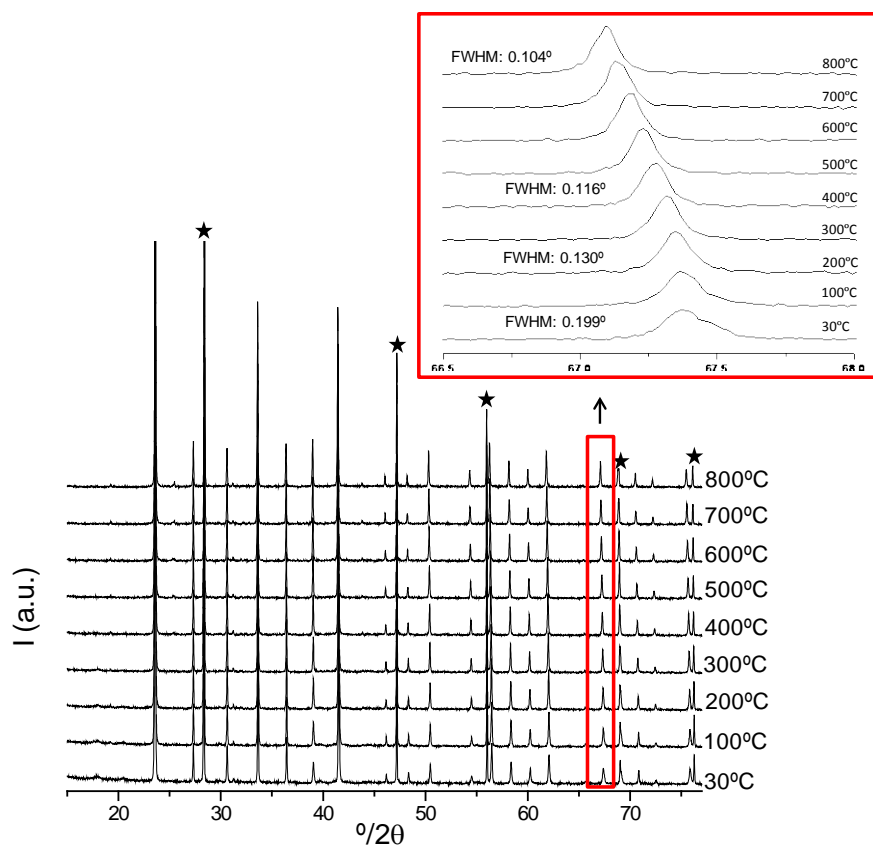


Figure 4.6. Selected region of the HT-LXRPD ($\lambda=1.5406 \text{ \AA}$) data for doped ye'elimitite. Stars indicate silicon reflections. Inset details the pseudocubic 622 reflection.

As a summary, this study has proved that stoichiometric ye'elimitite undergoes a cubic-to-orthorhombic phase transition at 470°C (on cooling) likely due to the freezing and spatial ordering of the sulfate anions which can be rotating

above the transition temperature. Moreover, doped ye'elimitite undergoes a related cubic-to-pseudocubic phase transition at 525°C also likely due to the freezing of the sulfate anions. However, the long-range ordering of the sulfate anions does take place, due to the presence of the dopants, avoiding the orthorhombic structure to develop. The difference in phase transition temperature between both polymorphs is likely due to the effect of the dopants which stabilize the static disorder of the sulfate anions within the cages.

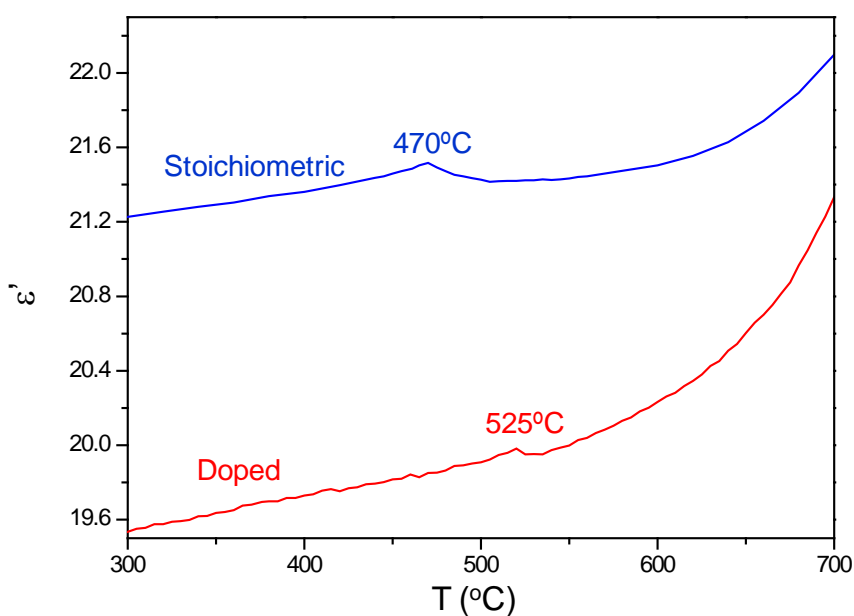


Figure 4.7. Permittivity signal for stoichiometric ye'elimitite and doped ye'elimitite.

4.2.4. HT-polymorphs of ye'elimitite: structural study.

Both ye'elimites were thoroughly studied at 800°C (article #4). Firstly, the pattern at 800°C of stoichiometric ye'elimitite was auto-indexed using DICVOL06 (Boultif and Louer 2004) in a cubic unit cell. The cubic structure was also verified by fitting the powder pattern with the cubic structure recently reported by Kurokawa et al. (2014). Table 4.3 shows the agreement factors obtained using both

4. Results and discussion

the published and refined structures. The final unit cell parameter obtained was $a=9.2497(1)$ Å.

The 800°C powder pattern for doped ye'elimite was also autoindexed using DICVOL06 (Boultif and Louer 2004) in a cubic unit cell. Figures of merit (De Wolff 1972) for this indexation were much higher than those obtained at RT (Table 1 in article #4). This is another indication that the HT-form is truly cubic. A Rietveld refinement of the 800°C pattern of doped ye'elimite was performed using the previously reported split-atom model for the sulfate anion (Kurokawa et al. 2014). The refinement in space group $I\bar{4}3m$ was very good and a proof of this fact was the low R-factors (see Table 4.3) and the flatness of the difference curve of the Rietveld plot (Figure 5 in article #4). The final refined unit cell parameter at 800°C was $a=9.2544(1)$ Å.

4.3. Synthesis of C_4AF .

Tetracalcium aluminoferrite (C_4AF) was prepared by mixing suitable amounts of $CaCO_3$ (99.95%, Alfa Aesar), Al_2O_3 (99.997%, Alfa Aesar) and Fe_2O_3 (99.945%, Alfa Aesar), to obtain approximately 5 g of sample. The raw mixture was ground for 5 minutes in an agate mortar and heated at 1000°C for 4 hours. After that, the powder was ground in an agate mortar and was pelletized. Finally, the pellets were heated at 1350°C for 4 hours (heating rate of 10 °C/min) followed by quenching from high temperature with an air flow (article #7).

This first synthesis of 5 grams of C_4AF was studied by LXRPD and the Rietveld method. The analysis of the sample was of 95.2(3) wt% of C_4AF with minor amounts of two crystalline phases: 2.6(3) wt% of Fe_2O_3 (hematite) and 2.2(3) wt% of $Ca_{12}Al_{14}O_{33}$ ($C_{12}A_7$). The derived unit cell parameters for C_4AF were: $a=5.5687(2)$ Å, $b=14.5250(7)$ Å, $c=5.3500(2)$ Å and $V=432.73(4)$ Å³.

In a second stage, this synthetic method was employed to obtain 50 g of sample for the hydration studies. In this case, the powder was ground in a Micro-deval machine with a cylinder container and steel balls for 45 min and was pelletized (600 mm diameter and 1000 MPa). The heating and cooling conditions were the same just described. This sample was studied by SXRPD and the Rietveld method. For this synthesis, the only additional phase was C_3A , 1.94(6) wt%. The derived unit cell parameters for C_4AF from SXRPD, were: $a=5.56638(4)\text{Å}$, $b=14.5227(1)\text{Å}$, $c=5.34835(4)\text{Å}$ and $V=432.354(8)\text{Å}^3$. Figure 4.8 shows the Rietveld plot for this sample. As the quality of the SXRPD was very high, we could optimize the Fe/Al ratio in the octahedral and tetrahedral sites (constrained to an overall Fe/Al ratio of 1.00). The resulting value was 0.746(2) of Fe occupancy at the octahedral site and therefore 0.254(2) of Fe occupancy at the tetrahedral site.

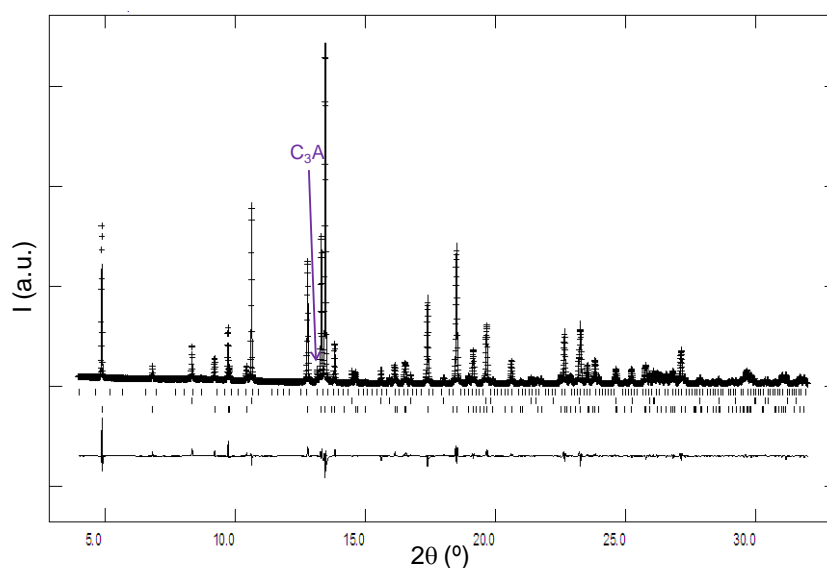


Figure 4.8. SXRPD Rietveld plot for C_4AF ($\lambda=0.6202(2)\text{Å}$). The tic marks are the allowed Bragg reflections. C_4AF : lower row, Quartz (internal standard): middle row and C_3A : upper row.

We are aware that different cooling rates could change Fe/Al distributions at these sites but to study the possible consequences of this variation on the hydration properties of C_4AF is not a target of this Thesis.

It is important to point out that the SXRPD Rietveld plot of the synthetic C_4AF (Figure 4.8) shows narrower reflections than C_4AF present in a Portland clinker (De la Torre, 2003). This fact indicates that the tetracalcium aluminoferrite found in a clinker matrix has smaller particle sizes. Moreover, the Fe/Al ratio of this phase can also be different in clinkers.

4.4. Application of the structural studies to the analysis of CSA and BCSA cements.

After the study of these revised crystal structures, dicalcium silicate and ye'elimite, they were used to perform RQPA of cements in order to prove the importance of choosing the best crystal structure description for each component.

Firstly, the refined orthorhombic structure of ye'elimite was used to describe a commercial CSA cement which contained large amounts of this phase. The R_F values from the Rietveld refinement of ye'elimite phase in CSA were 6.9% and 4.8% for the reported orthorhombic structure (Calos et al. 1995) and for the new revised structure, respectively. Moreover, the disagreement value for the whole pattern was 8.7% using the Calos et al. (1995) structure and 7.6% for the structure reported in this Thesis. Lower R_F values indicates that the structure description used fits better the experimental patterns yielding to more accurate results (article #3).

Secondly, the combination of the structural descriptions of α'_H-C_2S and doped-ye'elimite revised in this PhD Thesis were used to quantify these phases in an active BCSAF clinker (Álvarez-Pinazo et al. 2012) doped with 2 wt% B_2O_3 , added as borax. This study has not been previously published and it is original of this Thesis. Only the revised structure of α'_H-C_2S was used to perform the RQPA of an active BCSAF clinker in article #2. This clinker contains three main phases, α'_H-

C₂S, pseudocubic ye'elimite and tetracalcium aluminoferrite (see Table 4.6). Table 4.6 includes disagreement factors (R_F and R_{WP}) of the fits performed by using the revised crystal structure reported in this Thesis for α'_H-C₂S and pseudocubic ye'elimite and those obtained when crystal structures from bibliography are used, i.e. Mumme et al. (1995) for α'_H-C₂S and Saalfeld and Depmeier (1972) for ye'elimite. The lower R_F and R_{WP} values mean better fits and consequently more accurate RQPA.

Table 4.6. Rietveld quantitative phase analyses, expressed in weight percentages, for an active BCSAF clinker (Álvarez-Pinazo et al. 2012), using the refined structure descriptions obtained in this Thesis for α'_H-C₂S and doped-ye'elimite (upper row) and the Mumme et al. (1995) and Saalfeld and Depmeier (1972) (bottom row). R_{WP} and R_F for α'_H-C₂S and pseudocubic ye'elimite disagreement factors are also included.

α' _H -C ₂ S (wt%)	R _F (α' _H) (%)	Pseudocubic ye'elimite (wt%)	R _F (ye'elimite) (%)	C ₄ AF (wt%)	R _{WP} (%)
58.2(2)	4.4	31.2(1)	4.8	10.7(2)	4.6
53.7(2)	5.4	32.1(2)	6.6	14.2(2)	5.2

Figure 4.9 shows the LXRPD Rietveld plot of BCSAF clinker using the new revised structures. A similar study was done in article #2 but only the α'_H-C₂S revised structure was used (not ye'elimite) and for this reason the obtained disagreement values were not so good as in this new study.

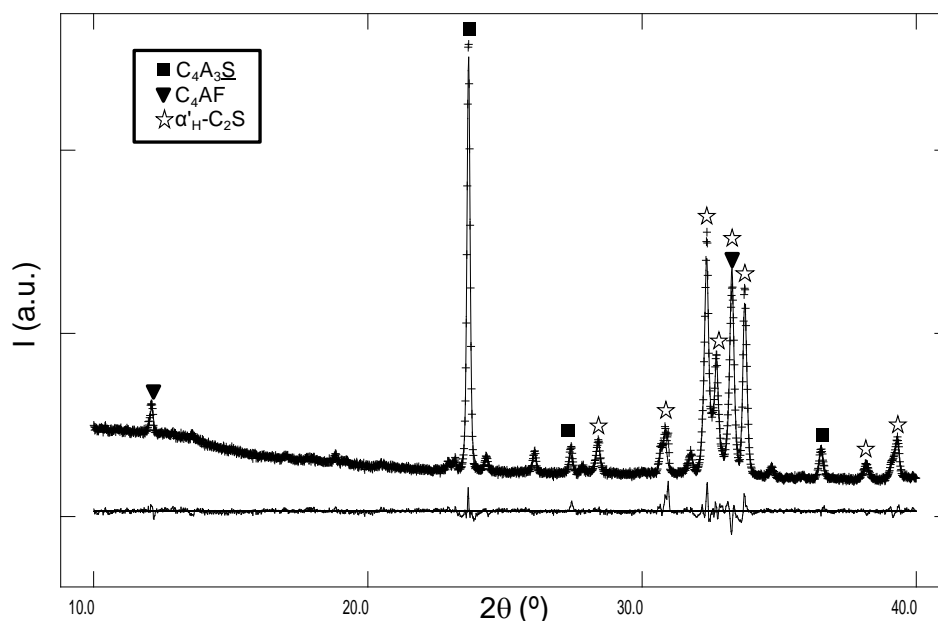


Figure 4.9. LXRPD Rietveld plot ($\lambda=1.5406 \text{ \AA}$) for active BCSAF (Álvarez-Pinazo et al. 2012) clinker using the crystal structures reported in this PhD Thesis for $\alpha'_H\text{-C}_2\text{S}$ and pseudocubic ye'elimate).

4.5. Hydration studies.

After the preparation and characterization of the anhydrous samples the next step is to better understand their hydration mechanisms. It is important to have in mind that the hydration of dicalcium silicate as a single phase is not an aim of this PhD work as it has been previously studied (Jelenic et al. 1978; Kim and Hong 2004; Benarchid et al. 2005) and it takes place at later ages (more than 28 days). The hydration mechanism of dicalcium silicate in the presence of ye'elimate has been studied in this PhD Thesis. However, the hydration mechanism of ye'elimate is of great interest and it has been one of the main objectives of this PhD work. This hydration study is mainly focus to understand the ye'elimate hydration mechanism as a function of ye'elimate polymorphism, water content, amount of

sulfate source and the presence of other phases. To finish this work, the hydration of tetracalcium aluminoferrite has also been studied. For this complex research, LXRPD and SXRPD have been employed. Moreover, these data have been correlated to calorimetric data, thermal analysis and SEM studies in some cases.

The sample preparation of hydrated samples was different depending on the XRPD set up. For the *in-situ* SXRPD study all the anhydrous mixtures were mixed with 15 wt% SiO₂ (99.56%, ABCR) as an internal standard (De la Torre et al. 2001). Pastes were *ex-situ* prepared by mixing sample with water and immediately loaded into glass capillaries of 0.5 mm of diameter with a syringe. The capillaries were sealed with grease. For the *ex-situ* LXRPD study, pastes were poured into hermetically closed Teflon® tubes in the form of cylinder until 1 day without movement. Then, the samples were demoulded and stored within demineralised water at 20°C. Pieces were taken out at specific hydration ages. The pastes were milled to fine powder in an agate mortar. In order to stop the hydration process, the procedure was filtration in a Whatman system with acetone twice and finally with ether. These samples were stored in a closed desiccator (without vacuum application) to avoid further hydration and/or carbonation.

It also important to clarify that different w/s ratios have been used in this Thesis. Firstly, the stoichiometric ye'elimite was selected in order to optimize/investigate the amount of water. On the hand one, this sample was measured with a w/s ratio (0.58) that corresponds to the stoichiometric amount of water according to reaction [1.8] with 10% of excess. Then, a next w/s ratio was selected that corresponds to the double of the previous value (1.16) to study the effect of larger water excess on hydration mechanisms. For the study of the hydration of all the samples of ye'elimite (including the samples with gypsum and anhydrite) the second criterion was selected in order to accelerate their hydration reactions. For the samples containing tetracalcium aluminoferrite or dicalcium silicate the water content was selected using a proportional ratio to the BCSAF cements according to Álvarez-Pinazo et al. (2012).

4.5.1. Hydration of ye'elinite

The hydration mechanism of stoichiometric ye'elinite (st-ye'elinite) was initially studied (article #5) at early ages by *in-situ* SXRPD with internal standard methodology to determine the ACn contents. Moreover, the pastes were also prepared into cylinders and studied with the external standard methodology, G-factor, at 2 and 7 days by *ex-situ* LXRPD. Different w/s ratios were used to study the influence on hydration of this parameter.

The stoichiometric ye'elinite was firstly studied with a w/s of 0.58 (st-C₄A₃S-0.58). It was clear that for this w/s ratio the dissolution rate was very slow, since up to 30 hours very small amount of ye'elinite was dissolved and there were not new crystalline hydrates. Figure 4.10(a) shows degree of reaction of C₄A₃S in these experimental conditions. After 2 days, ye'elinite was partially dissolved and the precipitation of small quantities of AFm and AFt were quantified. For longer hydration times, the formation of AFm is favored not only from ye'elinite reaction but also likely due to AFt dissolution. Figure 4.11 shows a selected range of the SXRPD and LXRPD raw patterns recorded at different hydration ages with peaks due to a given phase labeled (Table 3 in article #5 shows the RQPA results as a function of hydration time).

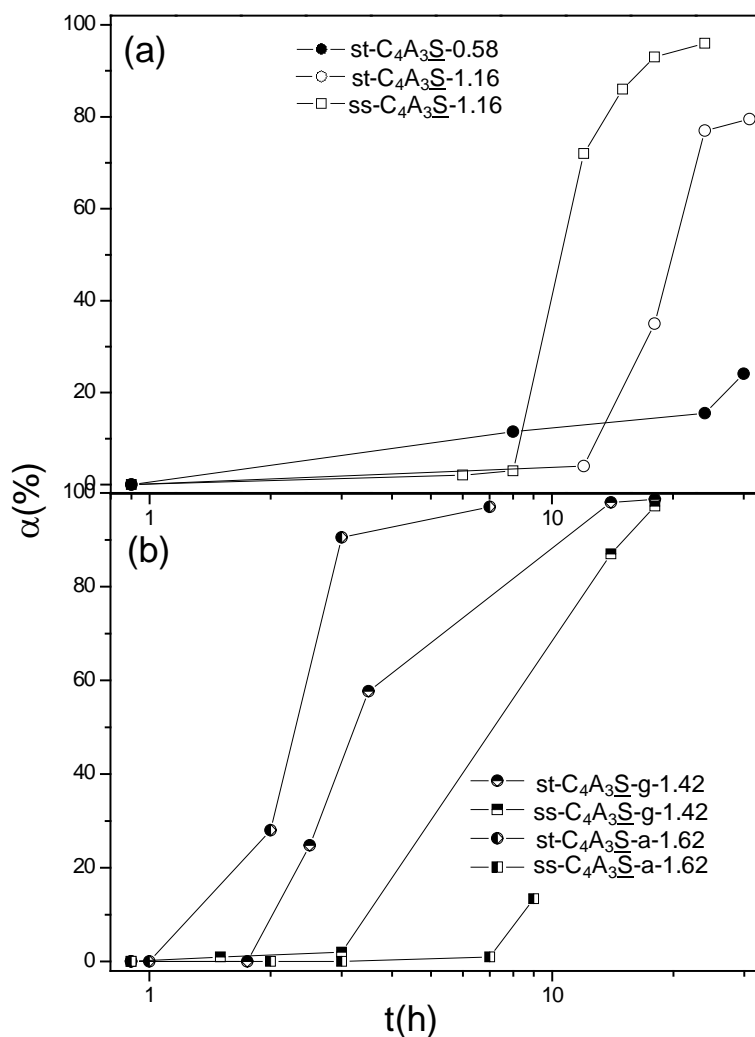


Figure 4.10. Degree of dissolution/reaction [α] of ye'elimitite as a function of time for (a) st-C₄A₃S and ss-C₄A₃S pastes without additional sulfate source; and (b) st-C₄A₃S and ss-C₄A₃S pastes with gypsum or anhydrite.

After this study, stoichiometric ye'elimitite sample with w/s of 1.16 was also prepared as it is well known that higher amounts of water enhance ye'elimitite reactivity (Winnefeld and Barlag 2010). Table 4.7 gives RQPA results for st-C₄A₃S-1.16 from SXRPD and LXRPD data. Moreover, Figure 4.10(a) shows the degree of reaction of ye'elimitite with water using different w/s ratios. Observing

4. Results and discussion

this figure, it is confirmed that reactivity of ye'elite has been enhanced by increasing w/s value. In addition, the total heat released after 7 days of hydration for this sample, 555 J/g, was higher than that for st-C₄A₃S-0.58 sample, 391 J/g, which is in full agreement with a larger reaction degree. In this case, the main hydration product was AFm, at all hydration times, indicating that higher amounts of water favor reaction [1.8]. It is supposed from a mass balance point of view that if the hydration is complete the same AFm/AFt ratio should be present. However, the hydration of ye'elite is not complete with a w/s of 0.58 but it is with a w/s of 1.16. For this reason, we found a higher AFm/AFt ratio at higher w/s, making the system to be closer to the equilibrium, reaction [1.8]. This behavior is in agreement with that previously reported by Winnefeld and Barlag (2010), where only AFm was obtained with a w/s ratio of 2.0.

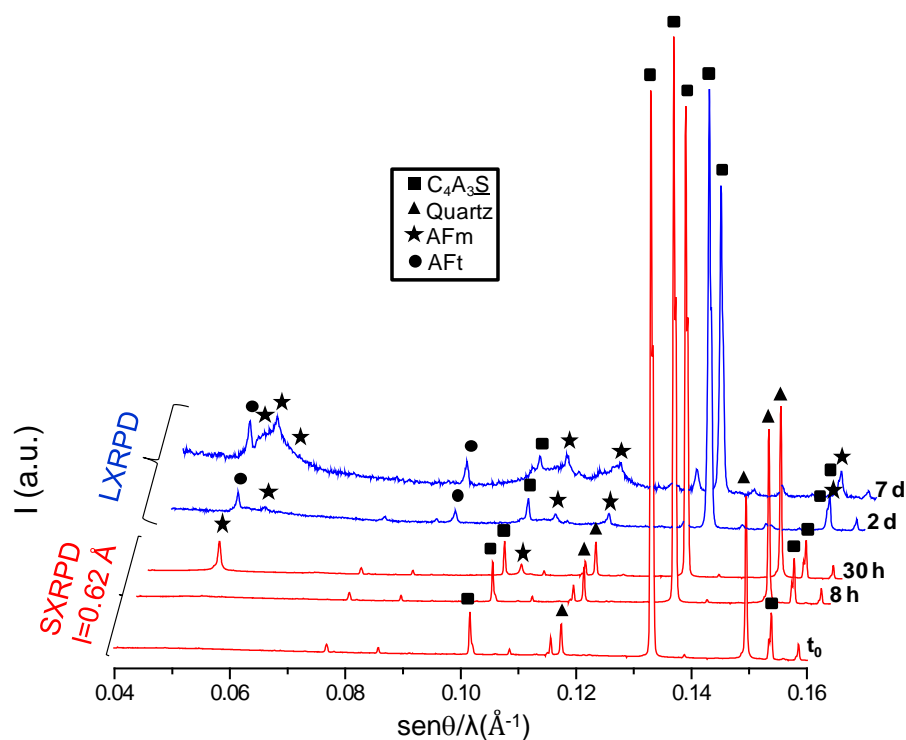


Figure 4.11. Selected range of the SXRPD ($\lambda=0.61975$ (1) \AA) and LXRPD ($\lambda=1.5406$ \AA) raw patterns for st-C₄A₃S-0.58 recorded at different hydration ages. The main peaks due to a given phase are labeled.

Table 4.7. Quantitative phase analysis results (wt%) for st-C₄A₃S-1.16 paste, as a function of hydration time obtained by SXRPD* and LXRPD[#].

	t ₀ *	12h*	18h*	24h*	31h*	2d [#]	7d [#]
st-C ₄ A ₃ S	44.9(1)	43.0(1)	29.4(1)	10.3(3)	9.2(3)	4.6(2)	2.9(2)
AFt	-	-	2.3(1)	1.1(2)	1.0(2)	9.2(3)	6.8(3)
AFm [§]	-	-	7.1(1)	22.0(2)	22.2(2)	25.1(4)	25.8(5)
ACn	1.4(1)					44.1(5)	46.5(6)
+FW	+53.7**=55.1	57.0(1)	61.2(1)	66.5(2)	67.6(2)	+17***=61.1	+17.9***=64.4

**Theoretical free water content

*** Obtained from the TGA study

[§]SXRPD patters were fitted with one AFm (Allmann 1977); In LXRPD pattern fit the value is the total of the three phases.

It is important to bear in mind that stopping procedure has affected the mineralogical composition, especially AFm-type phases. For the *in-situ* synchrotron experiment, the hydration was not stopped and higher crystallinity of AFm was found. It was fitted by using the crystal structure of AFm reported by Allmann (1977) and refining unit cell parameters. On the other hand, as the *ex-situ* LXRPD data were collected for stopped-hydration samples, broader peaks due to AFm-type phases were observed (see stars in Figure 4.11). In order to fit those broader peaks, the structure reported by Allmann (1977) was introduced three times in the GSAS experimental file and c values were modified. This was due to the lack of different crystal structures published for AFm-type phases.

Table 4.7 includes the ACn values obtained from internal and external standard methodologies of the mixture of st-C₄A₃S with w/s=1.16. The first column gives t₀ values obtained from the SXRPD pattern of the anhydrous sample. FW in t₀ column is the theoretical value. Remaining values obtained from internal standard method encompass not only ACn but also FW (not chemically bound water) and are expressed as a single value. This is due to the inability of the internal standard methodology to distinguish between different not-diffracting phases. On the other hand, data obtained with G-factor methodology from LXRPD, 2 days and 7 days, corresponds only to ACn values, since FW was removed by the stopping hydration procedure. The FW contents were determined by the difference between the ‘theoretical/mixed’ water and the combined water determined from

4. Results and discussion

TGA study (from RT to 600°C) of the stopped-hydration sample. It is important to highlight that the results obtained by the internal standard method are in agreement with those obtained at later ages with the external standard showing the consistence of both methodologies.

Secondly, the hydration mechanism for doped or solid solution ye'elinite (ss-ye'elinite) has been also studied with a w/s of 1.16. Table 4.8 shows RQPA results at the measured ages. It is important to know that the results reported in the article #5 were obtained using the crystal structure for doped ye'elinite published by Saalfeld and Depmeier (1972) since this study was published before obtaining a revised crystal structure for the doped polymorph. However, RQPA results have been updated in this Thesis by using the revised pseudocubic ye'elinite structure discussed in the previous section. The main difference has been that the amorphous contents have decreased due to the better Rietveld fits and hence the RQPA results are more accurate with the revised crystal structure.

Table 4.8. Quantitative phase analysis results (wt%) for ss-C₄A₃S-1.16 paste, as a function of hydration time obtained by SXRPD* and LXRPD[#].

	t ₀ *	6h*	8h*	12h*	15h*	18h*	24h*	2d [#]	7d [#]
ss-C ₄ A ₃ S	45.6(1)	45.1(1)	44.3(1)	12.2(2)	6.1(2)	3.9(3)	1.9(2)	0.8(1)	0
AFt	-	0.6(2)	0.9(2)	5.6(2)	6.4(3)	6.8(3)	7.0(3)	14.7(1)	12.7(1)
AFm [§]	-	-	-	13.6(2)	16.5(2)	18.8(2)	18.5(2)	13.4(1)	14.3(1)
ACn	0.7(2)	54.4(2)	54.8(2)	68.7(2)	71.0(2)	71.4(2)	72.6(2)	58.0(5)	61.0(5)
+FW	+53.7**=54.4							+13.1***=71.1	+12***=73.0

**Theoretical free water content

*** Obtained from the TGA study

§SXRPD patters were fitted with one AFm (Allmann 1977); In LXRPD pattern fit the value is the total of the three phases.

Comparing Tables 4.7 and 4.8 and observing Figure 4.10, it can be stated that solid-solution ye'elinite reacts at a faster pace as more than 13 wt% of AFm and 5 wt% of AFt are quantify after 12 hours while no hydration phase can be found in st-ye'elinite at the same time. Moreover, the increase of w/s ratio affected the hydration of st-ye'elinite by promoting the formation of AFm. As an example, Figure 4.12 a and b shows Rietveld plots of st-C₄A₃S-1.16 and ss-C₄A₃S-1.16,

respectively, at 12 hours of hydration in order to show the big differences in the reaction degree. In addition to a faster kinetics, solid-solution ye'elinite yielded much larger relative amounts of AFt. Observing Figure 4 in article #5, AFt crystallization in ss- C_4A_3S is higher than in the stoichiometric sample. Moreover, ~17% and ~10% of hydrated sulfate groups for st- C_4A_3S and ss- C_4A_3S , respectively were mainly incorporated into ACn phase(s) and/or in pore solution.

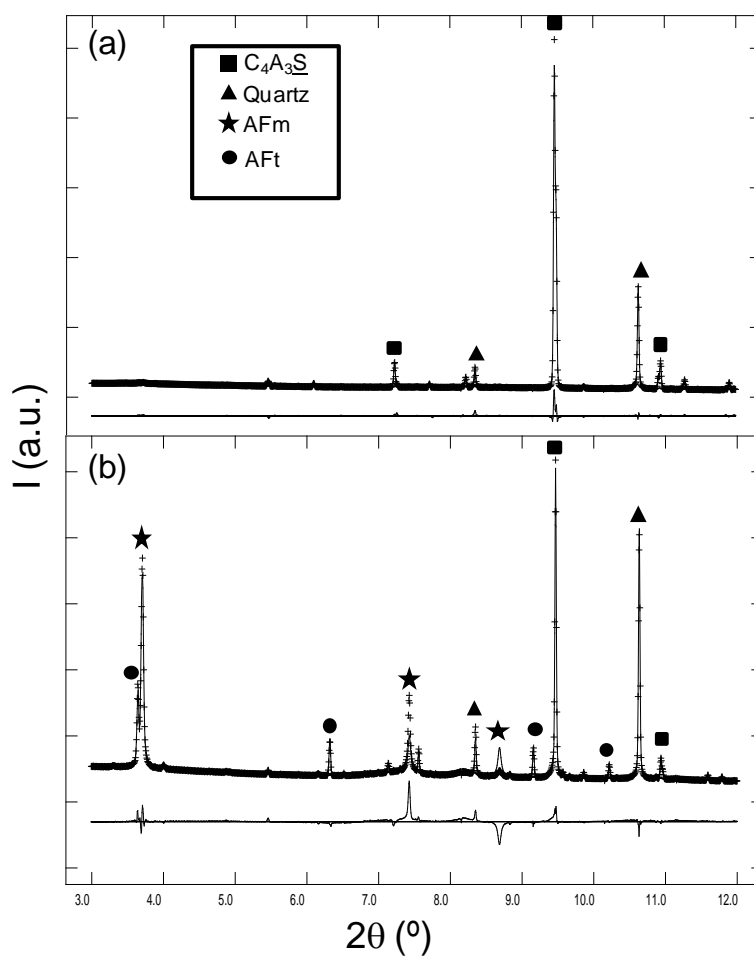


Figure 4.12. SXRPD ($\lambda=0.61975(1)$ Å) Rietveld plots for a) st- C_4A_3S -1.16 and b) ss- C_4A_3S -1.16, at 12 hours of hydration, with the main peaks due to a given phase labeled.

4. Results and discussion

It is important to highlight that calorimetric data, showed that more heat was released by the solid-solution sample (577 J/g at 7 days) in comparison to stoichiometric ye'elimite (555 J/g), due to a larger reaction degree and also to a larger relative amount of crystallized ettringite at seven days.

In summary, comparing both polymorphs, some findings should be highlighted: i) stoichiometric ye'elimite reacts slower than solid-solution ye'elimite and ii) solid-solution ye'elimite produces higher amounts of ettringite than stoichiometric ye'elimite in similar hydrating conditions.

Moreover, the increase of w/s ratio affects the hydration of st-ye'elimite by promoting the formation of AFm.

4.5.2. Reactivity of ye'elimites with gypsum.

The hydration of ye'elimite, stoichiometric and solid solution, with gypsum was studied by *in-situ* SXRPD at very early ages because the presence of gypsum accelerates the hydration reaction of ye'elimite.

In order to understand the role of polymorphism in the hydration mechanism, st-C₄A₃S-g-1.42 and ss-C₄A₃S-g-1.42 mixtures were prepared in which each polymorph was mixed with gypsum in the molar ratio of reaction [1.7] and water was added in excess. For both pastes, the reaction almost finished after 14 hours of hydration. RQPA results obtained from SXRPD are given in Tables 4.9 and 4.10. It can be observed that the overall reactivity of these two samples has followed reaction [1.7]. AFt is the only crystalline hydrated product, consequently there should be an amorphous phase with stoichiometry close to AH₃·nH₂O.

It can be also observed that ACn and FW contents for both pastes slightly diminished with time. It is worth noting that the opposite behavior is observed for samples without gypsum (Tables 4.7 and 4.8). This is mainly due to the larger amounts of ettringite and the absence of AFm-type phases.

Table 4.9. Quantitative phase analysis results (wt %) for st-C₄A₃S-g-1.42 paste, as a function of hydration time obtained by SXRPD.

	t₀	1h45m	2h30m	3h30m	14h	18h
st-C₄A₃S	22.9(1)	23.4(1)	17.3(1)	9.7(1)	0.4(1)	0.3(1)
CSH₂	12.8(1)	12.0(1)	8.2(1)	3.1(1)	0.3(1)	0.3(1)
AFt	-	5.4(1)	15.0(1)	28.0(1)	47.8(1)	47.5(1)
ACn+FW	6.1(1)+58.1* ⁼ 64.2	59.2(1)	59.6(1)	59.2(1)	51.4(1)	51.9(1)

*Theoretical free water content

Table 4.10. Quantitative phase analysis results (wt %) for ss-C₄A₃S-g-1.42 paste, as a function of hydration time obtained by SXRPD.

	t₀	1h30m	3h	14h	18h
ss-C₄A₃S	26.3(1)	25.8(1)	25.3(1)	3.2(1)	0.7(1)
CSH₂	13.4(2)	14.3(2)	14.3(2)	1.5(1)	0.3(1)
AFt	-	0.2(1)	0.8(2)	32.9(1)	37.8(1)
ACn+FW	2.2(1)+58.1* ⁼ 60.3	59.6(1)	59.6(1)	62.5(1)	61.2(1)

*Theoretical free water content

The main difference found between the hydration of st-C₄A₃S-g-1.42 and that of ss-C₄A₃S-g-1.42 is related to the reaction pace, Figure 4.10(b). The hydration kinetics in st-ye'elimite is faster than in ss-ye'elimite at early ages. Figure 4.13 shows the SXRPD raw patterns for both samples at similar early hydration ages for the sake of comparison. This effect was corroborated by calorimetric measurements since most of the heat evolved by stoichiometric sample is centered around 6 hours while that the signal of ss-C₄A₃S is placed close to 12 hours. Figure 4.14 shows the calorimetric data for both samples.

It is important to highlight that the hydration of stoichiometric ye'elimite has been accelerated in the presence of gypsum when compared to the hydration behavior of this phase without gypsum, Figure 4.10. However, for the solid solution ye'elimite, the presence of gypsum has only a little effect in the kinetics of hydration.

4. Results and discussion

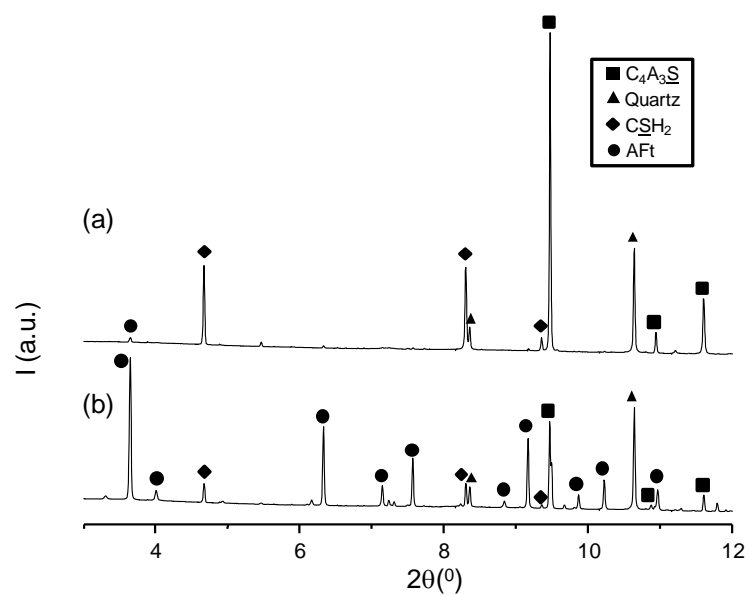


Figure 4.13. Selected range of a SXRPD ($\lambda=0.61975(1)$ Å) raw pattern for (a) ss-C₄A₃S-g-1.42 at 3 h and (b) st-C₄A₃S-g-1.42 at 3.5 h, with the main peaks due to a given phase labeled.

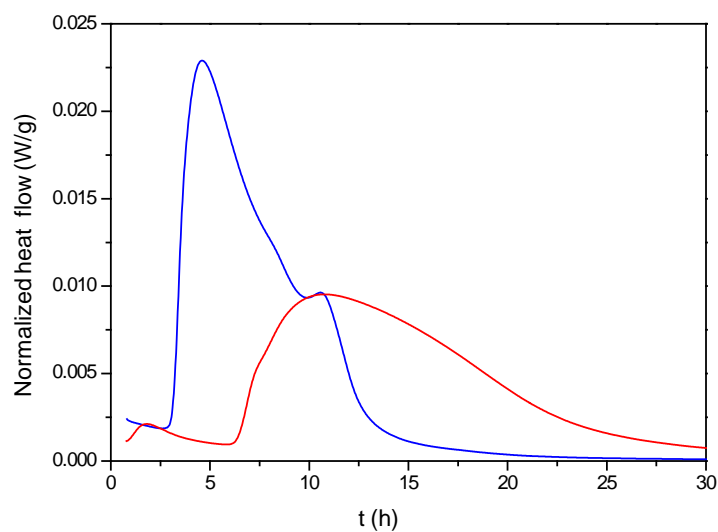


Figure 4.14. Conduction calorimetric curves for st-C₄A₃S-g-1.42 (blue line) and ss-C₄A₃S-g-1.42 (red line).

Finally, anhydrite was also used to study its influence on the hydration mechanism of ye'elimite, stoichiometric and doped (see Table 6 and 7 in article #5). The main difference with reference to the gypsum study was that the hydration mechanism was much slower because anhydrite was dissolved at a very low pace, as expected, Figure 4.10(b). In that case the main hydration product was again AFt.

4.5.3. Reactivity of ye'elimite with C₄AF.

The hydration of ye'elimite (stoichiometric and doped) in combination with C₄AF has been studied by *in-situ* SXRPD to characterize the hydration processes which have taken place at early-ages (article #7).

Firstly, st-ye'elimite, ferrite and gypsum were mixed in proportions close to those obtained for BC SAF reported by Álvarez-Pinazo et al. (2012) with a water/solid ratio of 1.0 (C₄AF-st-C₄A₃S₂-g-1.0). This paste has been studied at early ages, up to 46 hours. Figure 4.15(a) shows the full quantitative phase analysis results as a function of time. Initially, only reaction to form AFt took place. Then, when gypsum was totally consumed AFm phase crystallized and AFt started to consume/decrease. The formation of AFm was favored not only from ye'elimite reaction but also likely from AFt dissolution, see reaction [1.12]. The time evolution of ACn and FW contents had a complementary behavior. It can be observed that these values slightly diminished with time during the crystallization of AFt and it is worth noting that the opposite behavior was observed when AFm started to appear.

4. Results and discussion

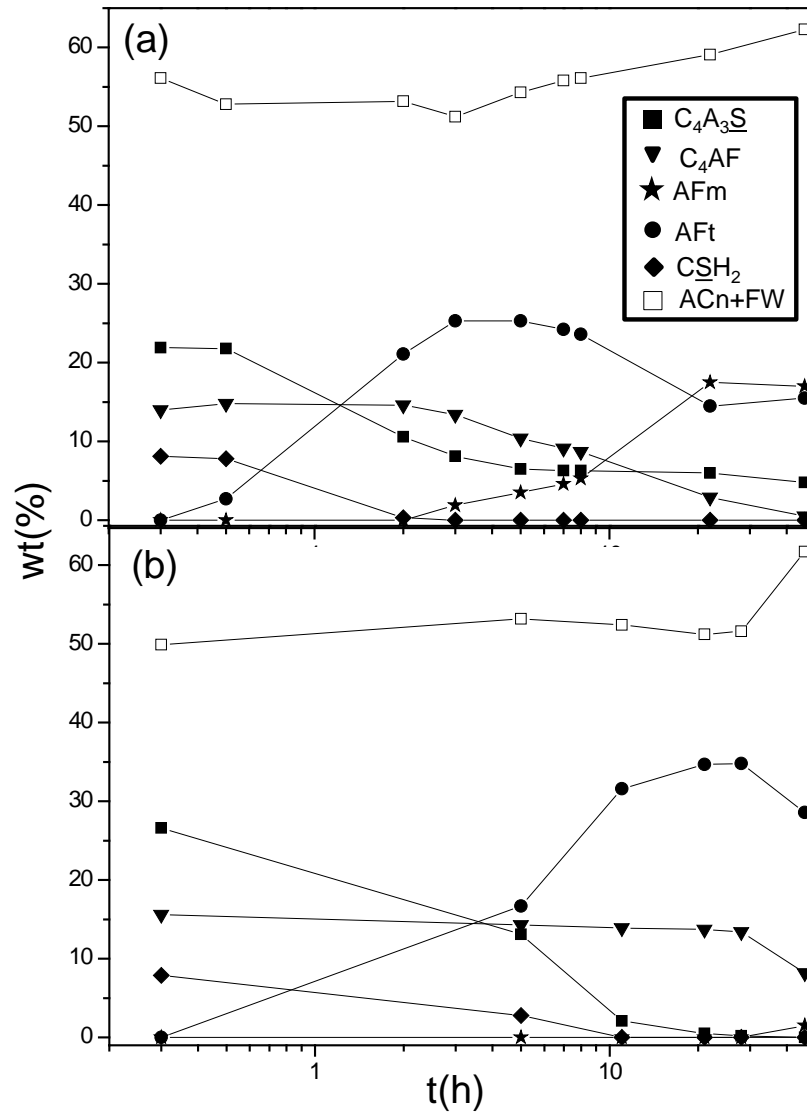


Figure 4.15. Full quantitative phase analysis results for (a) C_4AF -st- C_4A_3S -g-1.0 and (b) C_4AF -ss- C_4A_3S -g-1.0.

Moreover, st-ye'elite with C_4AF and gypsum was also studied with 0.7 and 1.3 w/s ratios up to 12 hours in order to study the water influence at very early ages. Tables 5 and 6 (in article #7) show the phase assemblages with time for both mixtures. It is well known that higher amounts of water enhance ye'elite

reactivity (Winnefeld and Barlag 2010) and this behavior has also been confirmed here. Figure 4.16 shows degree of reaction of ye'elite in the mixture with gypsum and C_4AF with different w/s ratios. This figure shows the enhanced ye'elite hydration with higher amounts of water. Moreover, the results obtained for these samples indicate that higher amounts of water favor the formation of AFm because the reaction is complete and the system is closer to the equilibrium, in agreement with the previous study of the hydration of ye'elite samples only with water (section 4.5.1). Figure 6 in article #7 shows the Rietveld plots of these mixtures with different w/s ratios where it is clearly shown that AFt phase is favored when w/s is low.

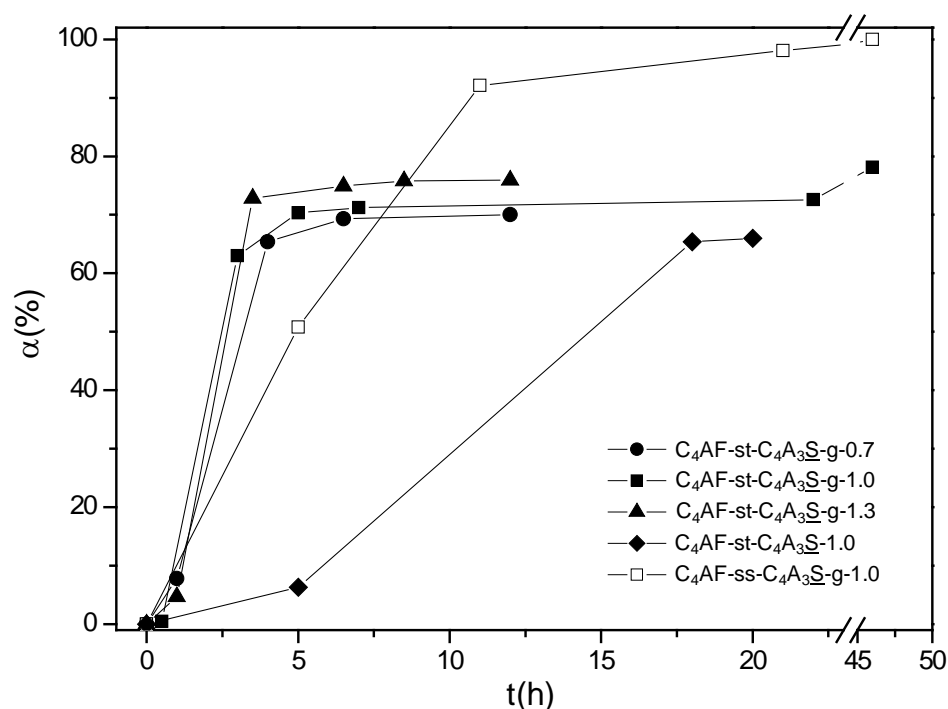


Figure 4.16. Degree of reaction $[\alpha]$ of ye'elite as a function of time for C_4AF with ye'elite pastes. Solid lines are just guide to the eyes.

4. Results and discussion

Secondly, doped ye'elimite was mixed with C_4AF and gypsum (C_4AF -ss- C_4A_3S -g-1.0) to determine its hydration behavior in these conditions. Figure 4.15(b) shows the full quantitative phase analysis results as a function of time. Here, ye'elimite started to consume fastly and AFt precipitated at early stage. Only when ss-ye'elimite ended up dissolving, C_4AF started to consume and AFm appeared. Furthermore, the ACn content was in agreement with this behavior, since it diminished with time during the crystallization of AFt and the opposite behavior was observed when AFm started to appear. Moreover, the total heat evolved at 2 days was 382 and 409 J/g for C_4AF -st- C_4A_3S -g-1.0 and C_4AF -ss- C_4A_3S -g-1.0, respectively. The total heat released for the C_4AF -ss- C_4A_3S -g-1.0 sample was higher due to the total consumption of ye'elimite and the precipitation of bigger amounts of ettringite.

The main difference between stoichiometric and doped ye'elimites, after 46 hours of hydration, is that the C_4AF -ss- C_4A_3S -g-1.0 sample yields much larger relative amounts of AFt, see Figure 4.17. Keeping this direct observation in mind, we can conclude that the differences in the hydration mechanisms between both ye'elimite polymorphs are intensified when ferrite is in the reaction medium.

A SEM-EDS study was also performed for C_4AF -st- C_4A_3S -g-1.0 and C_4AF -ss- C_4A_3S -g-1.0 pastes at 48 hours of hydration. Figure 4.18(a) shows Fe/Ca vs Al/Ca of these samples and Figure 4.18(b) shows a representative SEM photograph. It shows that most particles, with needle shape identified as AFt (Figure 4.18(b)) and with close compositions to theoretical ettringite (circle in Figure 4.18(a)) do not contain significant amounts of iron. Moreover, those particles without needle shape with composition similar to that of AFm neither contain iron in their structures, Figure 4.18. In addition, bright particles with high iron contents were also observed in SEM studies which may correspond to iron-rich amorphous phases and also a dark gray background with a very large Al/Ca ratio which could be related to aluminum-rich ACn phases (Song et al. 2015).

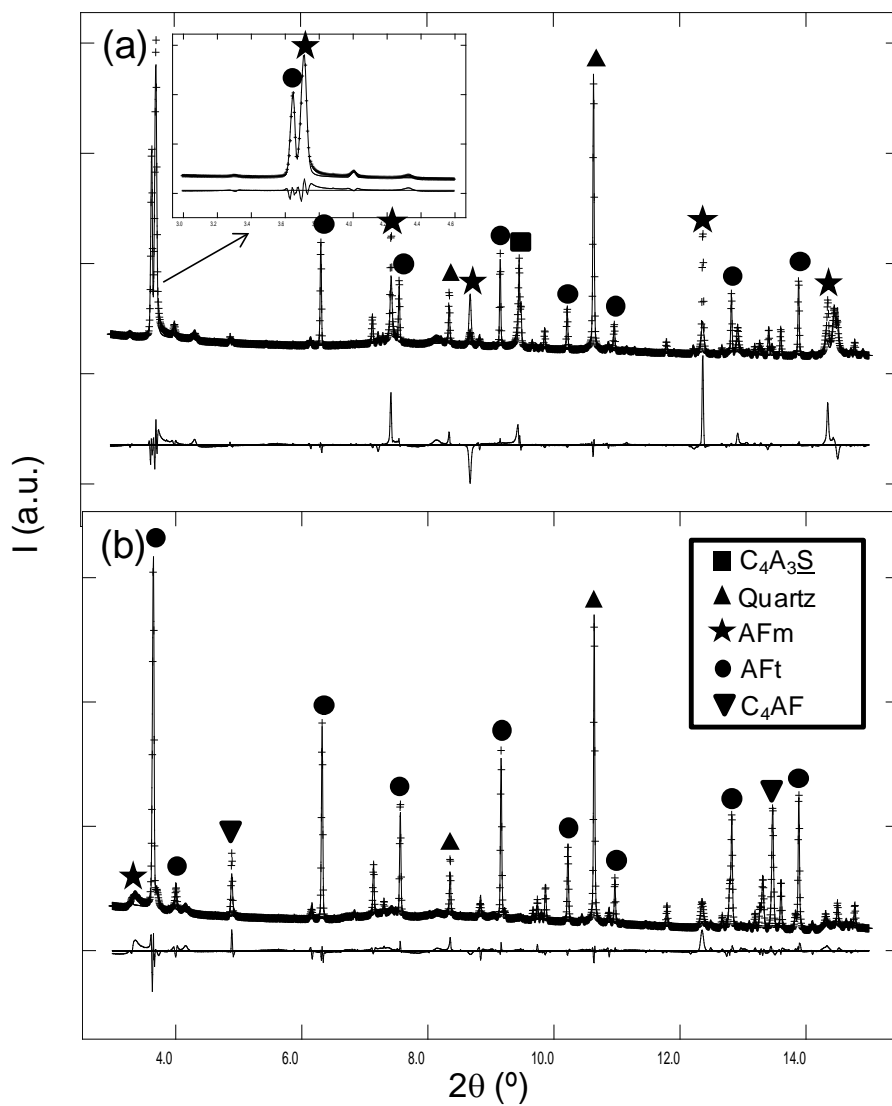


Figure 4.17. SXRPD ($\lambda=0.6202(2)$ Å) Rietveld plots for a) C_4AF -st- C_4A_3S -g-1.0 and b) C_4AF -ss- C_4A_3S -g-1.0, at 46 hours of hydration, with the main peaks due to a given phase labeled. Inset in (a): Enlargement of the low angle region.

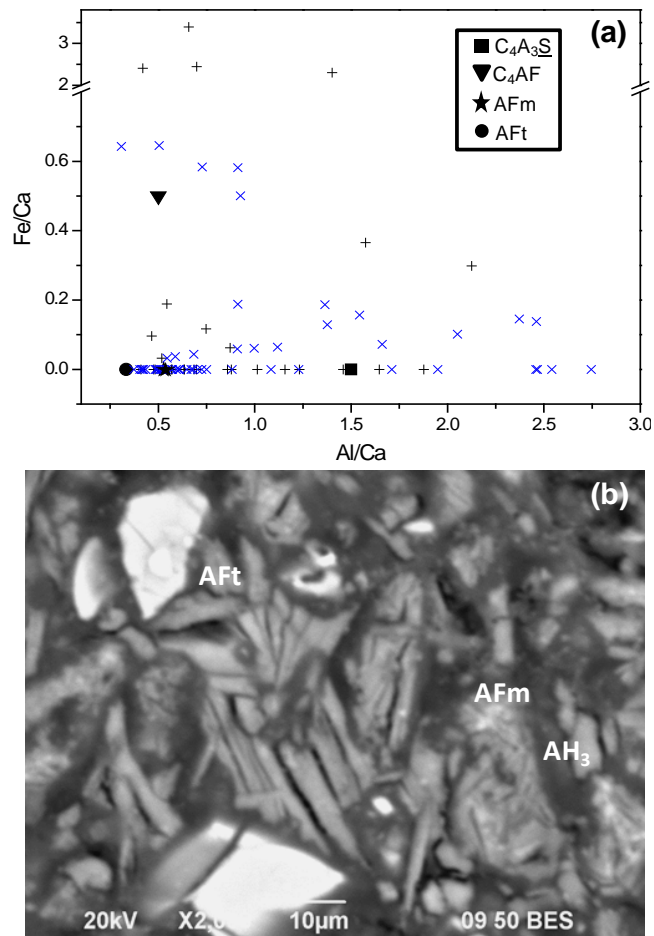


Figure 4.18. (a) Fe/Ca atomic ratio vs. Al/Ca atomic ratio for SEM-EDS study of C₄AF-st- C₄A₃S-g-1.0 (plus symbol) and C₄AF-ss-C₄A₃S-g-1.0 (crosses) at 48 hours. Solid symbols represent the theoretical composition of the phases. (b) SEM photograph of C₄AF-st-C₄A₃S-g-1.0.

Thirdly, the hydration of st-ye'elinite with ferrite and in absence of gypsum was also studied, C₄AF-st-C₄A₃S-g-1.0. Figure 4.19 shows a selected range of SXRPD raw patterns for this sample recorded as a function of time up to 20 h.

There is a clear difference with the C₄AF-st-C₄A₃S-g-1.0 sample. AFm was the only hydration product for this sample and AFt was not observed at any time due to the lack of extra sulfate in the mixture. According to this observation, it can

be demonstrated that the main responsible of the formation of AFt in these samples is the gypsum.

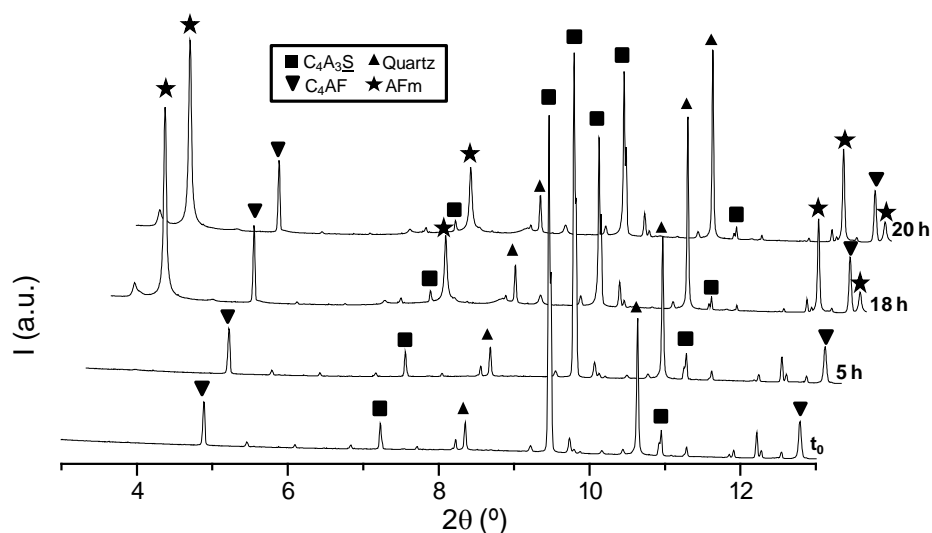


Figure 4.19. Selected range of SXRPD ($\lambda=0.6202(2)$ Å) raw patterns for C_4AF -st- C_4A_3S -1.0 recorded at different ages of hydration, with the main peaks due to a given phase labeled.

4.5.4. Reactivity of ye'elimite with dicalcium silicate.

Hydration mechanism of ye'elimite with dicalcium silicate (and gypsum) has been studied by *ex-situ* LXRPD in combination with the external standard method, G-factor, up to 6 months (article #6). The hydration mechanism of dicalcium silicate is so slow, that there is no point in performing hydration studies at early ages. In order to understand the role of C_2S polymorphs in combination with ye'elimite on the hydration mechanism four combinations were studied, see Table 4.11. The chosen proportions were those obtained in BCSAF cements (Álvarez-Pinazo et al. 2012). These results are not published yet.

4. Results and discussion

Table 4.11. Paste mix proportions in weight percentages (wt%) of dicalcium silicate, ye'elinite and gypsum.

Mixture	st-C ₄ A ₃ S wt%	ss-C ₄ A ₃ S wt%	β-C ₂ S wt%	α' _H -C ₂ S wt%	gypsum wt%	water/ solid
β-C ₂ S-st-C ₄ A ₃ S-g-0.67	32.9	-	54.9	-	12.2	0.67
β-C ₂ S-ss-C ₄ A ₃ S-g-0.67	-	32.9	54.9	-	12.2	0.67
α' _H -C ₂ S-st-C ₄ A ₃ S-g-0.67	32.9	-	-	54.9	12.2	0.67
α' _H -C ₂ S-ss-C ₄ A ₃ S-g-0.67	-	32.9	-	54.9	12.2	0.67

To study the reactivity of dicalcium silicate polymorphs, they were mixed with both polymorphs of ye'elinite and gypsum, Table 4.11. Figures 4.20 and 4.21 show the raw patterns of β-C₂S-st-C₄A₃S-g-0.67 and α'_H-C₂S-st-C₄A₃S-g-0.67 mixtures hydrated at 7, 28 and 180 days. Tables 4.12 and 4.13 give RQPA including ACn (determined by external standard methodology) and FW for all the studied mixtures. The first conclusion of this study is that the polymorphs of ye'elinite have not affected the hydration behavior of dicalcium silicate. Consequently, mixtures β-C₂S-st-C₄A₃S-g-0.67 and β-C₂S-ss-C₄A₃S-g-0.67 have presented an almost identical hydration behavior. The same can be stated for α'_H-C₂S-st-C₄A₃S-g-0.67 and α'_H-C₂S-ss-C₄A₃S-g-0.67.

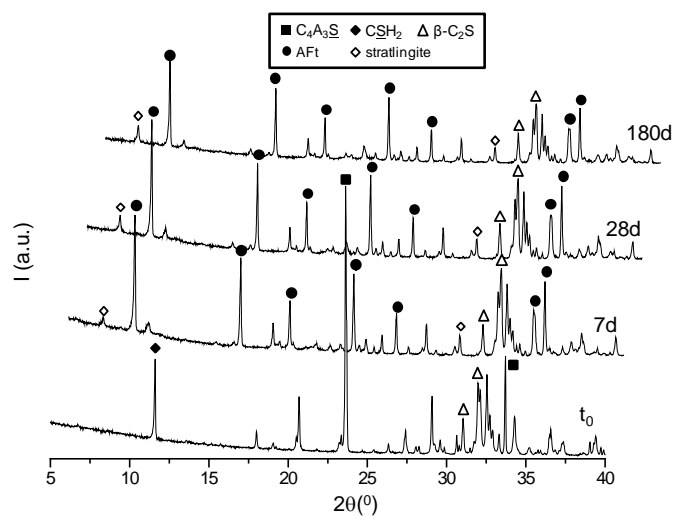


Figure 4.20. Selected range of LXPDP ($\lambda=1.5406 \text{ \AA}$) raw patterns for β-C₂S-st-C₄A₃S-g-0.67 recorded at different ages of hydration, with the main peaks due to a given phase labeled.

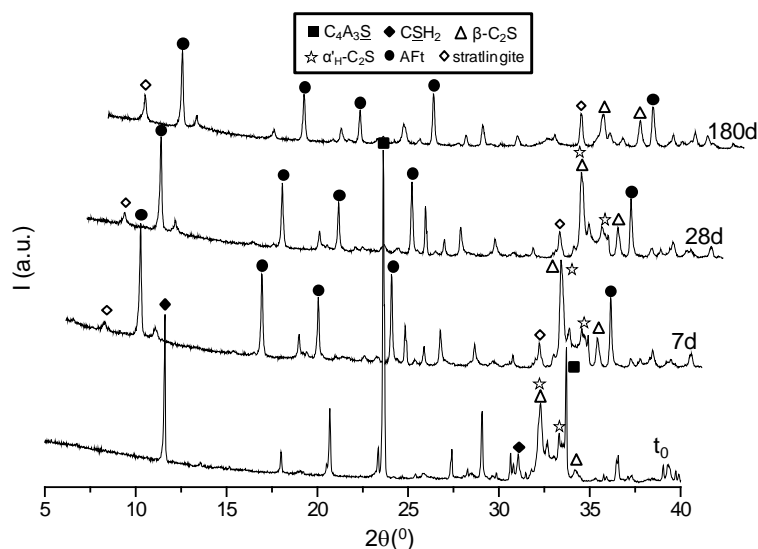


Figure 4.21. Selected range of LXRPD ($\lambda=1.5406 \text{ \AA}$) raw patterns for $\alpha'_H\text{-C}_2\text{S-st-C}_4\text{A}_3\text{S-g-0.67}$ recorded at different ages of hydration, with the main peaks due to a given phase labeled.

Table 4.12. Quantitative phase analysis results (wt%) for $\beta\text{-C}_2\text{S-st-C}_4\text{A}_3\text{S-g-0.67}$ and $\alpha'_H\text{-C}_2\text{S-st-C}_4\text{A}_3\text{S-g-0.67}$ pastes, as a function of hydration time obtained from LXRPD.

	$\beta\text{-C}_2\text{S-st-C}_4\text{A}_3\text{S-g-0.67}$				$\alpha'_H\text{-C}_2\text{S-st-C}_4\text{A}_3\text{S-g-0.67}$			
	t_0	7d	28d	180d	t_0	7d	28d	180d
C₄A₃S	14.9(1)	0.9(1)	0.9(1)	1.0(1)	15.7(1)	2.2(1)	2.6(1)	-
$\alpha'_H\text{-C}_2\text{S}$	-	-	-	-	20.0(3)	17.6(3)	13.9(4)	-
$\beta\text{-C}_2\text{S}$	21.7(1)	21.5(2)	20.6(2)	20.2(2)	7.4(3)	9.6(3)	9.3(3)	7.0(4)
CSH₂	5.7(1)	-	-	-	5.9(1)	-	-	-
$\gamma\text{-C}_2\text{S}$	2.5(2)	2.3(2)	2.2(2)	2.3(2)	-	-	-	-
Strat	-	2.6(2)	6.5(3)	8.6(3)	-	4.5(3)	6.4(3)	14.9(4)
AFt	-	20.5(2)	21.1(2)	22.5(2)	-	21.7(2)	19.9(2)	22.3(3)
Gib	-	0.6(1)	0.5(1)	0.6(1)	-	0.6(1)	0.5(1)	0.4(2)
Katoite	-	-	-	-	-	-	-	1.3(2)
CaCO₃	-	-	-	-	-	-	-	0.8(1)
AFm	-	-	-	-	-	0.7(1)	0.6(2)	0.9(2)
ACn	13.6(3)	35.7(4)	33.0(5)	30.0(5)	9.4(5)	28.6(6)	31.8(6)	49.5(7)
FW	41.6	16.0	15.1	14.9	41.6	14.6	14.9	2.9

4. Results and discussion

Table 4.13. Quantitative phase analysis results (wt%) for β -C₂S-ss-C₄A₃S-g-0.67 and α' _H-C₂S-ss-C₄A₃S-g-0.67 pastes, as a function of hydration time obtained from LXRPD.

	β -C ₂ S-ss-C ₄ A ₃ S-g-0.67				α' _H -C ₂ S-ss-C ₄ A ₃ S-g-0.67			
	t ₀	7d	28d	180d	t ₀	7d	28d	180d
C ₄ A ₃ S	16.2(1)	-	-	-	17.5(1)	-	-	-
α' _H -C ₂ S					19.0(1)	15.2(4)	11.8(4)	-
β -C ₂ S	22.7(2)	18.7(2)	20.1(2)	20.4(2)	8.0(3)	8.9(3)	9.8(3)	7.1(4)
C \overline{S} H ₂	5.8(1)	-	-	-	5.8(1)	-	-	-
γ -C ₂ S	2.3(2)	1.8(2)	2.0(2)	2.3(2)				
Strat	-	2.3(2)	6.7(2)	8.5(3)	-	6.0(3)	10.2(3)	14.9(4)
AFt	-	21.0(2)	23.5(2)	22.6(2)	-	20.3(2)	23.3(2)	25.7(1)
Gib	-	0.6(2)	0.5(1)	0.6(2)	-	0.5(1)	0.4(1)	0.4(2)
CaCO ₃	-	-	-	-	-	-	-	0.7(1)
ACn	11.4(3)	40.4(4)	32.9(4)	32.4(5)	8.1(3)	36.8(6)	32.7(6)	47.9(6)
FW	41.6	15.3	14.3	13.3	41.6	12.3	11.8	3.4

Table 4.14 shows the summary of the weight losses from the TGA study for β -C₂S-st-C₄A₃S-g-0.67 and β -C₂S-ss-C₄A₃S-g-0.67. For these studies, the temperature was varied from RT to 1000°C at a heating rate of 10 °C/min under a nitrogen flow. The weighed loss from RT to 600°C was computed to be water (chemically bounded water) and that from 600 to 1000°C was considered as CO₂. The weight losses are more or less constant with the time in pastes containing β -C₂S. This observation indicates that the hydration did not significantly continue at ages later than 7 days. This fact is in agreement with the quantitative phase analysis results for β -C₂S-st-C₄A₃S-g-0.67 and β -C₂S-ss-C₄A₃S-g-0.67, see Tables 4.12 and 4.13 (left) and Figure 4.20. After 7 days ye'elinite has fully reacted (in the ss-ye'elinite sample) and the main hydration product was AFt. However, it can be observed that the phase assemblage was not modified with the hydration age after 7 days. It is important to note that small amounts of stratlingite were also found at all ages. Stratlingite has been identified as a hydration product of belite by other authors (Álvarez-Pinazo et al. 2013; Andac and Glasser 1999) according to reaction [1.4]. However, the dissolution of dicalcium silicate was not taken place in the hydration of these samples. For this reason, we speculate that stratlingite could have been formed due to the presence of small amounts of belite or silicate phases

which were present in the amorphous fraction. Moreover, the ACn value dismissed with the time of hydration, supporting this hypothesis.

Table 4.14. Summary of the weight losses from the TGA study for the studied dicalcium silicate-containing pastes.

mixture	Hydration time / d	Theoretical weight loss [#] / %	Weight loss RT-600°C / %	Weight loss 600-1000°C / %
β -C ₂ S-st-C ₄ A ₃ S-g-0.67	7d	41.6	25.7	0.9
	28d	41.6	26.5	0.9
	180d	41.6	26.7	0.5
β -C ₂ S-ss-C ₄ A ₃ S-g-0.67	7d	41.6	26.3	0.9
	28d	41.6	27.3	0.7
	180d	41.6	28.3	0.5
α' _H -C ₂ S-st-C ₄ A ₃ S-g-0.67	7d	41.6	27.1	0.8
	28d	41.6	26.7	0.9
	180d	41.6	38.7	0.8
α' _H -C ₂ S-ss-C ₄ A ₃ S-g-0.67	7d	41.6	29.3	0.8
	28d	41.6	29.8	0.9
	180d	41.6	38.2	1.0

On the other hand, samples which contain the α' _H-C₂S polymorph, α' _H-C₂S-st-C₄A₃S-g-0.67 and α' _H-C₂S-ss-C₄A₃S-g-0.67, showed a different behavior in their hydration mechanisms in comparison to samples with β -dicalcium silicate. It has to be borne in mind that these samples also contain some amounts of β -polymorph, see Tables 4.12 and 4.13 (right). It is clear that there is an important increase in the weight losses of these pastes between 28 and 180 days (see Table 4.14) which indicates that α' _H-C₂S is (at least partly) reacting. Also, the phase assemblage is different between 7 and 180 days. Table 4.13 (right) shows the RQPA obtained by SXRPD for α' _H-C₂S-ss-C₄A₃S-g-0.67 sample. At 7 days, AFt was the main hydrated product and ye'elimite was totally dissolved. However, at 6 months, an important amount of stratlingite precipitated as a consequence of the total reaction of α' _H-C₂S. The ACn values increased at 180 days due to the formation of an amorphous phase, probably C-S-H. The same behavior can be observed in the α' _H-C₂S-st-C₄A₃S-g-0.67 sample, see Table 4.12 (right) and Figure 4.21.

As a summary, the main difference found between the hydration of samples

4. Results and discussion

which contain β -C₂S and that of α' _H-C₂S is related to the hydraulic activity of dicalcium silicate. Comparing the data reported in Table 4.12 and 4.13, it can be observed that only α' _H-C₂S reacts with the time and the β -C₂S is inactive up to 180 days of hydration. This fact proves a higher hydraulic activity for α' _H-C₂S than for β -C₂S independently of the ye'elinite polymorph present, which is in agreement with previous results obtained in sulfobelite cements (Cuberos et al. 2010).

However, these results could be in disagreement with Álvarez-Pinazo et al. (2013 and 2014). These authors concluded that β -C₂S present in BC SAF cements (also containing C₄AF) reacted at a higher pace than α' _H-C₂S present in active cements. Consequently, more research is needed to understand this behavior, including the role of C₄AF in the reaction of α' _H- and β -C₂S.

It is worth to highlight that as in almost all the hydrated samples of ye'elinite, hydration kinetics in ss-ye'elinite is faster than in st-ye'elinite. Ss-ye'elinite is totally consumed at 7 days (see Table 4.13) and there is a small amount of st-ye'elinite even at 180 days for β -C₂S-st-C₄A₃S₂-g-0.67 sample (see Table 4.12, left).

4.5.5. Hydration of C₄AF.

Initially, the hydration behavior of C₄AF with water was studied (article #7). The w/s ratio used was 0.8. C₄AF-0.8 sample has been characterized up to 5.5 hours by *in-situ* SXRPD with internal standard methodology for determining the ACn content. Table 2 in article #7 shows the phase assemblages at different ages. In agreement with reactions [1.9] and [1.10], C₃(A,F)H₆ crystallized. It has been reported that C₂AH₈ phase is formed after 5 minutes from hydration and then it abruptly converts into C₃(A,F)H₆ (Meller et al. 2004a). In this study, the first pattern was taken at 1 hour. Consequently big amounts of C₂AH₈ phase were not

expected and $C_3(A,F)H_6$ was the main phase after 5.5 hours of hydration. Figure 4.22 shows the degree of reaction of C_4AF as function of time.

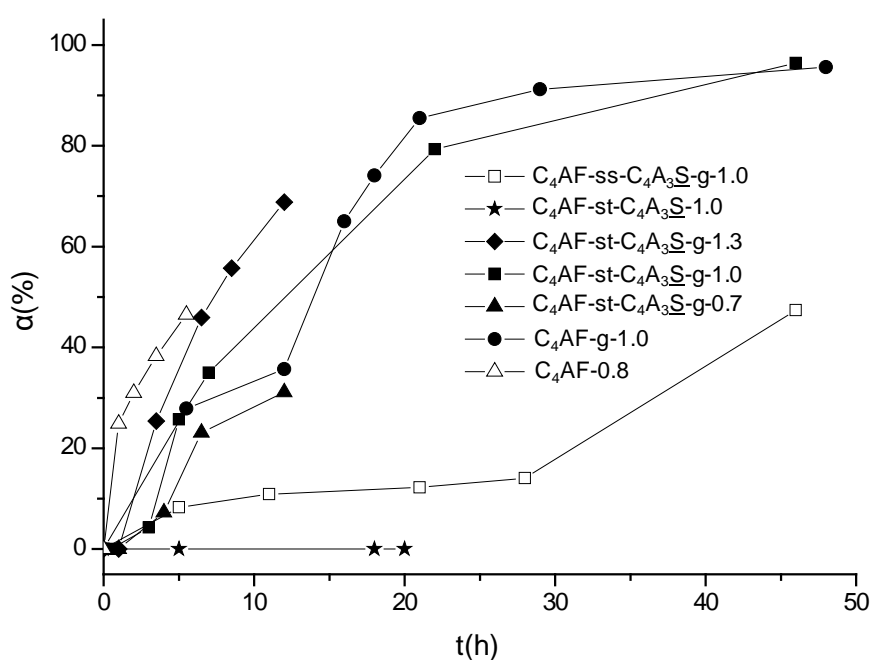


Figure 4.22. Degree of reaction [α] of C_4AF as a function of time for C_4AF pastes. Solid lines are just guide to the eyes.

Moreover, it can be observed that AC_n and FW values slightly diminished with time. This is mainly due to the precipitation of a crystalline phase, $C_3(A,F)H_6$, which is consuming free water, see Table 2 in article #7.

Later, high-resolution SXRPD was employed to study the crystal structure of crystalline $C_3(A,F)H_6$ obtained by direct hydration of C_4AF with w/s ratio of 1. The structural description reported by Lager et al. (1987), with space group $Ia\bar{3}d$, was used as a starting model for the structural Rietveld refinement. However, this structure does not include iron. The initial amount of iron, 0.20, was chosen using data reported in Table 1.6 (Taylor et al. 1997) by interpolating the refined unit cell parameter, a .

4. Results and discussion

The obtained disagreement factors were $R_{\text{WP}}=8.1\%$ and $R_{\text{F}}=4.8\%$ and the determined formula was $C_3A_{0.845}F_{0.155}H_6$. Figure 4.23 shows the final SXRPD Rietveld plot using the optimized structure. The final refined unit cell parameter and the cell volume were $a=12.60315(4) \text{ \AA}$ and $2001.88(2) \text{ \AA}^3$, respectively. The refined atomic parameters for this sample, measured at room temperature, are shown in Table 4.15.

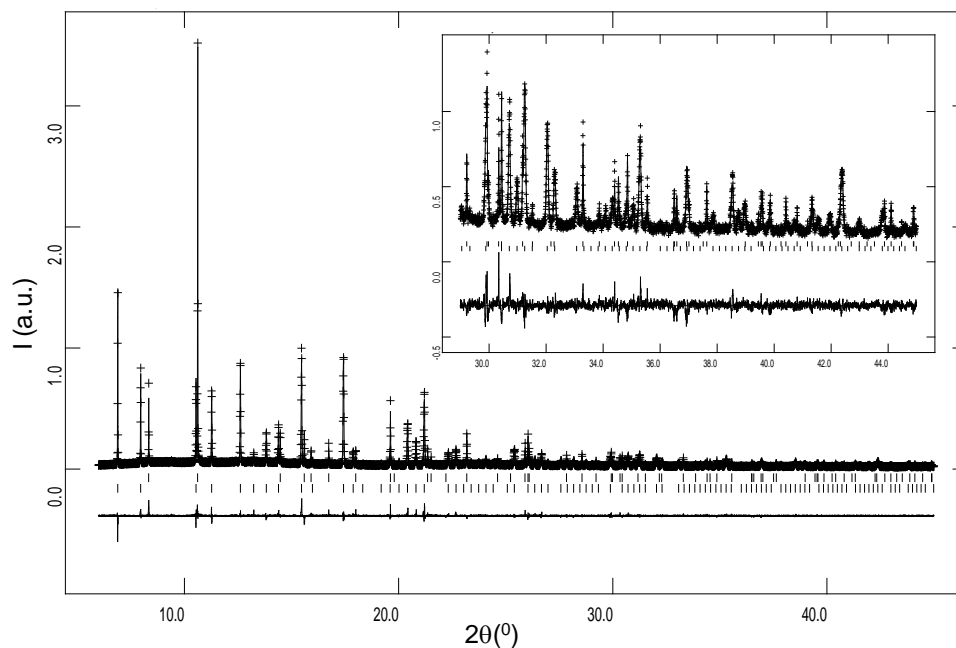


Figure 4.23. SXRPD Rietveld plot for $C_3A_{0.845}F_{0.155}H_6$ ($\lambda=0.6202(2) \text{ \AA}$). Inset details the high-angle range. The tic marks are the allowed Bragg reflections. C_4AF : lower row and Quartz (internal standard): upper row.

Table 4.15. Final (refined) atomic parameters (positional coordinates and ADPs) for $C_3A_{0.845}F_{0.155}H_6$ at room temperature

Atom	Ca	Al	O	Fe
Wyckoff position	24c	16a	96h	16a
occupation factor	1	0.845(5)	1	0.155(5)
x	0.1250	0.0000	0.0319(1)	0.0000
y	0.0000	0.0000	0.0519(2)	0.0000
z	0.2500	0.0000	0.46414(2)	0.0000
ADPs / \AA^2	0.0123(4)	0.0086(6)	0.0093(7)	0.0086(6)

Moreover, TEM, combined with EDS was also used in this sample to quantify the amount of iron in this hydrogarnet-type structure. Some particles of $C_3(A,F)H_6$ were analyzed and the obtained average composition matched relatively well that determined by the Rietveld methodology, see Table 3 in article #7; except for the iron content which is larger in TEM-EDS results. It is important to bear in mind that Rietveld methodology gives an average composition as the result of analyzing a representative sample. In any case, the most important result of this part is that the incorporation of iron in C_3AH_6 is possible and this phase is at least metastable. Moreover, as previously reported (Meller et al. 2004b), the Al/Fe ratio was greater than in the anhydrous phase. For this reason, it is assumed that iron also goes to an amorphous iron-rich gel, like the hydrated alumina-type gel, as hydration proceeds (Ectors et al. 2013, Meller et al. 2004b). Figure 4.24 shows TEM micrograph of $C_3A_{0.845}F_{0.155}H_6$ sample showing the expected cubic morphology, along (111) axis.

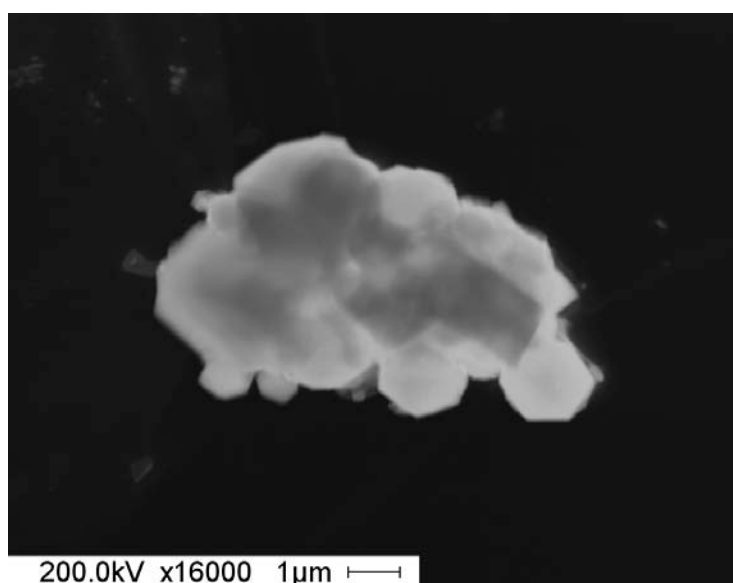


Figure 4.24. TEM micrograph of $C_3A_{0.845}F_{0.155}H_6$

4.5.6. Reactivity of C₄AF with gypsum.

The effect of the gypsum on the hydration mechanism of C₄AF has also been studied. Tetracalcium aluminoferrite was mixed with gypsum in a suitable proportion according to Meller et al. (2004a), and with a w/s ratio of 1.0 (C₄AF-g-1.0). Figure 4.25 shows the RQPA results obtained by analyzing *in-situ* SXRPD patterns up to 48 hours of hydration. In the first stage of the hydration, AFm-type phases were not identified and consequently only reaction [1.11] to form AFt took place. Later, when gypsum was totally consumed, the AFt started to decompose to yield an AFm-type phase, according to reactions [1.12] or [1.13]. To study the extension of both reactions is not an easy task but this (partial) conversion from AFt to AFm, reactions [1.12] and [1.13], have been studied and discussed previously by other authors (Meller et al. 2004a) and our results are in full agreement with their conclusions (Meller et al. 2004a).

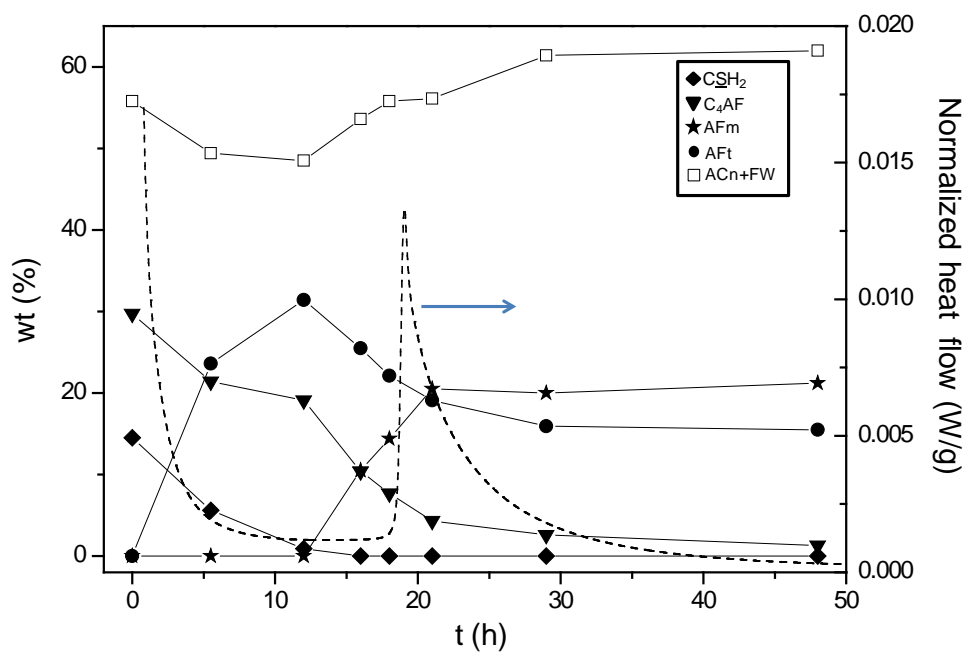


Figure 4.25. Full quantitative phase analysis results with time for C₄AF-g-1.0 (solid lines are guide to the eyes) and calorimetric heat flow curves (dashed line) are also displayed.

The time evolution of ACn and FW contents for this sample are also reported in Figure 4.25. Firstly, these values slightly diminished with time until 16 hours due to the presence of larger amounts of ettringite and the absence of AFm-type phases. Later, after 16 hours, the opposite behavior is observed because of the precipitation of AFm and the release of free water according to reaction [1.12]. Figure 4.22 shows the degree of reaction of C₄AF for this sample at all the studied ages.

Calorimetric data shows a broad signal between 20 and 30 hours of hydration likely associated to dissolution and precipitation processes, see Figure 4.25. This signal could be related to the AFm formation which occurs very close to that time from an independent study (SXRPD measurements). As the formation of AFt seems to occur very fast, the corresponding calorimetric signal cannot be recorded as a consequence of the 45 minutes of stabilization needed in the experimental set up used. Moreover, the total heat evolved after 48 h of hydration was 382 J/g.

A SEM-EDS study was performed for the C₄AF-g-1.0 sample on a polished section at 48 h of hydration in order to check if AFt and AFm phases had incorporated iron in their crystal structures. It is shown in Figure 3a in article #7 that those particles with needle and laminar shapes (SEM photograph) presented similar compositions to AFt and AFm, respectively and they contain non-negligible iron contents. These results also show that there are some bright particles observed by SEM with very high amount of iron which have been assigned as iron-bearing ACn phases. In addition to this, Figure 4.26 shows the fracture cross-section SEM micrograph of this sample. Small needle and laminar shape particles are clearly observed due to AFt and AFm phases respectively.

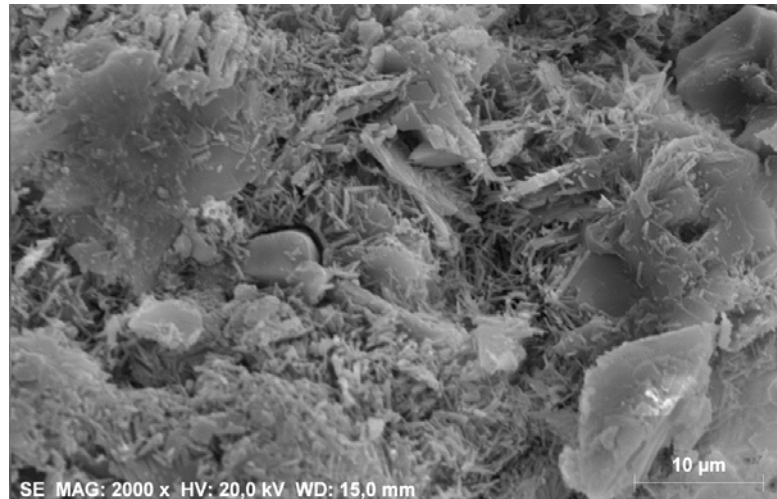


Figure 4.26. Fracture cross section SEM micrograph of C_4AF -g-1.0

4.5.7. Influence of ye'elimite in C_4AF hydration.

The hydration behavior of ye'elimite (both polymorph orthorhombic and pseudocubic) in the presence of C_4AF have been studied and discussed in section 4.5.3. Here, the hydration of C_4AF is discussed. As a summary, the mixture of tetracalcium aluminoferrite, gypsum and stoichiometric ye'elimite gave a mixture of AFt and AFm phases. However, C_4AF hydration was slightly slowed down in the presence of st-ye'elimite. The retarder effect of ye'elimite over C_4AF hydration was much stronger with doped ye'elimite and consequently AFt was the main hydration phase in this sample (see Figure 4.17(b)). It may seem that the dissolution of tetracalcium aluminoferrite was inhibited by the presence of the reaction products of ss-ye'elimite and this is likely the reason why only small quantities of AFm were quantified here. The retarder effect of ss-ye'elimite over C_4AF can be observed in Figure 4.22 which shows the degree of reaction of C_4AF for all the tetracalcium aluminoferrite-containing pastes at all the studied ages.

4.6. On-going research work.

At present, two different studies are been performing using different methodologies from those used in this PhD.

i) Ptychographic X-ray computed tomography (PXCT):

PXCT has been used to study the hydration of ye'elinite. PXCT is a non-invasive imaging technique based on the coherent properties of synchrotron radiation. The technique allows to obtain a three-dimensional mapping of the electron density of the studied sample (Miao et al. 2015; da Silva et al. 2015). It has a resolution close to 100 nm which makes the technique very appropriate for studying the microstructures in complex materials such as cement pastes (Trtik et al. 2013; da Silva et al. 2015).

The main goal has been the characterization of the microstructure of the pastes and the quantification of the electron and mass densities of the phases present in the samples. For the experiments, the samples were loaded inside a tapering capillary, filled with the appropriate amounts of distilled water, and both ends of the capillary were sealed immediately thereafter. After different hydration times, the samples (cement pastes) were investigated at cSAXS beamline, in Swiss Light Source synchrotron. For this experiment the pixel size was 40.8 nm.

Several samples has been studied by this technique and here we would like to highlight two of them, i) stoichiometric ye'elinite with water, at 6 days of hydration and ii) ye'elinite, gypsum and water, at 18 days of hydration. The main objective of this study is to study the amorphous 'gibbsite' and to estimate/determine its density which should vary if its hydration degree changes. It is also important to characterize the porosity which could develop in these hydration reactions.

For the st-ye'elinite with water sample at 6 days of hydration, Figure 4.27(a) show a selected tomogram of one slice in order to characterize the phase

4. Results and discussion

distributions. Moreover, Table 4.16 shows the measured electron and mass densities obtained for this sample and it can be observed that the mass densities match well the expected values for all the crystalline phases present in this sample. The resolution estimation for this measurement by Fourier shell correlation was 134 nm.

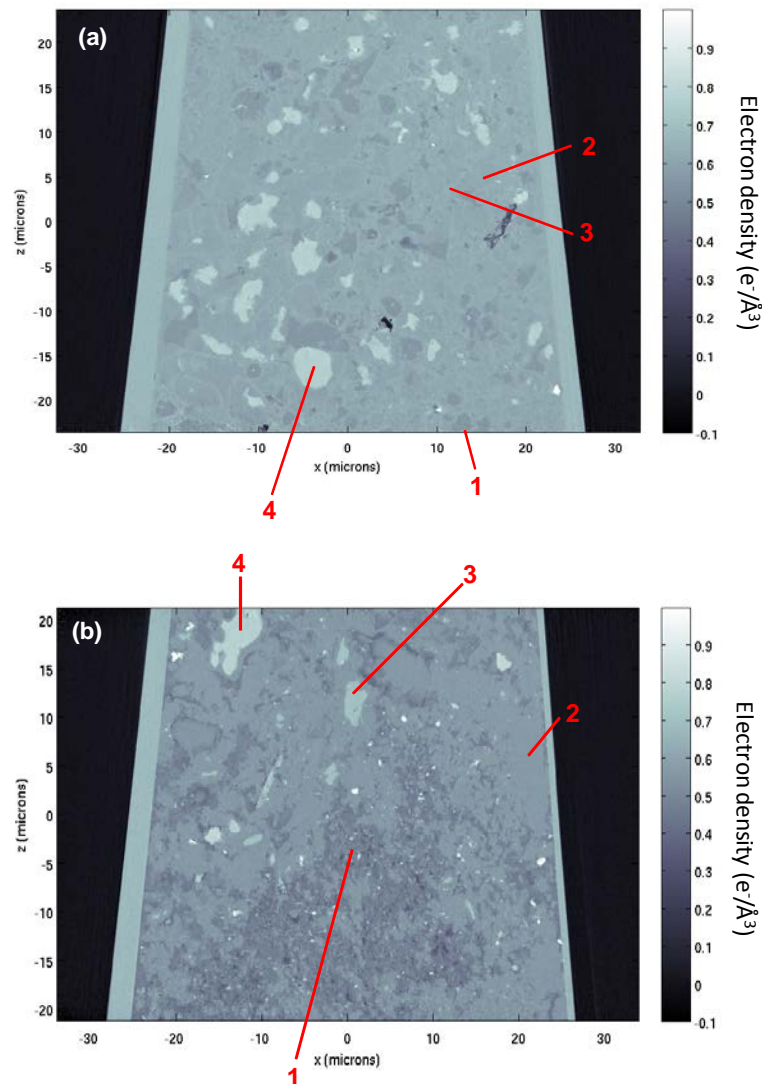


Figure 4.27. Tomogram of one slice obtained for (a) ye'elimite with water sample at 6 days of hydration and for (b) ye'elimite with gypsum and water sample at 18 days of hydration.

It is important to highlight that this study will allow us to understand the microstructure of amorphous gibbsite (amorphous aluminum hydroxide). The density of crystalline gibbsite, $\text{Al}(\text{OH})_3$, is well known, 2.40g/cm^3 but no similar density has been found in this study. For this reason, it could be supposed that all samples contain an amorphous phase, called gibbsite type-gel, $\text{Al}(\text{OH})_3 \cdot n\text{H}_2\text{O}$, which presents a variable amount of water (and so, its mass density is under debate).

Table 4.16. Densities obtained for the phases found in ye'elimité with water sample at 6 days of hydration obtain by PXCT.

Phase	Elect. Density ($\text{e}^-/\text{\AA}^3$)	Calculated mass density* (g/cm^3)	Theoretical mass density (g/cm^3)
H_2O	0.333	-	1.000
1. AFt	0.570	1.81	1.775
2. $\text{Al}(\text{OH})_3 \cdot n\text{H}_2\text{O}$	0.607	1.95	-
3. AFm	0.621	1.99	1.933
Cryst. gibbsite	0.741	-	2.398
4. Ye'elimité	0.765	2.53	2.602

*From the experiment

For ye'elimité with water sample, $\text{Al}(\text{OH})_3 \cdot n\text{H}_2\text{O}$ and AFm phases (mainly AFm), were found to have quite close experimental electron densities (≈ 0.60 & $\approx 0.62 \text{ e}^-/\text{\AA}^3$, respectively). We were not able to distinguish properly between both phases in the VOI (volume of interest) histogram (Figure 4.28(a)) but we have performed further studies using a bivariate histogram which combines the refractive index and the absorption index in order to clarify this issue.

For st-ye'elimité with gypsum and water sample at 18 days of hydration, Figure 4.27(b) show a selected tomogram of one slice in order to have a general idea of the phase distributions. The measured electron and mass densities obtained for this sample match well with the theoretical values, see Table 4.17. The resolution estimation for this measurement by Fourier shell correlation was 141nm.

4. Results and discussion

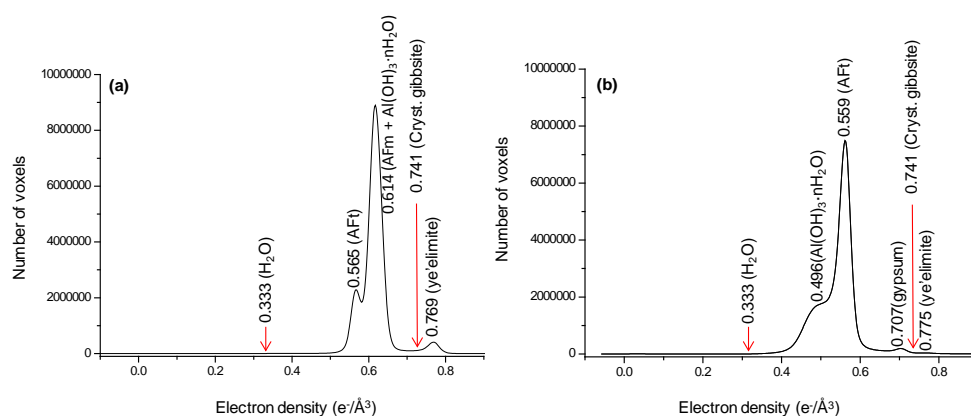


Figure 4.28. VOI histogram for (a) ye'elimite with water sample at 6 days of hydration and for (b) ye'elimite with gypsum and water sample at 18 days of hydration.

Table 4.17. Densities obtained for the phases found in ye'elimite with water sample at 18 days of hydration obtain by PXCT.

Phase	Elect. Density (e-/Å ³)	Calculated mass density* (g/cm ³)	Theoretical mass density (g/cm ³)
H ₂ O	0.333	-	1.000
1. Al(OH) ₃ ·nH ₂ O	0.479	1.54	-
2. AFt	0.564	1.79	1.775
3. Gypsum	0.703	2.28	2.304
Cryst. gibbsite	0.741	-	2.398
4. Ye'elimite	0.775	2.57	2.602

*From the experiment

The ye'elimite with gypsum sample should show a lot of ettringite (and little if any AFm phase) due to the presence of gypsum in the hydration medium according to the previous results obtained by SXRPD. This is precisely what it was observed from the analysis of the histogram, Figure 4.28(b). AFt was the main phase found in this sample jointly with amorphous aluminum hydroxide which has been identified in this sample with an electron density of 0.496 e-/Å³. Again, crystalline gibbsite and free water have not been identified in this sample.

Ana María Cuesta García

Moreover, small amounts of unreacted ye'elinite and gypsum were also found for this sample. Segmentation of the full tomogram of this sample will show the particle shapes of ettringite which is key to understand the performances of ye'elinite-containing cements.

It is important to highlight that two distinct microstructures are possible for 'amorphous gibbsite'. On the one hand, this phase may contain lattice water, i.e., water within the amorphous nanoparticles, even directly bound to aluminum. On the other hand, this phase may be composed by amorphous tiny nanoparticles of $\text{Al}(\text{OH})_3$ composition surrounded by free water. We must highlight that it is not possible to directly distinguish between these two possibilities with our estimated resolution (≈ 140 nm) in the two studies.

However, the absence of free water in these two samples, and the large variation of density between the two amorphous gibbsite samples point towards the mechanism of gibbsite nanoparticles surrounded by free water. The average density values determined for these two samples being the convolution of the density of gibbsite, 2.40 g/cm^3 , and free water, 1.00 g/cm^3 , within the resolution of the measurements. Furthermore, a third scenario with tiny partially hydrated gibbsite nanoparticles surrounded by free water, like in C-S-H gels, is also possible. A detailed analysis is in progress.

ii) high pressure SXRPD:

This experiment has been performed at the end of May-2015 at MSPD beamline of ALBA synchrotron. DAC has been used to obtain SXPDP patterns of hydrated phases under pressure. These works are important to derive mechanical properties of the hydrated phases as well as to study the stability of cement phases which may help to understand reaction mechanisms. The pressure transmitting medium is important as it should not induce any structural modification to the studied phase and it must be easy to work with. Silicone oil as well as

4. Results and discussion

methanol/ethanol mixtures have been used for studying hydrated cement phases at high pressures using DAC.

Pure iron-silicon-free katoite (C_3AH_6) has been the first sample tested in this study as reference material as its behavior under pressure is well known (Moon et al. 2011). Then, the most relevant result has been the study of the iron-katoite sample $C_3A_{0.845}F_{0.155}H_6$ from ambient pressure to close to 9 GPa using methanol/ethanol 4:1 as pressure transmitting medium. Figure 4.29 shows raw SXRPD patterns of iron Katoite at different pressures.

The Birch-Murnaghan equation of state (B.M. EoS) was used to calculate the bulk modulus of the iron-katoite. The third-order Birch–Murnaghan isothermal equation of state is given by (1.2):

$$P = \frac{3}{2}K_0[(V/V_0)^{-7/3} - (V/V_0)^{-5/3}] \left[1 + \frac{3}{4}(K'_0 - 4)((V/V_0)^{-2/3} - 1) \right] \quad (1.2)$$

The initial volume (V_0) estimated by for B.M. EoS was $2020.8(4.9) \text{ \AA}^3$ while the experimental value of V_0 was $2016.5(6) \text{ \AA}^3$, which gives us a high degree of confidence in the data. The y-intercept and slope of the weighted least-squares fit provide the bulk modulus K_0 and its derivative K'_0 (see Figure 4.30). The B.M. EoS with third order accounts well for the sets of data obtained and yielded a bulk modulus $K_0=54(2) \text{ GPa}$ with the pressure derivative $K'_0=5.5$, which is in agreement with the previously values reported for hydrogarnet (Moon et al. 2011). This study is in progress.

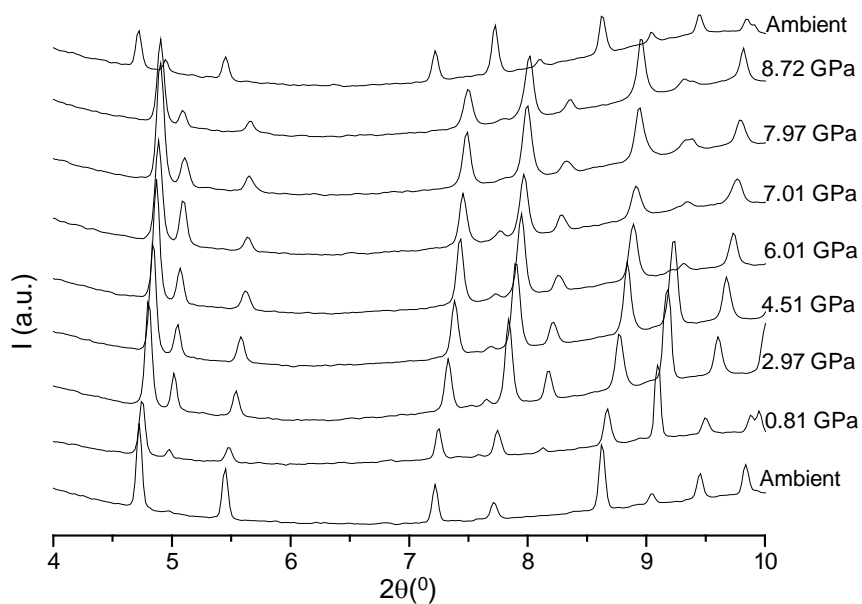


Figure 4.29. Integrated SRXPD ($\lambda=0.4246(1)$ Å) raw patterns of $C_3A_{0.845}F_{0.155}H_6$ as a function of pressure.

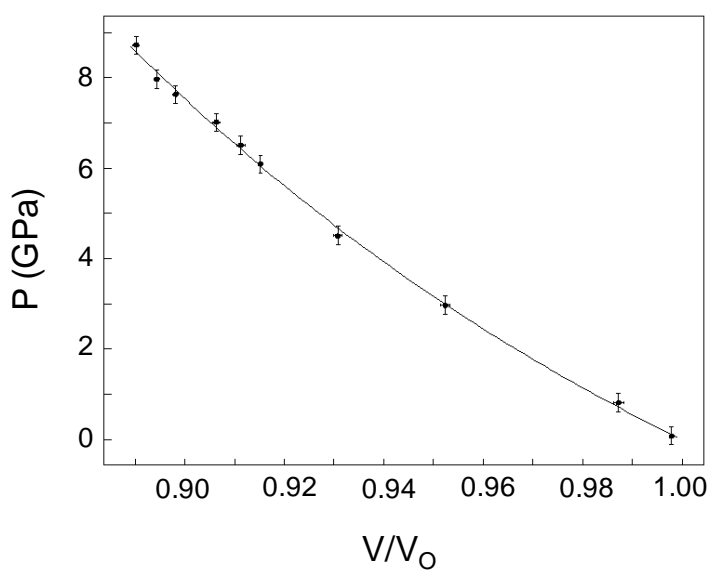


Figure 4.30. Pressure-volume behavior of iron-katoite with methanol/ethanol 4:1 as pressure medium. The line show third order B.M. EoS fitting.

5. Conclusions

5. Conclusions

In this PhD thesis about synthesis, characterization and hydration studies of single pure phases related to sulfoaluminate cements such as ye'elinite, dicalcium silicate and tetracalcium aluminoferrite, some important conclusions has been derived:

- The high temperature polymorphs of dicalcium silicate, β and α'_H , has been stabilized at RT and characterized. A β -form has been prepared with $\text{Ca}_2\text{Si}_{0.972}\text{Al}_{0.028}\text{O}_{3.986}\square_{0.014}$ and the stabilization of the high temperature form at RT has been allocated by replacing the silicate units and generating oxygen vacancies. The α'_H -dicalcium silicate has been stabilized by coupled sodium/boron doping. The chemical formula has been $\text{Ca}_{1.85}\text{Na}_{0.15}(\text{SiO}_4)_{0.85}(\text{BO}_3)_{0.15}$ and the mechanism of boron stabilization by BO_3^{3-} has been determined. Moreover, a new structural description has been reported.
- The RT crystal structure of stoichiometric ye'elinite, $\text{Ca}_4[\text{Al}_6\text{O}_{12}]\text{SO}_4$, has been studied by powder diffraction and atomistic calculations. Both methodologies agree that the most stable structure at room temperature and pressure is the Pcc2 orthorhombic phase.
- The crystal structure of doped ye'elinite, nominal stoichiometry: $\text{Ca}_{3.8}\text{Na}_{0.2}\text{Al}_{5.6}\text{Fe}_{0.2}\text{Si}_{0.2}\text{O}_{12}\text{SO}_4$, has also been studied by high-resolution SXRPD data. A pseudocubic structural description is reported based on $\bar{I}43m$ space group with a split-atom model for the sulfate anions.
- For stoichiometric ye'elinite, temperature-dependent XRPD, DSC, and permittivity data indicate a phase transition at 470 °C on heating from

orthorhombic to cubic phase which is accompanied by an disordering of the sulfate anions.

- For doped ye'elimite, a variable temperature permittivity study also shows a phase transition on heating at 525°C. The structural study of this phase at 800°C suggests a truly cubic structure. Consequently, a pseudocubic to cubic phase transition is occurring on heating.
- The crystal structures of ye'elimite (orthorhombic and pseudocubic) and dicalcium silicate (α'_H -form) reported in this Thesis enable more accurate mineralogical phase analysis of CSA and BCSA cements (when compared to those results obtained using previously-reported structures).
- We have shown that hydration kinetics of ye'elimite samples not only depends on the w/s ratio and the solubility of the additional sulfate source, but also on the polymorphism of ye'elimite. Firstly, in the absence of additional sulfate sources, stoichiometric ye'elimite reacts slower than doped ye'elimite and doped ye'elimite produces higher amounts of ettringite than stoichiometric ye'elimite in similar hydrating conditions. Moreover, in this environment, the formation of AFm-type phases from stoichiometric ye'elimite is strongly accelerated and favoured by high w/s ratios. On the other hand, in the presence of gypsum or anhydrite as additional sulfate sources, stoichiometric ye'elimite reacts faster than doped ye'elimite. In addition, the formation of AFm-type phases at late ages is avoided by the addition of gypsum and anhydrite being ettringite the only crystalline phase formed in this reaction medium.
- The hydration behaviour of stoichiometric and doped ye'elimite presents some differences in the presence of other phases. For instance, in tetracalcium aluminoferrite-containing mixtures, stoichiometric-ye'elimite dissolution is delayed; C_4AF reaction is enhanced which yields

5. Conclusions

higher amounts of AFm and comparatively lower amounts of AFt. In the same hydrating conditions, doped-ye'elimite dissolution is much faster and tetracalcium aluminoferrite dissolution delayed; which yields higher amounts of AFt and comparatively much lower amounts of AFm. Finally, the role of polymorphism of dicalcium silicate in the presence of ye'elimite has also been investigated. In the tested experimental conditions, both ye'elimite polymorphs yield mainly crystalline ettringite in the presence of dicalcium silicate and gypsum. However, we have demonstrated that the hydration degree of $\alpha'_H\text{-C}_2\text{S}$ is much larger than that of $\beta\text{-C}_2\text{S}$ in the investigated time range (up to six months) with the reported starting phase assemblage.

- The hydration mechanism of pure tetracalcium aluminoferrite phase has also been investigated in the presence and absence of gypsum. C_4AF in the presence of water hydrates to form mainly a hydrogarnet-type phase with iron, $\text{C}_3\text{A}_{0.84}\text{F}_{0.16}\text{H}_6$, as single crystalline phase (a revised crystal structure has been obtained). The presence of sulfates strongly modifies C_4AF hydration behavior. The hydration of C_4AF in the presence of gypsum gives AFt and amorphous aluminum hydroxide and once gypsum is completely dissolved crystalline AFm starts to precipitate jointly with more amorphous phase.

5. Conclusiones

5. Conclusiones

En esta tesis doctoral se ha sintetizado, caracterizado y estudiado la hidratación de fases puras presentes en cementos de sulfoaluminado de calcio, concretamente la ye'elimita, el silicato dicálcico y el ferrito aluminato tetracálcico. De este estudio se pueden derivar las siguientes conclusiones:

- Se han estabilizado a temperatura ambiente y caracterizado los polimorfos de alta temperatura, β y α'_H , del silicato dicálcico. El polimorfo beta se ha obtenido sustituyendo unidades silicato por aluminato con la correspondiente generación de vacantes de oxígeno según la estequiometría general $\text{Ca}_2\text{Si}_{0.972}\text{Al}_{0.028}\text{O}_{3.986}\square_{0.014}$. Por otro lado, el α'_H -silicato dicálcico se ha estabilizado realizando un dopaje simultáneo de sodio en la posición del calcio y de boro en la del silicio. La fórmula general de la disolución sólida obtenida es $\text{Ca}_{1.85}\text{Na}_{0.15}(\text{SiO}_4)_{0.85}(\text{BO}_3)_{0.15}$ donde el boro se encuentra formando unidades BO_3^{3-} triangulares planas. Además, se ha obtenido una nueva descripción estructural para esta fase.
- Se ha determinado la estructura cristalina a temperatura ambiente de la ye'elimita estequiométrica, $\text{Ca}_4[\text{Al}_6\text{O}_{12}]\text{SO}_4$, mediante difracción de rayos-X de laboratorio, de neutrones y por cálculo atómicos. Estas metodologías apuntan a que la estructura más estable para esta fase a temperatura ambiente y presión es la ortorrómbica con grupo espacial Pcc2.
- Se ha estudiado la estructura cristalina de la ye'elimita dopada, $\text{Ca}_{3.8}\text{Na}_{0.2}\text{Al}_{5.6}\text{Fe}_{0.2}\text{Si}_{0.2}\text{O}_{12}\text{SO}_4$, por difracción de rayos-X de sincrotrón de

alta resolución. La descripción estructural se ha realizado en el grupo espacial $I\bar{4}3m$, desdoblado las posiciones de los oxígenos del anión sulfato.

- La ye'elimita estequiométrica se ha caracterizado mediante termodifracción de rayos-X de laboratorio, calorimetría diferencial de barrido y medidas de permitividad. A 470°C, en calentamiento, se produce una transición de fase de ortorrómbica a cúbica acompañada de desorden en los aniones sulfato.
- La caracterización por termodifracción de rayos-X y medidas de permitividad demuestran que la ye'elimita dopada presenta una transición de fase a 525°C. Al calentar los picos de difracción se estrechan significativamente demostrando que la forma de baja temperatura posee una simetría inferior a la cúbica siendo pseudocúbica. Además, el estudio estructural de esta fase a 800°C sugiere la presencia de una estructura cúbica real.
- Las estructuras cristalinas determinadas de la ye'elimita (ortorrómbica y pseudocúbica) y del silicato dicálcico (forma α'_H) permiten hacer análisis mineralógicos de fases de cementos tipo CSA and BCSA con mejores factores de desacuerdo que cuando se realizan utilizando las estructuras previamente publicadas.
- Se ha mostrado que la cinética de hidratación de la ye'elimita depende de la relación agua/sólido, de la solubilidad de la fuente de sulfato adicional y de la forma polimórfica. En primer lugar, cuando la hidratación se realiza sin fuente de sulfato adicional, la ye'elimita estequiométrica reacciona más lentamente que la dopada, produciendo ésta más cantidad de etringita en comparación con la que produce la estequiométrica en las mismas condiciones. En este medio de reacción la formación de fases

5. Conclusions

tipo AFm en la hidratación de la ye'elimita estequiométrica se acelera y favorece usando mayores relaciones agua/sólido. En presencia de yeso o anhidrita, la ye'elimita estequiométrica reacciona más rápido que la dopada. Además, se evita la formación a altas edades de fases tipo AFm, siendo la etringita la única fase cristalina.

- La hidratación de la ye'elimita estequiométrica y dopada es diferente en presencia de otras fases. En mezclas que contienen ferrito aluminato tetracálcico, la disolución de la ye'elimita se retrasa y favorece la reacción del C_4AF formándose grandes cantidades de AFm y muy poca de AFt. En las mismas condiciones, la disolución de la ye'elimita dopada es mucho más rápida y la disolución del C_4AF se retrasa formándose grandes cantidades de AFt y muy poca de AFm. Por último, también se ha investigado el papel del polimorfismo del silicato dicálcico en presencia de la ye'elimita. En mezclas que contienen silicato dicálcico y yeso, ambos polimorfos conducen a la formación de etringita cristalina. Sin embargo, el grado de hidratación del polimorfo α'_H-C_2S es mayor que en el caso de β -silicato dicálcico en el rango de tiempo estudiado (hasta 6 meses) con respecto al ensamblaje de fases inicial.
- Se ha investigado el mecanismo de hidratación de la fase ferrito aluminato tetracálcico con y sin yeso. El C_4AF en presencia de agua se hidrata para formar una fase tipo hidrogranate con hierro $C_3A_{0.84}F_{0.16}H_6$ (se ha presentado también una nueva estructura cristalina para esta fase). La presencia de sulfato modifica sustancialmente el mecanismo de hidratación del C_4AF y conduce a la formación de AFt e hidróxido de aluminio amorfo. Una vez que se ha disuelto todo el yeso, la fase cristalina AFm empieza a precipitar junto con más fase amorfa. Por otro lado, la hidratación del C_4AF se ve inhibida por la presencia de ye'elimita dopada hasta 46 horas de hidratación.

6. References

6. References

A

- Adolfsson D, Menad N, Viggh E and Bjorkman B (2007), “Hydraulic properties of sulphoaluminate belite cement based on steelmaking slags”, *Adv Cem Res*, 19, 133-138.
- Allmann R (1977), “Refinement of the hybrid layer structure $[\text{Ca}_2\text{Al}(\text{OH})_6] \cdot 0.5(\text{SO}_4) \cdot 3\text{H}_2\text{O}$ ”, *Neues Jb Miner Monat*, 136-144.
- Álvarez-Pinazo G, Cuesta A, García-Maté M, , De la Torre A G, León-Reina L and Aranda M A G (2012), “Rietveld quantitative phase analysis of Yeelimites-containing cements”, *Cem Concr Res*, 42, 960-971.
- Álvarez-Pinazo G, Santacruz I, León-Reina L, Aranda M A G and De la Torre A G (2013), “Hydration Reactions and Mechanical Strength Developments of Iron Rich Sulfoaluminates Eco-cements”, *Ind Eng Chem Res*, 52,16606-16614.
- Álvarez-Pinazo G, Cuesta A, García-Maté M, Santacruz I, Losilla E R, Ordóñez L M, Sanfélix S G, Fauth F, Aranda M A G and De la Torre A G (2014), “In-situ early-age hydration study of sulfoaluminates cements by synchrotron powder diffraction”, *Cem Concr Res*, 56, 12-19.
- Andac M and Glasser F P (1999), “Pore solution composition of calciumsulfoaluminate cement”, *Adv Cem Res*, 11, 23-26.
- Andac O and Glasser F P (1994), “Polymorphism of calcium sulphoaluminate $(\text{Ca}_4\text{Al}_6\text{O}_{16} \cdot \text{SO}_3)$ and its solid solutions”, *Adv Cem Res*, 6, 57-60.
- Antao S M, Hassan I and Parise J B (2004), “Chromate aluminate sodalite, $\text{Ca}_8[\text{Al}_{12}\text{O}_{24}](\text{CrO}_4)_2$: phase transitions and high-temperature structural evolution of the cubic phase”, *Can Mineral*, 42, 1047-1056.
- Aranda M A G, Cuberos A J M, Cuesta A, Alvarez-Pinazo G, De la Torre A G, Schollbach K and Pöllmann H (2011), “Hydrating behaviour of activated

Ana María Cuesta García

belite sulfoaluminate cements”, *Proceedings of the 13th International Congress on the Chemistry of Cement*, Madrid, Spain.

Aranda M A G, De la Torre A G and León-Reina L (2012), “Rietveld quantitative phase analysis of OPC clinkers, cements and hydration products”, *Rev Mineral Geochem*, 74, 169-209.

Aranda M A G and De la Torre A G (2013), “Sulfoaluminate cement” in *Eco-efficient Concrete*, Pacheco-Torgal F, Jalali S, Labrincha J and John V M (Eds.), Woodhead Publishing, Cambridge, 488-522.

Aranda M A G, De la Torre A G and León-Reina L (2015), “Powder diffraction characterisation of cements”, *International Tables for Crystallography, Volume H, Powder Diffraction*, Eds. C. Gilmore, J. Kaduk, H. Schenk 2015 (in the press).

B

Barcelo L, Kline J, Walenta G and Gartner E (2014), “Cement and carbon emissions”, *Mater Struct*, 47, 1055-1065.

Barnes P, Fentiman C H and Jeffery J W (1980), “Structurally related dicalcium silicate phases”, *Acta Cryst*, A36, 353-356.

Barrer R M and Coler J F (1968), “Interaction of sodium vapour with synthetic sodalite: Sorption and formation of colour centres”, *J Phys Chem Solids*, 29, 1755-1758.

Benarchid M Y, Diouri A, Boukhari A, Aride J, Rogez J and Castanet R (2004), “Elaboration and thermal study of iron-phosphorus-substituted dicalcium silicate phase”, *Cem Concr Res*, 34, 1873-1879.

Benarchid M Y, Diouri A, Boukhari A, Aride J and Elkhadiri I (2005), “Hydration of iron-phosphorus doped dicalcium silicate phase”, *Mat Chem Phys*, 94, 190-194.

6. References

- Bensted J (1979), "Some hydration studies of α -dicalcium silicate", *Cem Concr Res*, 9, 97-101.
- Berger S, Cau-Dit-Coumes C, Le Bescop P and Daminot D (2011), "Influence of a thermal cycle at early age on the hydration of calcium sulfoaluminate cements with variable gypsum contents", *Cem Concr Res*, 41, 149-160.
- Bizzozero J, Gosselin C and Scrivener K L (2014), "Expansion mechanisms in calcium aluminate and sulfoaluminate systems with calcium sulfate", *Cem Concr Res*, 56, 190-202.
- Bonaccorsi E, Merlino S and Taylor H F W (2004), "The crystal structure of jennite, $\text{Ca}_9\text{Si}_6\text{O}_{18}(\text{OH})_6 \cdot 8(\text{H}_2\text{O})$ ", *Cem Con Res*, 34, 1481-1488.
- Bonaccorsi E, Merlino S and Kampf A R (2005), "The crystal structure of tobermorite 14 A (plombierite), a C - S - H phase", *J Am Cer Soc*, 88, 505-512.
- Borgmann C, Sauer J, Jüstel T, Kynast U and Schüth F (1999), "Efficiently emitting Rare Earth sodalites by phase transformation of zeolite X and by direct synthesis", *Adv Mater*, 11, 45-49.
- Boultif A and Louer D (2004), "Powder pattern indexing with the dichotomy method", *J Appl Cryst*, 37, 724-731.
- Bredig M A (1950), "Polymorphism of calcium orthosilicate", *J Am Ceram Soc*, 33, 188-192.
- Bullerjahn F, Schmitt D and Ben Haha M (2014), "Effect of raw mix design and of clinkering process on the formation and mineralogical composition of (ternesite) belite calcium sulfoaluminate ferrite clinker", *Cem Concr Res*, 2014, 59, 87-95.

C

- Calos N J, Kennard C H L, Whittaker A K and Davis R L (1995), "Structure of calcium aluminate sulfate $\text{Ca}_4\text{Al}_6\text{O}_{16}\text{S}$ ", *J Solid State Chem*, 1995, 119, 1-7.

Ana María Cuesta García

- Campbel D H (1999), “Microscopical examination and interpretation of portland cement and clinker Portland Cement Association”, Old Orchard RD., Skokie, USA.
- Catti M, Gazzoni G and Ivaldi G (1984), “Order-disorder in the α' -(Ca,Sr) $_2$ SiO $_4$ solid solution: a structural and statistical-thermodynamic analysis”, *Acta Cryst*, B40, 537-544.
- Cau Dit Coumes C, Courtois S, Peysson S, Ambroise J and Péra J (2009), “Calcium sulfoaluminate cement blended with OPC: a potential binder to encapsulate low-level radioactive slurries of complex chemistry”, *Cem Concr Res*, 39, 740-747.
- Champenois J B, Mesbah A, Cau-dit-Coumes C, Renaudin G, Leroux F, Mercier C, Revel B and Damidot D (2012), “ Crystal structures of Boro-AFm and Boro-AFt phases”, *Cem Concr Res*, 42, 1362-1370.
- Chen I A, Hargis C W and Juenger M C G (2012), “Understanding expansion in calcium sulfoaluminate-belite cements”, *Cem Concr Res*, 42, 51-60.
- Chen Y L, Lin C J, Ko M S, Lai Y C and Chang J E (2011), “Characterization of mortars from belite-rich clinkers produced from inorganic wastes”, *Cem Concr Comp*, 33, 261-266.
- Colville A A (1970), “The crystal structure of Ca $_2$ Fe $_2$ O $_5$ and its relation to the nuclear electric field gradient at the iron sites”, *Acta Cryst*, B26, 1469-1473.
- Colville A A and Geller S (1971), “The crystal structure of brownmillerite, Ca $_2$ FeAlO $_5$ ”, *Acta Cryst*, B27, 2311-2315.
- Colville A A and Geller S (1972), “The structures of Ca $_2$ Fe $_{1.43}$ Al $_{0.57}$ O $_5$ and Ca $_2$ Fe $_{1.28}$ Al $_{0.72}$ O $_5$ ”, *Acta Cryst*, B28, 3196-3200.
- Cuberos A J M, De la Torre A G, Álvarez-Pinazo G, Martín-Sedeño M C, Schollbach K, Pöllmann H and Aranda M A G (2010), “Active iron-rich belite sulfoaluminate cements: Clinkering and Hydration”, *Environ Sci Technol*, 44, 6855-6862.

Czaya R (1971), "Refinement of the structure of γ -Ca₂SiO₄", *Acta Cryst*, B27, 848-849.

D

da Silva J C, Trtik P, Diaz A, Holler M, Guizar-Sicairos M, Raabe J, Bunk O and Menzel A (2015), "Mass Density and Water Content of Saturated Never-Dried Calcium Silicate Hydrates", *Langmuir* 31, 3779-3783.

De la Torre A G, Bruque S and Aranda M A G (2001), "Rietveld quantitative amorphous content analysis", *J Appl Crystallogr*, 34, 196-202.

De la Torre A G (2003), "Estudio de cementos y materiales relacionados por el método de Rietveld", Tesis Doctoral, Universidad de Málaga.

De la Torre A G, Cuberos A J M, Álvarez-Pinazo G, Cuesta A and Aranda M A G (2011a), "In situ powder diffraction study of belite sulfoaluminate clinkering", *J Synch Rad*, 18, 506-514.

De la Torre A G, Cuberos A J M, Álvarez-Pinazo G, Cuesta A and Aranda M A G (2011b), "In-Situ Clinkering Study of Belite Sulfoaluminate Clinkers by Synchrotron X-Ray Powder Diffraction", *Proceedings of the 13th International Congress on the Chemistry of Cement*, Madrid, Spain.

Depmeier W (1987), "Aluminate sodalites — A family of inclusion compounds with strong host-guest interactions", *J Inclusion Phenom*, 5, 279-282.

Depmeier W (1988), "Aluminate sodalites — A family with strained structures and ferroic phase transitions", *Phys Chem Minerals*, 15, 419-426.

Depmeier W and Bühner W (1991), "Aluminate sodalites: Sr₈[Al₁₂O₂₄](MoO₄)₂ (SAM) at 293, 423, 523, 623 and 723 K and Sr₈[Al₁₂O₂₄](WO₄)₂ (SAW) at 293 K", *Acta Cryst*, B47, 197-206.

Depmeier W (2005), "The sodalite family", *Rev Mineral Geochem*, 57, 203-240.

De Wolff P M (1972), "The definition of the indexing figure of merit M₂₀", *J Appl Cryst*, 1972, 5, 243.

Ana María Cuesta García

Dilnesa BZ, Lothenbach B, Le Saout G, Renaudin G, Mesbah A, Filinchuk Y, Wichser A and Wieland E (2011) “Iron in carbonate containing AFm phases”, *Cem Concr Res*, 41, 311-323.

Dilnesa B Z, Lothenbach B, Renaudin G, Wichser A and Wieland E (2012), “Stability of monosulfate in the presence of iron”, *J Am Ceram Soc*, 95, 3305-3316.

Dilnesa B Z, Lothenbach B, Renaudin G, Wichser A and Kulik D (2014), “Synthesis and characterization of hydrogarnet $\text{Ca}_3(\text{Al}_x\text{Fe}_{1-x})_2(\text{SiO}_4)_y(\text{OH})_{4(3-y)}$ ”, *Cem Concr Res*, 59, 96-111.

Dinnebier R E and Billinge S J L (Eds.) (2008), “Powder Diffraction: Theory and Practice”, Royal Society of Chemistry, Publishing, Cambridge.

E

Ectors D, Neubauer J and Goetz-Neunhoeffler F (2013), “The hydration of synthetic brownmillerite in presence of low Ca-sulfate content and calcite monitored by quantitative in-situ-XRD and heat flow calorimetry”, *Cem Concr Res*, 54, 61-68.

Effenberger H, Kirfel A, Will G and Zobetz E (1983), “A further refinement of the crystal structure of thaumasite, $\text{Ca}_3\text{Si}(\text{OH})_6(\text{CO}_3)(\text{SO}_4)(\text{H}_2\text{O})_{12}$ ”, *Neues Jb Miner Monat*, 60-68.

El-Didamony H, El-Sokkari T M, Khalil KH A, Heikal M and Ahmed I A (2012), “Hydration mechanisms of calcium sulphoaluminate $\text{C}_4\text{A}_3\text{S}$, C_4AS phase and active belite $\beta\text{-C}_2\text{S}$ ”, *Ceram Silik*, 56, 389-395.

F

- Fauth F, Peral I, Popescu C and Knapp M (2013), “The new Material Science Powder Diffraction beamline at ALBA Synchrotron”, *Powder Diffr*, 28, S360-S370.
- Feng X, Liao G and Long S (1991), “On the Structure and the Hydration Rate of $3\text{CaO}_3 \cdot 3\text{Al}_2\text{O}_3 \cdot \text{CaSO}_4$ ”, *Il Cemento*, 88, 29-35.
- Ferro O, Galli E, Papp G, Quartieri S, Szakall S and Vezzalini G (2003), “A new occurrence of katoite and re-examination of the hydrogrossular group”, *Eur J Mineral*, 15, 419-426.
- Fierens P and Tirlocq J (1983), “Nature and concentration effect of stabilizing elements of Beta-dicalcium silicate on its hydration rate”, *Cem Concr Res*, 13, 267-276.
- François M, Renaudin G and Evrad O (1998), “A cementitious compound with composition $3\text{CaO} \cdot \text{Al}_2\text{O}_3 \cdot \text{CaCO}_3 \cdot 11\text{H}_2\text{O}$ ”, *Acta Cryst*, C54, 1214-1217.
- Fukuda K and Ito S (1999), “Improvement in reactivity and grindability of belite-Rich cement by remelting reaction”, *J Am Ceram Soc*, 82, 2177-2180.
- Fukuda K, Wakamatsu N and Ito S (2001), “Improvement in hydration reactivity of α -phase belite by remelting reaction”, *J Am Ceram Soc*, 84, 639-641.
- Fukuhara M, Goto S, Asage K, Daimon M and Kondo R (1981), “Mechanisms and kinetics of C_4AF hydration with gypsum”, *Cem Concr Res*, 407-414.

G

- Gajbhiye N S and Singh N B (2010), “Microwave assisted preparation of Fe^{3+} doped β -dicalcium silicate by sol-gel method”, *Mater Res Bull*, 45, 933-938.
- García-Maté M, Santacruz I, De la Torre A G, León-Reina L and Aranda M A G (2012), “Rheological and hydration characterization of calcium sulfoaluminate cements”, *Cem Concr Comp*, 34, 684-691.

Ana María Cuesta García

- García-Maté M, De la Torre A G, León-Reina L, Aranda M A G and Santacruz I (2013), “Hydration study of calcium sulfoaluminate cements blended with fly ash”, *Cem Concr Res*, 54, 12-20.
- García-Maté M, De la Torre A G, León-Reina L, Losilla E R, Aranda M A G and Santacruz I (2015), “Effect of calcium sulfate source on the hydration of calcium sulfoaluminate eco-cement”, *Cem Concr Comp*, 55, 53-61.
- Gartner E M, Yong J F, Damidot D A and Jawed I (2002), “Hydration of Portland cement” in *Structure and Performance of cements*, Bensted J and Barnes P (Eds.), Spon Press, London and New York, 57-113.
- Gartner E (2004), “Industrially interesting approaches to low-CO₂ cement”, *Cem Concr Res*, 34, 1489-1498.
- Gartner E and Li G (2006), “High-belite sulfoaluminate clinker: fabrication process and binder preparation”, World Patent Application WO2006/018569 A2.
- Gartner E and Macphee D E (2011), “A physico-chemical basis for novel cementitious binders”, *Cem Concr Res*, 41, 736-749.
- Gartner E and Hirao H (2015), “A review of alternative approaches to the reduction of CO₂ emissions associated with the manufacture of the binder phase in concrete” *Cem Concr Res*, <http://dx.doi.org/10.1016/j.cemconres.2015.04.012>
- Georgin J F, Ambroise J, Péra J and Reynouard J M (2008), “Development of self-leveling screed based on calcium sulfoaluminate cement: Modelling of curling due to drying”, *Cem Concr Comp*, 30, 769-778.
- Ghosh S N, Rao P B, Paul A K and Raina K J (1979), “The chemistry of the dicalcium silicate mineral”, *Mater Sci*, 14, 1554-1566.
- Glasser F P and Zhang L (2001), “High-performance cement matrices based on calcium sulfoaluminate-belite compositions”, *Cem Concr Res*, 31, 1881-1886.

- Goetz-Neunhoeffler F and Neubauer J (2006), “Refined ettringite ($\text{Ca}_6\text{Al}_2(\text{SO}_4)_3(\text{OH})_{12}\cdot 26\text{H}_2\text{O}$) structure for quantitative X-ray diffraction analysis”, *Powder Diffr*, 21, 4-11.
- Gualtieri A F, Riva V, Bresciani A, Maretti S, Tamburini M and Viani A (2014), “Accuracy in quantitative phase analysis of mixtures with large amorphous contents. The case of stoneware ceramics and bricks”, *J Appl Cryst*, 47, 835-846.
- Guirado F, Galis S Chinchón S and Rius J (1998) “Crystal Structure Solution of Hydrated High-Alumina Cement from X-ray Powder Diffraction Data” *Angew Chem Int Ed*, 37, 72-75.

H

- Halstead P E and Moore A E (1962), “The composition and crystallography on an anhydrous calcium aluminosulphate occurring in expanding cement”, *J Appl Chem*, 12, 413-417.
- Hargis C W, Kirchheim A P, Monteiro P J M and Gartner E.M (2013) “Early age hydration of calcium sulfoaluminate (synthetic ye’elinite, $\text{C}_4\text{A}_3\text{S}$) in the presence of gypsum and varying amounts of calcium hydroxide”, *Cem Concr Res*, 48, 105-115.
- Hargis C W, Moon J, Lothenbach B, Winnefeld F, Wenk H R and Monteiro P J M (2014a), “Calcium sulfoaluminate sodalite ($\text{Ca}_4\text{Al}_6\text{O}_{12}\text{SO}_4$) crystal structure evaluation and bulk modulus determination”, *J Am Ceram Soc*, 97, 892-898.
- Hargis C W, Telesca A and Monteiro P J M (2014b), “ Calcium sulfoaluminate (Ye’elinite) hydration in the presence of gypsum, calcite and vaterite”, *Cem Concr Res*, 65, 15-20.
- Hartman M R and Berliner R (2006), “Investigation of the structure of ettringite by time-of-flight neutron powder”, *Cem Concr Res*, 36, 364-370.

Ana María Cuesta García

Hartmann M R, Brady S K, Berliner R and Conradi M S (2006), “The evolution of structural changes in ettringite during thermal decomposition”, *J Solid State Chem*, 179, 1259-1272.

Hesse C, Goetz-Neunhoeffler F and Neubauer J (2011), “A new approach in quantitative in-situ XRD of cement pastes: Correlation of heat flow curves with early hydration reactions”, *Cem Concr Res*, 41, 123-128.

Heyns A M, Range K J and Wildenauer M (1990), “The vibrational spectra of NbBO_4 , TaBO_4 , NaNb_3O_8 and NaTa_3O_8 ”, *Spectrochim Acta*, 46A, 1621-1628.

Hurlbut C S and Klein C (1985), “Manual of Mineralogy”, 20th ed., John Wiley & Sons, New York.

I

Ichikawa M, Ikeda S and Komukai Y (1994), “Effect of cooling rate and Na_2O content on the character of the interstitial”, *Cem Concr Res*, 24, 1092-1096.

Il'inets A M and Bikbau M Y (1990), “Structural Mechanism of Polymorphic Transitions of Dicalcium Silicate, Ca_2SiO_4 . Part II: Refinement of Crystal Structure of High-Temperature α'_L . Modification of Dicalcium Silicate Ca_2SiO_4 ”, *Kristallografiya*, 35, 91-93.

Insley H (1936), “Structural Characteristics of Some Constituents of Portland Cement Clinker”, *Journal of Research of the National Bureau of Standards*, Washington, D.C., 17, 353-361.

Ioannou S, Reig L, Paine K and Quillin K (2014), “Properties of a ternary calcium sulfoaluminate-calcium sulphate-fly ash cement”, *Cem Concr Res*, 56, 2014, 75-83.

J

- Janotka I and Krajci L (1999), “An experimental study on the upgrade of sulfoaluminate-belite cement systems by blending with Portland cement”, *Adv Cem Res*, 11, 35-41.
- Janotka I, Krajci U and Mojumdar S C (2007), “Performance of sulphoaluminate-belite cement with high C_4A_3S content”, *Cer Silik*, 51, 74-81.
- Jansen D, Stabler CH, Goetz-Neunhoeffler F, Dittrich S and Neubauer J (2011), “Does ordinary Portland cement contain amorphous phase? A quantitative study using an external standard method”, *Powder Diffr*, 26, 31-38.
- Jansen D, Goetz-Neunhoeffler F, Lothenbach B and Neubauer J (2012a), “The early hydration of Ordinary Portland Cement (OPC): An approach comparing measured heat flow with calculated heat flow from QXRD”, *Cem Concr Res*, 42, 134-138
- Jansen D, Neubauer J, Goetz-Neunhoeffler F, Haerzschel R and Hergeth WD (2012b), “Change in reaction kinetics of a Portland cement caused by a superplasticizer — Calculation of heat flow curves from XRD data”, *Cem Concr Res*, 42, 327-332.
- Jelenic I, Bezjak A and Bujan M (1978), “Hydration of B_2O_3 -stabilized α' - and β -modifications of dicalcium silicate”, *Cem Concr Res*, 8, 173-180.
- Jelenic I and Bezjak A (1982), “Electron Diffraction Evidence for Superstructures in β -Modification of Dicalcium Silicate”, *Cem Concr Res*, 12, 785-788.
- Jost K H, Ziemer B and Seydel R (1977), “Retermination of the structure of β -dicalcium silicate”, *Acta Cryst*, B33, 1696-1700.
- Jost K H and Ziemer B (1984), “Relations between the crystal structures of calcium silicates and their reactivity against water”, *Cem Concr Res*, 14, 177-184.
- Juenger M and Chen I (2011), “Composition-Property Relationships in Calcium Sulfoaluminate Cements”, *Proceedings of the 13th International Congress on the Chemistry of Cement*, Madrid, Spain.

Ana María Cuesta García

Juenger M C G, Winnefeld F, Provis J L and Ideker J H (2011), “Advances in alternative cementitious binders”, *Cem Concr Res*, 41, 1232-1243.

Juenger M C G and Siddique R (2015), “Recent advances in understanding the role of supplementary cementitious materials in concrete”, *Cem Concr Res*, <http://dx.doi.org/10.1016/j.cemconres.2015.03.018>

Jupe A C, Turrillas X, Barnes P, Colston S L, Hall C, Hausermann D and Handfland M (1996), “Fast in situ x-ray-diffraction studies of chemical reactions: A synchrotron view of the hydration of tricalcium aluminate”, *Phys Rev B*, 53, 14697-14700.

K

Kantro D L and Weise C H (1979), “Hydration of various beta-dicalcium silicate preparations”, *J Am Cer Soc*, 62, 621-626.

Kim Y-M and Hong S-H (2004), “Influence of minor ions on the stability and hydration rates of β -dicalcium silicate”, *J Am Ceram Soc*, 87, 900-905.

Klein A (1963), “Calcium aluminosulfate and expansive cements containing same”, US Patent 3155526.

Klochko K, Cody G D, Tossell J A, Dera P and Kaufman A J (2009), “Re-evaluating boron speciation in biogenic calcite and aragonite using ^{11}B MAS NMR”, *Geochimica et Cosmochimica Acta*, 73, 1890-1900.

Kondo R (1965), “The Synthesis and Crystallography of a Group of a new Compounds Belonging to the Hauyne Type Structure”, *J Ceram Assoc Jpn*, 73, 1-8.

Kurokawa D, Takeda S, Colas M, Asaka T, Thomas P and Fukuda K (2014), “Phase transformation of $\text{Ca}_4[\text{Al}_6\text{O}_{12}]\text{SO}_4$ and its disordered crystal structure at 1073K”, *J Solid State Chem*, 215, 265-270.

Kwan S, La Rosa J and Grutzeck MW (1995), “ ^{29}Si and ^{27}Al MASNMR study of stratlingite”, *J Am Ceram Soc*, 78, 1921-1926.

L

- Lager G A, Armbruster T H and Faber J (1987), "Neutron and X-ray diffraction study of hydrogarnet $\text{Ca}_3\text{Al}_2(\text{O}_4\text{H}_4)_3$ ", *A Miner*, 72, 756-765.
- Larson A C and Von Dreele R B (1994), Los Alamos national laboratory report LA-UR-86-748, Los Alamos.
- Lawrence D (2003), "Physicochemical and mechanical properties of Portland cements" in *Lea's Chemistry of Cement and Concrete* by Peter Hewlett, Elsevier Science & Technology Books Pub, 343-419.
- Leardini L, Martucci A and Cruciani G (2012), "The unusual thermal expansion of pure silica sodalite probed by in situ time-resolved synchrotron powder diffraction" *Microporous Mesoporous Mater*, 151, 163-171.
- Le Saoût G, Lothenbach B, Hori A, Higuchi T and Winnefeld F (2013), "Hydration of Portland cement with additions of calcium sulfoaluminates", *Cem Concr Res*, 43, 81-94.
- Li G S, Walenta G and Gartner E M (2007), "Formation and hydration of low- CO_2 cements based on belite, calcium sulfoaluminate and calcium aluminoferrite", *Proceedings of the 12th International Congress on the Chemistry of Cement*, Montreal, Canada.
- Locher F W (2006), "Cement: principles of production and use", Verlag Bau + Technik GmbH, Düsseldorf.

M

- Ma B, Li X, Shen X, Mao Y and Huang H (2014), "Enhancing the addition of fly ash from thermal power plants in activated high belite sulphoaluminate cement", *Const Build Mat*, 52, 261-266.

- Madsen I C, Scarlett N V Y and Kern A (2011), "Description and survey of methodologies for the determination of amorphous content via X-ray powder diffraction", *Z Kristallogr*, 226, 944-955.
- Martín-Sedeño M C, Cuberos A J M, De la Torre A G, Álvarez-Pinazo G, Ordóñez L M, Gateshki M and Aranda M A G (2010), "Aluminum-rich belite sulfoaluminate cements: clinkering and early age hydration", *Cem Concr Res*, 40, 359-369.
- Matkovic B, Carin V, Gacesa T, Halle R, Jelenic I and Young J F (1981), "Influence of BaSO₄ on the Formation and Hydration Properties of Calcium Silicates: I, Doped Dicalcium Silicates", *Am Ceram Soc Bull*, 60, 825-829.
- Matschei T, Lothenbach B and Glasser F P (2007), "The AFm phase in Portland cement", *Cem Concr Res*, 37, 118-130.
- McCaffrey R (2002), "Climate change and the cement industry", *Global Cement and Lime Magazine Environmental Special Issue*, 15-19.
- Meller N, Hall C, Jupe A C, Colston S L, Jacques S D M, Barnes P and Phipps J (2004a), "The paste hydration of brownmillerite with and without gypsum: a time resolved synchrotron diffraction study at 30, 70, 100 and 150 °C", *J Mat Chem*, 14, 428-435.
- Meller N, Hall C and Crawshaw J (2004b), "ESEM evidence for through-solution transport during brownmillerite hydration", *J Mat Sci*, 39, 6611-6614.
- Meredith P, Donald A M, Meller N and Hall C (2004), "Tricalcium aluminate hydration: Microstructural observations by in-situ electron microscopy", *J Mater Sci*, 39, 997-1005.
- Merlini M, Artioli G, Meneghini C, Cerulli T, Bravo A and Cella F (2007), "The early hydration and the set of Portland cements: In situ X-ray powder diffraction studies", *Powder Diffr*, 22, 201-208.
- Merlino S, Bonaccorsi E and Armbruster T (2000), "The real structure of clinotobermorite and tobermorite 9 Å: OD character, polytypes, and structural relationships", *Eur J Mineral*, 12, 411-429.

6. References

- Merlino S, Bonaccorsi E and Armbruster T (2001), “The real structure of Tobermorite 11 Å: normal and anomalous forms, OD character and polytypic modifications”, *Eur. J. Mineral*, 13, 577-590.
- Mesbah A, François M, Cau-dit-Coumes C, Frizon F and Filinchuk Y (2011) “Crystal structure of Kuzel’s salt $3\text{CaO}\cdot\text{Al}_2\text{O}_3\cdot\frac{1}{2}\text{CaSO}_4\cdot\frac{1}{2}\text{CaCl}_2\cdot 11\text{H}_2\text{O}$ determined by synchrotron powder diffraction”, *Cem Concr Res*, 41, 504-509.
- Miao J, Ishikawa T, Robinson I K and Murnane M M (2015), “Beyond crystallography: diffractive imaging using coherent x-ray light sources”, *Science*, 348, 530-535.
- Midgley C M (1952), “The crystal structure of β dicalcium silicate”, *Acta Cryst*, 5, 307-312.
- Monnier A, Srdanov V I, Stucky G D and Metiu H (1994), “The Properties of Electrons in Sodalite Saturated with Alkali Atoms”, *J Chem Phys*, 100, 6944-6952.
- Moore A E and Taylor H F W (1970), “Crystal structure of ettringite”, *Acta Cryst*, B26, 386-393.
- Möschner G, Lothenbach B, Winnefeld F, Ulrich A, Figi R and Kretzschmar R (2009), “Solid solution between Al-ettringite and Fe-ettringite ($\text{Ca}_6[\text{Al}_{1-x}\text{Fe}_x(\text{OH})_6]_2(\text{SO}_4)_3\cdot 26\text{H}_2\text{O}$)”, *Cem Concr Res*, 39, 482-489.
- Moran K L, Harrison W T A, Kamber I, Gier T E, Bu X, Herren D, Behrens P, Eckert H and Stucky G D (1996), “Synthesis, Characterization and Tunable Electronic/Optical Properties of II–VI Semiconductor Species Included in the Sodalite Structure”, *Chem Mater*, 8, 1930-1943.
- Morin V, Walenta G, Gartner E, Termkhajornkit P, Baco I and Casabonne J M (2011), “Hydration of a Belite-Calcium Sulfoaluminate- Ferrite cement: Aether™”, *Proceedings of the 13th International Congress on the Chemistry of Cement*, Madrid, Spain.

Ana María Cuesta García

Morsli K, De la Torre A G, Stöber S, Cuberos A J M, Zahir M and Aranda M A G (2007a), “Quantitative Phase Analysis of Laboratory Active Belite Clinkers by Synchrotron Powder Diffraction”, *J Amer Cer Soc*, 90, 3205-3212.

Morsli K, De la Torre A G, Zahir M and Aranda M A G (2007b), “Mineralogical Phase Analysis of Alkali and Sulfate Bearing Belite Rich Laboratory Clinkers”, *Cem Concr Res*, 37, 639-646.

Moon J, Oh J E, Balonis M, Glasser F P and Monteiro P J M (2011), “Pressure induced reactions amongst calcium aluminate hydrate phases”, *Cem Concr Res*, 41, 571-578.

Mumme W G, Hill R J, Bushnell-Wye G and Segnit E R (1995), “Rietveld structure refinement, crystal chemistry and calculated powder diffraction data for the polymorphs of dicalcium silicate and related phases”, *N Jb Miner Abh*, 169, 35-68.

Mumme W, Cranswick L and Chakoumakos B (1996), “Rietveld crystal structure refinements from high temperature neutron powder diffraction data for the polymorphs of dicalcium silicate”, *N Jb Miner Abh*, 170, 171-188.

N

Nettleship I, Slavick K G, Kim Y J and Kriven W M (1992), “Phase transformation in dicalcium silicate: I, Fabrication and phase stability of fine-grained β -phase”, *J Am Cer Soc*, 75, 2400-2406.

O

O'Connor B H and Raven M D (1988), “Application of the Rietveld refinement procedure in assaying powdered mixtures”, *Powder Diffr*, 3, 2-6.

Odler I (2000), “Special Inorganic Cements”, Taylor and Francis, London.

- Ogura M, Morozumi K, Elangovan S P, Tanada H, Ando H and Okubo T (2008), “Potassium-doped sodalite: A tectoaluminosilicate for the catalytic material towards continuous combustion of carbonaceous matters”, *App Catal B*, 77, 294-299.
- Ono Y, Kawamura S and Soda Y (1969), “Microscopic observations of alite and belite and hydraulic strength of concrete”, *Proceedings of the 5th International Congress on the Chemistry of Cement*, Tokyo, Japan.
- Ono Y (1995), “Ono’s Method, Fundamental Microscopy of Portland Cement Clinker”, Chichibu Onoda Cement Corp., No. 2-4-2, Ohsaku, Sakura, Chiba, 285, Japan, 229 pp.

P

- Palou M, Majling J, Dovál M, Kozanková J and Mojumdar S C (2005), “Formation and stability of crystallohydrates in the non-equilibrium system during hydration of SAB cements”, *Cer Silik*, 49, 230-236.
- Park C K (2001), “Phase transformation and hydration of dicalcium silicate containing stabilizers”, *J Ceram Soc Jap*, 109, 380-386.
- Passaglia E and Rinaldi R (1984), “Katoite, a new member of the $\text{Ca}_3\text{Al}_2(\text{SiO}_4)_3\text{--Ca}_3\text{Al}_2(\text{OH})_{12}$ series and a new nomenclature for the hydrogrossular group of minerals”, *Bull Mineral*, 107, 605-618.
- Pecharsky V and Zavalij P (2005), “Fundamentals of Powder Diffraction and Structural Characterization of Materials”, Springer, New York.
- Peixing Z, Yimin C, Piping S, Guanying Z, Wenmel H and Jiaguo W (1992), “The crystal structure of $\text{C}_4\text{A}_3\text{S}$ ”, *Proceedings of the 9th International Congress on the Chemistry of Cement*, New Delhi, India.
- Pelletier L, Winnefeld F and Lothenbach B (2010), “The ternary system Portland cement–calcium sulphoaluminate clinker–anhydrite: Hydration mechanism and mortar properties”, *Cem Concr Comp*, 32, 497-507.

Ana María Cuesta García

- Pelletier-Chaignat L, Winnefeld F, Lothenbach B, Le Saout G, Müller C J and Famy C (2011), “Influence of the calcium sulphate source on the hydration mechanism of portland cement–calcium sulfoaluminate clinker–calcium sulphate binders”, *Cem Concr Comp*, 33, 551-561.
- Pera J and Ambroise J (2004), “New applications of calcium sulfoaluminate cement”, *Cem Concr Res*, 34, 671-676.
- Petch H E (1961), “The hydrogen positions in portlandite, $\text{Ca}(\text{OH})_2$, as indicated by the electron distribution”, *Acta Cryst*, 14, 950-957.
- Phair J W (2006), “Green chemistry for sustainable cement production and use”, *Green Chem*, 8, 763-780.
- Porrás-Vázquez J M, De la Torre A G, Losilla E R and Aranda M A G (2007), “Oxide and proton conductivity in aluminum-doped tricalcium oxy-silicate”, *Solid State Ion*, 178, 1073-1080.
- Pritts M and Daugherty K E (1976), “The effect on stabilizing agents on the hydration rate of $\beta\text{-C}_2\text{S}$ ”, *Cem Concr Res*, 6, 783-796.

Q

- Quillin K (2001), “Performance of belite–sulfoaluminate cements”, *Cem Concr Res*, 31, 1341-1349.

R

- Raab B and Pöllmann H (2011), “ $\text{C}_2\text{AH}_8\text{-}2\text{CaO}\cdot\text{Al}_2\text{O}_3\cdot(8\pm n)\text{H}_2\text{O}$ - main hydration products of CAC”, *Z Kristallogr Proc*, 1, 349-353.
- Rapin J P and Francois M (2001), “The double-layered hydroxide $3\text{CaO}\cdot\text{Al}_2\text{O}_3\cdot 0.5\text{CaBr}_2\cdot 0.5\text{CaCl}_2\cdot 10\text{H}_2\text{O}$ ”, *Acta Cryst*, C57, 137-138.
- Rapin J P, Noor N M and Francois M (1999a), “The double layered hydroxide $3\text{CaO}\cdot\text{Al}_2\text{O}_3\cdot\text{CaBr}_2\cdot 10\text{H}_2\text{O}$ ”, *Acta Cryst*, C55, IUC9900092.

6. References

- Rapin J P, Walcarius A, Lefevre G and Francois M (1999b), "A double-layered hydroxide, $3\text{CaO}\cdot\text{Al}_2\text{O}_3\cdot\text{CaI}_2\cdot 10\text{H}_2\text{O}$ ", *Acta Cryst*, C55, 1957-1959.
- Regourd M, Bigare M, Forest J and Guinier A (1968), "Synthesis and Crystallographic Investigation of Some Belites", *Proceedings of the 5th International Congress on the Chemistry of Cement*, Tokyo, Japan.
- Remy C and Andrault D (1997), "High-Temperature, High-Pressure X-ray Investigation of Dicalcium Silicate", *J Am Ceram Soc*, 80, 851-860.
- Renaudin G, Kubel F, Rivera J P and Francois M (1999), "Structural phase transition and high temperature phase structure of Friedels salt, $3(\text{CaO})(\text{Al}_2\text{O}_3)(\text{CaCl}_2)\cdot 10(\text{H}_2\text{O})$ ", *Cem Concr Res*, 29, 1937-1942.
- Renaudin G and François M (1999), "The lamellar Double-hydroxide (LDH) compound with composition $3\text{CaO}\cdot\text{Al}_2\text{O}_3\cdot\text{Ca}(\text{NO}_3)_2\cdot 10\text{H}_2\text{O}$ ", *Acta Cryst*, C55, 835-838.
- Richardson I G (1999), "The nature of C-S-H in hardened cements", *Cem Concr Res*, 29, 1129-1147.
- Rietveld H M (1967), "Line profiles of neutron powder-diffraction peaks for structure refinement", *Acta Cryst*, 22, 151-152.
- Rietveld H M (1969), "A profile refinement method for nuclear and magnetic structures", *J Appl Crystallogr*, 2, 65-71.
- Rinaldi R, Sacerdoti M and Passaglia E (1990), "Straetlingite: crystal structure, chemistry and a reexamination of its polytype vertumnite", *Eur J Mineral*, 2, 841-849.
- Rivas Mercury J M, Pena P, De Aza A H, Turrillas X, Sobrados I and Sanz J (2007), "Solid-state ^{27}Al and ^{29}Si NMR investigations on Si-substituted hydrogarnets", *Acta Materialia*, 55, 1183-1191.
- Rogers D E and Aldridge L P (1977), "Hydrates of calcium ferrites and calcium aluminoferrites", *Cem Concr Res*, 7, 399-410.
- Rousselot I, Taviot-Gueho C, Leroux F, Leone P, Palvadeau P and Besse JP (2002), "Insights on the structural chemistry of hydrocalumite and

Ana María Cuesta García

hydrotalcite-like materials: investigation of the series $\text{Ca}_2\text{M}^{(3+)}(\text{OH})_6\text{Cl}_2(\text{H}_2\text{O})(\text{M}^{(3+)})$: Al, Ga, Fe, and Sc) by x-ray powder diffraction”. *J Solid State Chem*, 167, 137-144.

Runcevski T, Dinnebier R E, Magdysyuk O V and Pöllmann H (2012), “Crystal structures of calcium hemicarboaluminate and carbonated calcium hemicarboaluminate from synchrotron powder diffraction data”, *Acta Cryst*, B 68, 493–500.

S

Saalfeld H (1975), “X-Ray Investigation of Single Crystals of $\beta\text{-Ca}_2\text{SiO}_4$ (Larnite) at High Temperatures”, *Am Mineral*, 60, 824-827.

Saalfeld H and Depmeier W (1972), “Silicon-free compounds with sodalite structure”, *Kristall und Technik*, 7, 229-233.

Saalfeld H and Wedde M (1974), “Refinement of the crystal structure of gibbsite, $\text{Al}(\text{OH})_3$ ”, *Z Kristallogr*, 139, 129-135.

Sacerdoti M and Passaglia E (1985), “The crystal structure of katoite and implications within the hydrogrossular group of minerals”, *Bull Mineral*, 108, 1-8.

Sacerdoti M and Passaglia E (1988), “Hydrocalumite from Latium, Italy: its crystal structure and relationship with related synthetic phases”, *Neues Jb Miner Monat*, 462-475.

Sahu S and Majling J (1993), “Phase compatibility in the system $\text{CaO-SiO}_2\text{-Al}_2\text{O}_3\text{-Fe}_2\text{O}_3\text{-SO}_3$ referred to sulphoaluminate belite cement clinker”, *Cem Concr Res*, 23, 1331-1339.

Santacruz I, De la Torre A G, Álvarez-Pinazo G, Cabeza A, Cuesta A, Sáenz J and Aranda M.A.G (2015). “Structure of stratlingite and effect of hydration methodology on microstructure”, DOI: 10.1680/adcr.14.00104.

6. References

- Scarlett N V Y and Madsen I C (2006), “Quantification of phases with partial or no known crystal structures”, *Powder Diffr*, 21, 278-284.
- Schmidt R and Poellmann H (1999), ICDD Grant-in-aid. Martin-Luther-Uni., Halle, Germany.
- Scrivener K L, Juilland P and Monteiro P J M (2015), “Advances in understanding hydration of Portland cement”, *Cem Concr Res*, <http://dx.doi.org/10.1016/j.cemconres.2015.05.025>
- Setter N, Mendoza-Alvarez M E, Depmeier W and Schmid H (1984) “Aluminate sodalite $\text{Sr}_8[\text{Al}_{12}\text{O}_{24}](\text{CrO}_4)_2$ a new ferroelectric”, *Ferroelectrics*, 56, 49-52.
- Sharp J H, Lawrence C D and Yang R (1999), “Calcium sulphoaluminate cements—Low-energy cements, special cements or what?”, *Adv Cem Res*, 11, 3-13.
- Silver A H and Bray P J (1958), “Nuclear Magnetic Resonance Absorption in Glass. I. Nuclear Quadrupole Effects in Boron Oxide, Soda-Boric Oxide, and Borosilicate Glasses”, *J Chem Phys*, 29, 984-990.
- Smaalen SV, Dinnebier R, Katzke H and Depmeier W (1997), “Structural Characterization of the High-Temperature Phase Transition in $\text{Ca}_8[\text{Al}_{12}\text{O}_{24}](\text{MoO}_4)_2$ Aluminate Sodalite using X-ray Powder Diffraction” *J State Solid Chem*, 129, 130-143.
- Smith D K, Majumdar A and Ordway F (1965), “The crystal structure of [gamma]-dicalcium silicate”, *Acta Cryst*, 18, 787-795.
- Smith D K, Johnson G G, Scheible A, Wims A M, Johnson J L and Ullmann G (1987), “Quantitative X-ray powder diffraction method using the full diffraction pattern”, *Powder Diffr*, 2, 73-77.
- Snellings R, Bazzoni A and Scrivener K (2014), “The existence of amorphous phase in Portland cements: Physical factors affecting Rietveld quantitative phase analysis”, *Cem Concr Res*, 59, 139-146.
- Song F, Yu Z, Yang F, Lu Y and Liu Y (2015), “Microstructure of amorphous aluminum hydroxide in belite-calcium sulfoaluminate cement”, *Cem Concr Res*, 71, 1-6.

Ana María Cuesta García

Sun Q, Li J and Wang J (2011), “Effect of borate concentration on solidification of radioactive wastes by different cements”, *Nucl Engin Design*, 241, 4341-4345.

Susuki K and Yamaguchi G (1968), “A Structural Study on α' - Ca_2SiO_4 ”, Proceedings of the 5th International Congress on the Chemistry of Cement, Tokyo, Japan.

T

Taplin J H (1959), “A method for following the hydration reactions in Portland cement paste”, *Australian J Appl Sci*, 10, 329-345.

Taylor H F W (1986), “Chemistry of cement hydration”, *Proceedings of the 8th International Congress on the Chemistry of Cement*, Rio de Janeiro, Brazil.

Taylor H F W (1997), “Cement Chemistry”, Thomas Telford, London.

Taylor J C and Zhu R (1992), “Simultaneous use of observed and calculated standard profiles in quantitative XRD analysis of minerals by the multiphase Rietveld method: the determination of pseudorutile in mineral and products”, *Powder Diffr*, 7, 152-161.

Telesca A, Marroccoli M, Pace M L, Tomasulo M, Valenti G L and Monteiro P J M (2014), “A hydration study of various calcium sulfoaluminate cements”, *Cem Concr Comp*, 53, 233-238.

Teoreanu I, Filoti G, Hritcu C, Bucea L, Spânu V, Ciocanel S and Ivascu M (1979), “Interaction mechanism of $2\text{CaO}\cdot\text{Fe}_2\text{O}_3$ and $4\text{CaO}\cdot\text{Al}_2\text{O}_3\cdot\text{Fe}_2\text{O}_3$ with water, at various pressures and temperatures”, *Il Cemento*, 76, 19-28, 1979.

Toby B H (2001), “EXPGUI, a graphical user interface for GSAS”, *J Appl Crystallogr*, 34, 210-213.

Touzo B, Scrivener K L and Glasser F P (2013), “Phase compositions and equilibria in the $\text{CaO}\text{-Al}_2\text{O}_3\text{-Fe}_2\text{O}_3\text{-SO}_3$ system, for assemblages containing ye'elimite and ferrite $\text{Ca}_2(\text{Al,Fe})\text{O}_5$ ”, *Cem Concr Res*, 54, 77-86.

Trtik P, Diaz A, Guizar-Sicairos M, Menzel A and Bunk O (2013), “Density mapping of hardened cement paste using ptychographic X-ray computed tomography”, *Cem Concr Comp* 36, 71-77.

Tukia M, Hölsä J, Lastusaari M and Niittykoski J (2005), “Eu³⁺ doped rare earth orthoborates, RBO₃ (R = Y, La and Gd), obtained by combustion synthesis”, *Opt Mater*, 27, 1516-1522.

U

Udagawa S, Urabe K, Takada K and Natsume M (1979), “Studies on the dusting of Ca₂SiO₄”, The crystal structure of α'-Ca₂SiO₄”, *Cem Assoc Jpn Rev, Gen Meet, Tech Sess*, 33, 35-38.

Udagawa S, Urabe K, Natsume M and Yano T (1980), “Refinement of the crystal-structure of γ-Ca₂SiO₄”, *Cem Concr Res*, 10, 139-144.

W

Wesselsky A and Jensen O M (2009), “Synthesis of pure Portland cement phases”, *Cem Concr Res*, 39, 973-980.

Winnefeld F and Barlag S (2010), “Calorimetric and thermogravimetric study on the influence of calcium sulfate on the hydration of ye'elinite”, *J Therm Anal Calorim*, 101, 949-957.

Winnefeld F and Lothenbach B (2010), “Hydration of calcium sulfoaluminate cements - Experimental findings and thermodynamic modeling”, *Cem Concr Res*, 40, 1239-1247.

Wu Z D (1995), “Hydrates of the calcium sulphoaluminate cement – aluminum hydroxide”, *China Build Mater Sci Technol*, 4, 7-10.

Y

- Yamaguchi G and Takagi S (1969), “The analysis of Portland cement clinker”, *Proceeding of the 5th International Congress on the Chemistry of Cement*, Tokyo, Japan.
- Yamnova N A, Zubkova N V, Eremin N N, Zadov A E and Gazeev V M (2011), “Crystal structure of Larnite β -Ca₂SiO₄ and specific features of polymorphic transitions in dicalcium orthosilicate”, *Kristallografiya*, 56, 235-245.
- Yano T, Urabe K, Ikawa H, Teraushi T, Ishizawa N and Udagawa S (1993), “Structure of alpha-dicalcium silicate hydrate”, *Acta Cryst*, C49, 1555-1559.

Z

- Zhang P, Chen Y, Shi L, Zhang G and Huang W W J (1992). “The crystal structure of C₄A₃S”, *Proceedings of the 9th International Congress on the Chemistry of Cement*, New Delhi, India.
- Zhang L, Su M Z and Wang Y M (1999), “Development of the use of sulfo- and ferro-aluminate cements in China”, *Adv Cem Res*, 11, 15-21.
- Zhao Y, Lu L, Wang S, Gong C and Huang Y (2013), “Modification of dicalcium silicates phase composition by BaO, SO₃ and MgO”, *J Inorg Organomet Polym*, 23, 930-936.
- Zhou Q and Glasser F P (2001), “Thermal stability and decomposition mechanisms of ettringite at <120°C”, *Cem Concr Res*, 31, 1333-1339.
- Zhou Q, Milestone N B and Hayes M (2006), “An alternative to Portland cement for waste encapsulation-the calcium sulfoaluminate cement system”, *J Haz Mater*, 136, 120-129.
- Ziemer B, Altrichter B and Jesenak V (1984), “Effect of SO₃ on formation and hydraulic reactivity of belite”, *Cem Concr Res*, 14, 686-692.

Annex I: Other publications

Other publications

- A.G. de la Torre, A.J.M. Cuberos, G. Álvarez-Pinazo, **A. Cuesta**, M.A.G. Aranda. “In situ powder diffraction study of belite sulfoaluminate clinkering” *Journal of Synchrotron Radiation*, 2011, 18, 506-514.
- G. Álvarez-Pinazo, **A. Cuesta**, M. García-Maté, I. Santacruz, A. G. De la Torre, L. León-Reina and M. A. G. Aranda. “Rietveld quantitative phase analysis of Yeelimite-containing cements” *Cement and Concrete Research*, 2012, 42, 960-971.
- G. Álvarez-Pinazo, **A. Cuesta**, M. García-Maté, I. Santacruz, E. R. Losilla, L.M. Ordóñez, S. G. Sanfélix, F. Fouth, M.A.G. Aranda, A. G. De la Torre. “In-situ early-age hydration study of sulfobelite cements by synchrotron powder diffraction”. *Cement and Concrete Research*, 2014, 56, 12-19.
- **Cuesta**, G. Álvarez-Pinazo, M.García-Maté, I. Santacruz, M.A.G. Aranda, A. G. De la Torre, L. León-Reina. “Rietveld quantitative phase analysis with Molybdenum radiation”. *Powder Diffraction*, 2015, 30, 25-35.
- M. García-Maté, I. Santacruz, **A. Cuesta**, L. León-Reina, M.A.G. Aranda, I. Baco, V. Morin, G. Walenta, E. Gartner and A. G. De la Torre. “Amorphous determination in calcium sulfoaluminate materials by external and internal methods”. *Advanced cement research*, 2015, 27, 417-423.
- I. Santacruz, A.G De la Torre, G. Álvarez-Pinazo, A.Cabeza, **A. Cuesta**, J. Sanz, M. A G Aranda “Structure of stratlingite and effect of hydration methodology on microstructure” *Advances in cement research*, 2015, doi: /10.1680/adcr.14.00104.

Annex II: Copyright permissions

a#1: Mechanism of stabilization of dicalcium silicate solid solution with aluminium

Cuesta A, Aranda M A G, Sanz J, De la Torre A G and Losilla E R (2014b),
“Mechanism of stabilization of dicalcium silicate solid solution with aluminium”,
Dalton Trans, 43, 2176-2182.

Acknowledgement

Reproduced by permission of The Royal Society of Chemistry

<http://pubs.rsc.org/en/content/articlelanding/2014/dt/c3dt52194j#!divAbstract>

a#2: Reactive belite stabilization mechanisms by boron bearing dopants

Rightslink® by Copyright Clearance Center

https://s100.copyright.com/AppDispatchServlet



Home Account Info Help Live Chat



Title: Reactive belite stabilization mechanisms by boron-bearing dopants
Author: Ana Cuesta, Enrique R. Losilla, Miguel A.G. Aranda, Jesús Sanz, Ángeles G. De la Torre
Publication: Cement and Concrete Research
Publisher: Elsevier
Date: April 2012
Copyright © 2012 Elsevier Ltd. All rights reserved.

Logged in as:
ana cuesta
Account #: 3000916509
[LOGOUT](#)

Order Completed

Thank you very much for your order.

This is a License Agreement between ana cuesta ("You") and Elsevier ("Elsevier"). The license consists of your order details, the terms and conditions provided by Elsevier, and the [payment terms and conditions](#).

[Get the printable license.](#)

License Number	3657711482324
License date	Jun 28, 2015
Licensed content publisher	Elsevier
Licensed content publication	Cement and Concrete Research
Licensed content title	Reactive belite stabilization mechanisms by boron-bearing dopants
Licensed content author	Ana Cuesta, Enrique R. Losilla, Miguel A.G. Aranda, Jesús Sanz, Ángeles G. De la Torre
Licensed content date	April 2012
Licensed content volume number	42
Licensed content issue number	4
Number of pages	9
Type of Use	reuse in a thesis/dissertation
Portion	full article
Format	both print and electronic
Are you the author of this Elsevier article?	Yes
Will you be translating?	No
Title of your thesis/dissertation	Preparation and hydration of model ecocement phases. Characterization by diffraction and cognate methods.
Expected completion date	Nov 2015
Estimated size (number of pages)	250
Elsevier VAT number	GB 494 6272 12
Permissions price	0.00 EUR
VAT/Local Sales Tax	0.00 EUR / 0.00 GBP
Total	0.00 EUR

[ORDER MORE...](#) [CLOSE WINDOW](#)

Copyright © 2015 Copyright Clearance Center, Inc. All Rights Reserved. [Privacy statement](#). [Terms and Conditions](#).
Comments? We would like to hear from you. E-mail us at customer@copyright.com

a#3: Structure, atomistic simulations, and phase transition of stoichiometric yeelinite

RightsLink® by Copyright Clearance Center

<https://s100.copyright.com/AppDispatchServlet>


Home Create Account Help Live Chat


ACS Publications Title: Structure, Atomistic Simulations, and Phase Transition of Stoichiometric Yeelinite
Most Trusted. Most Cited. Most Read.

Author: Ana Cuesta, Angeles G. De la Torre, Enrique R. Losilla, et al
Publication: Chemistry of Materials
Publisher: American Chemical Society
Date: May 1, 2013
 Copyright © 2013, American Chemical Society

LOGIN
 If you're a copyright.com user, you can login to RightsLink using your copyright.com credentials. Already a RightsLink user or want to learn more?

PERMISSION/LICENSE IS GRANTED FOR YOUR ORDER AT NO CHARGE

This type of permission/license, instead of the standard Terms & Conditions, is sent to you because no fee is being charged for your order. Please note the following:

- Permission is granted for your request in both print and electronic formats, and translations.
- If figures and/or tables were requested, they may be adapted or used in part.
- Please print this page for your records and send a copy of it to your publisher/graduate school.
- Appropriate credit for the requested material should be given as follows: "Reprinted (adapted) with permission from (COMPLETE REFERENCE CITATION). Copyright (YEAR) American Chemical Society." Insert appropriate information in place of the capitalized words.
- One-time permission is granted only for the use specified in your request. No additional uses are granted (such as derivative works or other editions). For any other uses, please submit a new request.

BACK

CLOSE WINDOW


Copyright © 2015 Copyright Clearance Center, Inc. All Rights Reserved. [Privacy statement](#). [Terms and Conditions](#).
 Comments? We would like to hear from you. E-mail us at customercare@copyright.com

Ana María Cuesta García

a#4: Pseudocubic crystal structure and phase transition in doped ye'elimité

Rightslink® by Copyright Clearance Center

https://s100.copyright.com/AppDispatchServlet



Home Create Account Help Live Chat

ACS Publications Most Trusted. Most Cited. Most Read.

Title: Pseudocubic Crystal Structure and Phase Transition in Doped Ye'elimité
Author: Ana Cuesta, Ángeles G. De la Torre, Enrique R. Losilla, et al
Publication: Crystal Growth and Design
Publisher: American Chemical Society
Date: Oct 1, 2014
Copyright © 2014, American Chemical Society

LOGIN
If you're a [copyright.com](#) user, you can login to RightsLink using your [copyright.com](#) credentials. Already a [RightsLink user](#) or want to [learn more?](#)

PERMISSION/LICENSE IS GRANTED FOR YOUR ORDER AT NO CHARGE

This type of permission/license, instead of the standard Terms & Conditions, is sent to you because no fee is being charged for your order. Please note the following:

- Permission is granted for your request in both print and electronic formats, and translations.
- If figures and/or tables were requested, they may be adapted or used in part.
- Please print this page for your records and send a copy of it to your publisher/graduate school.
- Appropriate credit for the requested material should be given as follows: "Reprinted (adapted) with permission from (COMPLETE REFERENCE CITATION). Copyright (YEAR) American Chemical Society." Insert appropriate information in place of the capitalized words.
- One-time permission is granted only for the use specified in your request. No additional uses are granted (such as derivative works or other editions). For any other uses, please submit a new request.

BACK **CLOSE WINDOW**

Copyright © 2015 Copyright Clearance Center, Inc. All Rights Reserved. [Privacy statement](#). [Terms and Conditions](#).
Comments? We would like to hear from you. E-mail us at customercare@copyright.com

1 de 1

06/05/2015 14:50

a#5: Hydration mechanisms of two polymorphs of synthetic ye'elimité

Rightslink® by Copyright Clearance Center

https://s100.copyright.com/AppDispatchServlet



Title: Hydration mechanisms of two polymorphs of synthetic ye'elimité
Author: A. Cuesta, G. Álvarez-Pinazo, S.G. Sanfélix, I. Peral, M.A.G. Aranda, A.G. De la Torre
Publication: Cement and Concrete Research
Publisher: Elsevier
Date: September 2014
 Copyright © 2014 Elsevier Ltd. All rights reserved.

Logged in as:
 ana cuesta
 Account #:
 3000916509
[LOGOUT](#)

Order Completed

Thank you very much for your order.

This is a License Agreement between ana cuesta ("You") and Elsevier ("Elsevier"). The license consists of your order details, the terms and conditions provided by Elsevier, and the [payment terms and conditions](#).

[Get the printable license.](#)

License Number	3657720133736
License date	Jun 28, 2015
Licensed content publisher	Elsevier
Licensed content publication	Cement and Concrete Research
Licensed content title	Hydration mechanisms of two polymorphs of synthetic ye'elimité
Licensed content author	A. Cuesta, G. Álvarez-Pinazo, S.G. Sanfélix, I. Peral, M.A.G. Aranda, A.G. De la Torre
Licensed content date	September 2014
Licensed content volume number	63
Licensed content issue number	n/a
Number of pages	10
Type of Use	reuse in a thesis/dissertation
Portion	full article
Format	both print and electronic
Are you the author of this Elsevier article?	Yes
Will you be translating?	No
Title of your thesis/dissertation	Preparation and hydration of model ecocement phases. Characterization by diffraction and cognate methods.
Expected completion date	Nov 2015
Estimated size (number of pages)	250
Elsevier VAT number	GB 494 6272 12
Permissions price	0.00 EUR
VAT/Local Sales Tax	0.00 EUR / 0.00 GBP
Total	0.00 EUR

[ORDER MORE...](#) [CLOSE WINDOW](#)

Copyright © 2015 Copyright Clearance Center, Inc. All Rights Reserved. [Privacy statement](#). [Terms and Conditions](#).
 Comments? We would like to hear from you. E-mail us at customercare@copyright.com

Figure 1.5.

Rightslink Printable License

<https://s100.copyright.com/App/PrintableLicenseFrame.jsp?publisher...>

JOHN WILEY AND SONS LICENSE TERMS AND CONDITIONS

Jun 28, 2015

This Agreement between ana cuesta ("You") and John Wiley and Sons ("John Wiley and Sons") consists of your license details and the terms and conditions provided by John Wiley and Sons and Copyright Clearance Center.

License Number	3657701083765
License date	Jun 28, 2015
Licensed Content Publisher	John Wiley and Sons
Licensed Content Publication	Journal of the American Ceramic Society
Licensed Content Title	Calcium Sulfoaluminate Sodalite (Ca ₄ Al ₆ O ₁₂ SO ₄) Crystal Structure Evaluation and Bulk Modulus Determination
Licensed Content Author	Craig W. Hargis, Juhyuk Moon, Barbara Lothenbach, Frank Winnefeld, Hans-Rudolf Wenk, Paulo J. M. Monteiro
Licensed Content Date	Dec 12, 2013
Pages	7
Type of use	Dissertation/Thesis
Requestor type	University/Academic
Format	Print and electronic
Portion	Figure/table
Number of figures/tables	1
Original Wiley figure/table number(s)	Figure 1
Will you be translating?	No
Title of your thesis / dissertation	Preparation and hydration of model ecocement phases. Characterization by diffraction and cognate methods.
Expected completion date	Nov 2015
Expected size (number of pages)	250
Requestor Location	ana cuesta UNIVERSITY OF MALAGA CAMPUES TEATINOS S/N MALAGA, Spain 29071 Attn: ANA CUESTA
Billing Type	Invoice
Billing Address	ana cuesta UNIVERSITY OF MALAGA CAMPUES TEATINOS S/N MALAGA, Spain 29071 Attn: ANA CUESTA
Total	0.00 EUR
Terms and Conditions	

Figure 1.6 and 1.11.

Rightslink® by Copyright Clearance Center

https://s100.copyright.com/AppDispatchServlet

The screenshot shows the RightsLink interface. On the left is the journal cover for 'Journal of Thermal Analysis and Calorimetry'. To the right, the following metadata is displayed:

- Title:** Calorimetric and thermogravimetric study on the influence of calcium sulfate on the hydration of ye'elinite
- Author:** Frank Winnefeld
- Publication:** Journal of Thermal Analysis and Calorimetry
- Publisher:** Springer
- Date:** Jan 1, 2009
- Copyright © 2009, Akadémiai Kiadó, Budapest, Hungary

Additional information on the right includes 'Logged in as: ana cuesta' and 'Account #: 3000916509'. Navigation buttons for 'Home', 'Account Info', 'Help', and 'Live Chat' are visible at the top. A 'LOGOUT' button is located below the account information.

Order Completed

Thank you very much for your order.

This is a License Agreement between ana cuesta ("You") and Springer ("Springer"). The license consists of your order details, the terms and conditions provided by Springer, and the [payment terms and conditions](#).

[Get the printable license.](#)

License Number	3657710414234
License date	Jun 28, 2015
Licensed content publisher	Springer
Licensed content publication	Journal of Thermal Analysis and Calorimetry
Licensed content title	Calorimetric and thermogravimetric study on the influence of calcium sulfate on the hydration of ye'elinite
Licensed content author	Frank Winnefeld
Licensed content date	Jan 1, 2009
Volume number	101
Issue number	3
Type of Use	Thesis/Dissertation
Portion	Figures
Author of this Springer article	No
Country of republication	other
Original figure numbers	Figures 1 and 6
Title of your thesis / dissertation	Preparation and hydration of model ecocement phases. Characterization by diffraction and cognate methods.
Expected completion date	Nov 2015
Estimated size(pages)	250
Total	0.00 EUR

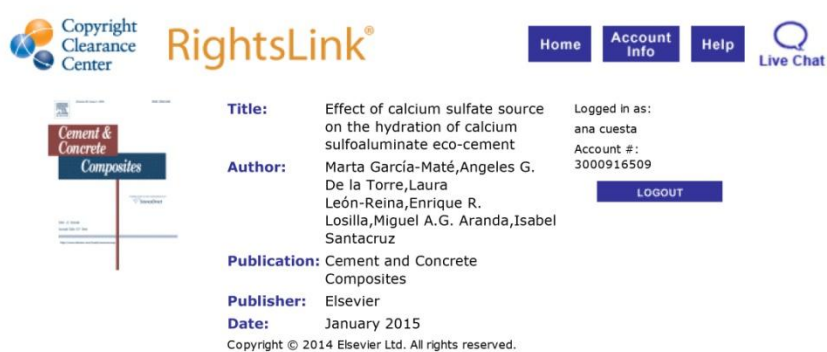
CLOSE WINDOW

Copyright © 2015 Copyright Clearance Center, Inc. All Rights Reserved. [Privacy statement](#). [Terms and Conditions](#). Comments? We would like to hear from you. E-mail us at customercare@copyright.com

Figure 1.7.

Rightslink® by Copyright Clearance Center

https://s100.copyright.com/AppDispatchServlet



The screenshot shows the RightsLink interface. At the top left is the Copyright Clearance Center logo. To its right is the RightsLink logo. Further right are navigation buttons for Home, Account Info, Help, and Live Chat. Below the logos is a thumbnail of the journal cover for 'Cement & Concrete Composites'. The main content area displays the following information:

- Title:** Effect of calcium sulfate source on the hydration of calcium sulfoaluminate eco-cement
- Author:** Marta García-Maté, Angeles G. De la Torre, Laura León-Reina, Enrique R. Losilla, Miguel A.G. Aranda, Isabel Santacruz
- Publication:** Cement and Concrete Composites
- Publisher:** Elsevier
- Date:** January 2015

Logged in as: ana cuesta
Account #: 3000916509
A LOGOUT button is visible.

Copyright © 2014 Elsevier Ltd. All rights reserved.

Order Completed

Thank you very much for your order.

This is a License Agreement between ana cuesta ("You") and Elsevier ("Elsevier"). The license consists of your order details, the terms and conditions provided by Elsevier, and the [payment terms and conditions](#).

[Get the printable license.](#)

License Number	3657710657840
License date	Jun 28, 2015
Licensed content publisher	Elsevier
Licensed content publication	Cement and Concrete Composites
Licensed content title	Effect of calcium sulfate source on the hydration of calcium sulfoaluminate eco-cement
Licensed content author	Marta García-Maté, Angeles G. De la Torre, Laura León-Reina, Enrique R. Losilla, Miguel A.G. Aranda, Isabel Santacruz
Licensed content date	January 2015
Licensed content volume number	55
Licensed content issue number	n/a
Number of pages	9
Type of Use	reuse in a thesis/dissertation
Portion	figures/tables/illustrations
Number of figures/tables /illustrations	1
Format	both print and electronic
Are you the author of this Elsevier article?	No
Will you be translating?	No
Title of your thesis/dissertation	Preparation and hydration of model ecocement phases. Characterization by diffraction and cognate methods.
Expected completion date	Nov 2015
Estimated size (number of pages)	250
Elsevier VAT number	GB 494 6272 12
Permissions price	0.00 EUR
VAT/Local Sales Tax	0.00 EUR / 0.00 GBP
Total	0.00 EUR

[ORDER MORE...](#)

[CLOSE WINDOW](#)

Copyright © 2015 Copyright Clearance Center, Inc. All Rights Reserved. [Privacy statement](#). [Terms and Conditions](#).
Comments? We would like to hear from you. E-mail us at customer-care@copyright.com

Figure 1.8.

Rightslink® by Copyright Clearance Center

https://s100.copyright.com/AppDispatchServlet



Copyright Clearance Center **RightsLink®** Home Account Info Help Live Chat

ACS Publications **Title:** Active Iron-Rich Belite Sulfoaluminate Cements: Clinkering and Hydration
Author: Antonio J. M. Cuberos, Ángeles G. De la Torre, G. Álvarez-Pinazo, et al
Publication: Environmental Science & Technology
Publisher: American Chemical Society
Date: Sep 1, 2010
 Copyright © 2010, American Chemical Society

Logged in as: ana cuesta
 Account #: 3000916509
 LOGOUT

PERMISSION/LICENSE IS GRANTED FOR YOUR ORDER AT NO CHARGE

This type of permission/license, instead of the standard Terms & Conditions, is sent to you because no fee is being charged for your order. Please note the following:

- Permission is granted for your request in both print and electronic formats, and translations.
- If figures and/or tables were requested, they may be adapted or used in part.
- Please print this page for your records and send a copy of it to your publisher/graduate school.
- Appropriate credit for the requested material should be given as follows: "Reprinted (adapted) with permission from (COMPLETE REFERENCE CITATION). Copyright (YEAR) American Chemical Society." Insert appropriate information in place of the capitalized words.
- One-time permission is granted only for the use specified in your request. No additional uses are granted (such as derivative works or other editions). For any other uses, please submit a new request.

If credit is given to another source for the material you requested, permission must be obtained from that source.

BACK

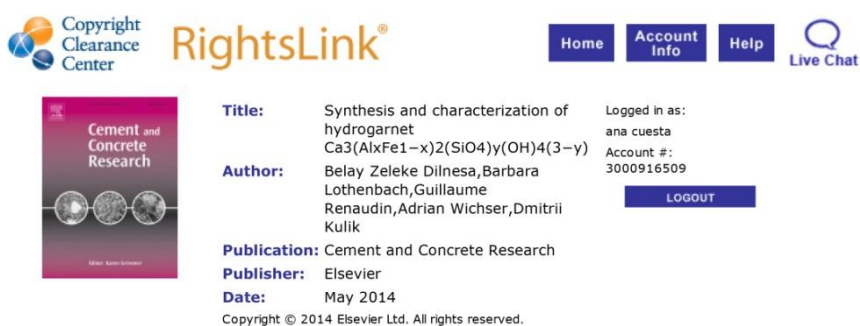
CLOSE WINDOW

Copyright © 2015 Copyright Clearance Center, Inc. All Rights Reserved. [Privacy statement](#). [Terms and Conditions](#).
 Comments? We would like to hear from you. E-mail us at customercare@copyright.com

Figure 1.10.

Rightslink® by Copyright Clearance Center

https://s100.copyright.com/AppDispatchServlet



The screenshot shows the RightsLink interface. At the top left is the Copyright Clearance Center logo. To its right is the RightsLink logo. Further right are navigation buttons for Home, Account Info, Help, and Live Chat. Below the logos is a book cover for 'Cement and Concrete Research'. To the right of the cover, the article details are listed: Title: Synthesis and characterization of hydrogarnet $\text{Ca}_3(\text{Al}_x\text{Fe}_{1-x})_2(\text{SiO}_4)_y(\text{OH})_4(3-y)$; Author: Belay Zeleke Dilnesa, Barbara Lothenbach, Guillaume Renaudin, Adrian Wichser, Dmitrii Kulik; Publication: Cement and Concrete Research; Publisher: Elsevier; Date: May 2014. On the right side, the user is logged in as 'ana cuesta' with account number 3000916509 and a LOGOUT button. At the bottom, there is a copyright notice: Copyright © 2014 Elsevier Ltd. All rights reserved.

Order Completed

Thank you very much for your order.

This is a License Agreement between ana cuesta ("You") and Elsevier ("Elsevier"). The license consists of your order details, the terms and conditions provided by Elsevier, and the [payment terms and conditions](#).

[Get the printable license.](#)

License Number	3657711086851
License date	Jun 28, 2015
Licensed content publisher	Elsevier
Licensed content publication	Cement and Concrete Research
Licensed content title	Synthesis and characterization of hydrogarnet $\text{Ca}_3(\text{Al}_x\text{Fe}_{1-x})_2(\text{SiO}_4)_y(\text{OH})_4(3-y)$
Licensed content author	Belay Zeleke Dilnesa, Barbara Lothenbach, Guillaume Renaudin, Adrian Wichser, Dmitrii Kulik
Licensed content date	May 2014
Licensed content volume number	59
Licensed content issue number	n/a
Number of pages	16
Type of Use	reuse in a thesis/dissertation
Portion	figures/tables/illustrations
Number of figures/tables /illustrations	2
Format	both print and electronic
Are you the author of this Elsevier article?	No
Will you be translating?	No
Title of your thesis/dissertation	Preparation and hydration of model ecocement phases. Characterization by diffraction and cognate methods.
Expected completion date	Nov 2015
Estimated size (number of pages)	250
Elsevier VAT number	GB 494 6272 12
Permissions price	0.00 EUR
VAT/Local Sales Tax	0.00 EUR / 0.00 GBP
Total	0.00 EUR

[ORDER MORE...](#)

[CLOSE WINDOW](#)

Copyright © 2015 Copyright Clearance Center, Inc. All Rights Reserved. [Privacy statement](#). [Terms and Conditions](#). Comments? We would like to hear from you. E-mail us at customecare@copyright.com

Figure 4.2.

Rightslink® by Copyright Clearance Center

https://s100.copyright.com/AppDispatchServlet



The screenshot shows the RightsLink interface. On the left is the Copyright Clearance Center logo. In the center is the RightsLink logo. On the right are navigation buttons: Home, Account Info, Help, and Live Chat. Below the logo is a thumbnail of a journal article cover titled "Geochimica et Cosmochimica Acta". To the right of the thumbnail, the following information is displayed:

- Title:** Re-evaluating boron speciation in biogenic calcite and aragonite using 11B MAS NMR
- Author:** Kateryna Klochko, George D. Cody, John A. Tossell, Przemyslaw Dera, Alan J. Kaufman
- Publication:** Geochimica et Cosmochimica Acta
- Publisher:** Elsevier
- Date:** 1 April 2009

Logged in as: ana cuesta
Account #: 3000916509
A LOGOUT button is visible.

Copyright © 2009 Elsevier Ltd. All rights reserved.

Order Completed

Thank you very much for your order.

This is a License Agreement between ana cuesta ("You") and Elsevier ("Elsevier"). The license consists of your order details, the terms and conditions provided by Elsevier, and the [payment terms and conditions](#).

[Get the printable license.](#)

License Number	3658680350061
License date	Jun 30, 2015
Licensed content publisher	Elsevier
Licensed content publication	Geochimica et Cosmochimica Acta
Licensed content title	Re-evaluating boron speciation in biogenic calcite and aragonite using 11B MAS NMR
Licensed content author	Kateryna Klochko, George D. Cody, John A. Tossell, Przemyslaw Dera, Alan J. Kaufman
Licensed content date	1 April 2009
Licensed content volume number	73
Licensed content issue number	7
Number of pages	11
Type of Use	reuse in a thesis/dissertation
Portion	figures/tables/illustrations
Number of figures/tables /illustrations	1
Format	both print and electronic
Are you the author of this Elsevier article?	No
Will you be translating?	No
Title of your thesis/dissertation	Preparation and hydration of model ecocement phases. Characterization by diffraction and cognate methods.
Expected completion date	Nov 2015
Estimated size (number of pages)	250
Elsevier VAT number	GB 494 6272 12
Permissions price	0.00 EUR
VAT/Local Sales Tax	0.00 EUR / 0.00 GBP
Total	0.00 EUR

[ORDER MORE...](#) [CLOSE WINDOW](#)

Copyright © 2015 Copyright Clearance Center, Inc. All Rights Reserved. [Privacy statement](#). [Terms and Conditions](#). Comments? We would like to hear from you. E-mail us at customercare@copyright.com

